AFCRL-67-0049

A REAL TIME FOURIER TRANSFORM SYNTHESIZER

J. E. Hoffman, Jr.

Electro-Dynamics Laboratories
Departments of Electrical Engineering, Physics, and Chemistry
UTAH STATE UNIVERSITY
Logan, Utah

Contract No. AF19(628)-3825

Project No. 8663

SCIENTIFIC REPORT No. 7

1 November 1966

Dr. G. A. Vanasse

This research was sponsored by the Advanced Research Projects Agency
under ARPA Order No. 450

Prepared for
Air Force Cambridge Research Laboratories
Office of Aerospace Research
UNITED STATES AIR FORCE
Bedford, Massachusetts

AFCRL-67-0049

A REAL-TIME FOURIER TRANSFORM SYNTHESIZER

J.E. Hoffman, Jr.

Electro-Dynamics Laboratories
Departments of Electrical Engineering, Physics, and Chemistry
UTAH STATE UNIVERSITY
Logan, Utah

SCIENTIFIC REPORT NO. 7

Contract No. AF19(628)-3825

1 November 1966

This research was sponsored by the
Advanced Research Projects Agency

ARPA Order No. 450

Project No. 8663

Prepared for

Air Force Cambridge Research Laboratories
Office of Aerospace Research
UNITED STATES AIR FORCE
Bedford, Massachusetts

ABSTRACT

A study of the relationship between the interferogram F(x) obtained in Fourier spectroscopy and the corresponding spectral distribution E(ν) is made. It is found that the spectral distribution is the Fourier cosine transform of the interferogram.

Various computational techniques for performing the required transformation are studied, and a Real-Time Fourier Transform Synthesizer is described. It has been designed to be compatible with a lamellar grating interferometer but could be used just as well with a well-compensated Michelson interferometer. The system used to obtain the point of zero path difference is described in detail. A novel approach is used to obtain the cosine functions required in the synthesis of the cosine transform. All the computations except the summation are done in analog form, while the summation is done digitally. The result of the computation, the spectral distribution, is available as soon as the interferogram is obtained. Errors in the technique are discussed and methods of compensating for them are enumerated.

Data have been obtained for several test functions, and the synthesized spectra are compared with the theoretical values. Several actual interferograms have been obtained, and the results of the spectral synthesis are presented.

CONTENTS

INTRODUCTION

In the infrared, there are two reasons for using an interferometer. First, an interferometer views a source with a much larger entrance aperture than a spectrometer and allows more energy to reach the detector. This is called "aperture gain." Second, all spectral elements in a bandwidth determined by the resolving power of the instrument are scanned simultaneously during the full time of the observation. If T is the observation time per spectral element and N is the number of elements, it is found that the interferometer makes N times as many measurements of each spectral element. If the system is detector-noise limited, variations in the signal due to random detector noise vary inversely as the square root of the observation time [1] and this, in turn, depends on the number of spectral elements being observed. This fact, the gain of the square root of N in the signal-to-noise ratio of the recorded signal, is known as the "Fellgett advantage." Hence, the ratio of the net gain of an interferometer over a spectrometer is the aperture gain times the Fellgett advantage [2].

An interferometer may be used as a spectrometer by measuring the radiation falling on the central fringe of a two-beam interferometer as a function of path difference. The average value of a chart recording of the radiation as a function of path difference is called an interferogram.

The spectral distribution may be obtained by calculating the Fourier transform of the interferogram. A digital computer is generally used to perform the transformation. The use of a digital computer has a disadvantage in that the spectrum is not available for immediate analysis.

This research is undertaken to determine the feasibility of computing spectra in real time and building a computer to perform this task.

TWO-BEAM INTERFEROMETERS AND A DISCUSSION OF INTERFEROGRAMS

Interferometers

A two-beam interferometer is a device which splits an incoming wavefront into two parts by amplitude or wavefront division. It introduces a delay in the path of one part and then recombines the two parts. The Michelson interferometer is an example of the type which operates by amplitude division, see Figure 1 . The beamsplitter, providing it is non-absorbing and has a reflectance of 0.5, divides the light into two equal parts and recombines them after a relative delay of σ thus causing them to interfere. The delay is produced by introducing different optical paths for the different parts of the divided beam. One mirror is fixed while the other can be displaced parallel to itself with a constant velocity v. If M_2 is shifted through distance d to position M_2', the time delay associated with this path is increased by 2 d/c where c is the speed of light. The geometrical path is increased by 2d. The optical path is increased by 2md where m is the index of refraction. A compensator is included in one path to equalize the paths in material other than air. The Michelson interferometer exhibits circular symmetry, and the detector is placed in the central fringe of the interference pattern.

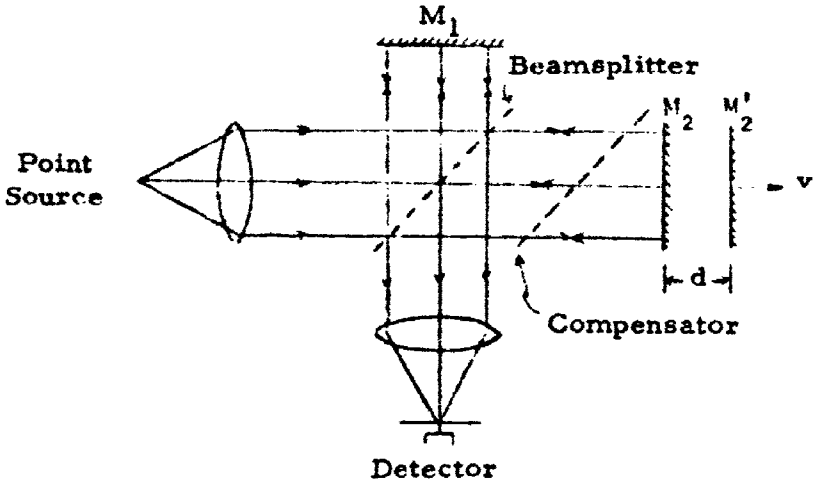
M1
Beamsplitter
M2
M'2
Point
Source
v
d
Compensator
Detector

Figure 1

An interferometer which makes use of wavefront division is the lamellar grating. Figure 33 shows a system in which the lamellar grating is used, and Figure 17 shows a cross section through the facets. The odd-numbered facets are fixed, and the even-numbered ones are mounted in such a manner that they are movable over a total distance of one inch. In this particular case, both sets of facets are made of steel although other materials, such as glass, have been used. The grating is 6 inches square, and each facet is 6 inches long and 1/16 inch wide. The faces of the facets have a deposited gold coating to increase the reflectance in the infrared. Each facet acts as a narrow mirror, and the path difference is introduced by changing the groove depth. Interference takes place in a plane located at the faces of the foremost facets. The detector is placed in the central grating order.

Lamellar grating interferometers are used in the infrared region of the spectrum. The one used in this research is designed for wavelengths longer than 10 microns. They are not used in the visible region because it is impossible to machine and polish the surface of the facets to the required tolerances.

The illumination received by the detector is modulated by translating the movable section of the grating or one mirror of the Michelson interferometer. When this is done linearly with time, the detector response is modulated at a frequency

$$f_{\nu_o} = 2\nu_o v$$

where v is the velocity of the mirror, or moving facets, and ν_o is the wavenumber. Also, $\nu_o = 1/\lambda_o$, where λ_o is the wavelength.

For monochromatic illumination, the detector response is sinusoidal and would continue indefinitely. When several monochromatic components are present, the detector response is the sum of a series of sinusoidal functions, one for each of the components. Thus, the output of an interferometer, called an "interferogram," is synthesized by means of the summation of trigonometric functions with amplitudes determined by the spectrum of the incident illumination. By computing the Fourier transform of the interferogram, it is possible to make a harmonic analysis of it and thence to determine the intensities of the frequency components. Thus, the spectrum may be obtained.

Derivation of equations

In the infrared, one is dealing with frequencies on the order of 10^{12}-10^{15} cycles per second. Present detectors cannot respond to frequencies higher than about 10^7 cps. When higher frequencies fall upon these detectors, they respond to the time average intensity of the illumination. Time dependence will be ignored in the following work, although it can be shown that the time origin is arbitrary.

The following derivation is applicable to the case of the Michelson interferometer or the lamellar grating. Consider an electromagnetic wave of single frequency ν_o,

$$v(\delta) = v_o e^{-i2\pi\nu_o\delta} \tag{1}$$

where

ν_o is in wavenumbers and is equal to $1/\lambda_o$,

λ_o is the wavelength in centimeters,

v_o is the amplitude of the wave, and

δ is the distance from some arbitrary origin.

The beamsplitter, or the grating, divides the wave into two parts $v_1(\delta)$ and $v_2(\delta)$ such that $av_1 = v_2$. For the Michelson, "a" may be a constant, a complex quantity, or a frequency dependent, as determined by the characteristics of the beamsplitter. It is nearly unity for the lamellar grating.

Let the difference in optical path length between $v_1(\delta)$ and $v_2(\delta)$, as measured from the beamsplitter or the front face of the grating, be x. Then

$$v_1(\delta) = v_1 e^{-i2\pi\nu_o\delta} \tag{2}$$

and

$$v_2(\delta) = a v_1 e^{-i2\pi\nu_o(\delta + x)} \tag{3}$$

At the recombination point, the sum of these is

$$v(\delta) = v_1(\delta) + v_2(\delta) = v_1 e^{-i2\pi\nu_o\delta}(1 + a e^{-i2\pi\nu_o x}) \tag{4}$$

This equation demonstrates that the origin of δ is arbitrary and may be chosen equal to zero.

At any point in space, the intensity is given by

$$I = v(\delta)\, v^*(\delta) \tag{5}$$

where $v^*(\delta)$ represents the complex conjugate of $v(\delta)$. Therefore,

$$I = v_1^2 \left[1 + a^2 + a(e^{i2\pi\nu_o x} + e^{-i2\pi\nu_o x})\right] \tag{6}$$

For an ideal beamsplitter, $v_1 = v_2$, so "a" = 1 in this case also. Since it is only a function of x, equation (6) may be rewritten as

$$I(x) = 2\, v_1^2 \left[1 + \cos 2\pi\nu_o x\right] \tag{7}$$

If a broad spectral source is being observed, equation (1) becomes

$$v(\delta) = \int_{-\infty}^{\infty} v(\nu)\, e^{-i2\pi\nu\delta} d\nu \tag{8}$$

With this substitution, equation (4) becomes

$$v(\delta) = \int_{-\infty}^{\infty} v(\nu)\,(1 + e^{-i2\pi\nu x}) e^{-i2\pi\nu\delta} d\nu \tag{9}$$

This equation is a Fourier transform relationship so that

$$v_r(\nu) = v(\nu)(1 + e^{-i2\pi\nu x}) = \int_{-\infty}^{\infty} v(\delta) e^{i2\pi\nu\delta} d\delta \tag{10}$$

In order to obtain the intensity as a function of x, $v_r(\nu) * v_r^*(\nu)$ must be integrated over all frequencies, where * denotes convolution. Therefore,

$$\frac{I(x)}{2} = \int_{-\infty}^{\infty} |v(\nu)|^2 (1 + \cos 2\pi\nu x) d\nu \tag{11}$$

Now, redefine the variables and let

$$\frac{I(x)}{2} = E(x) = \text{total illuminance}$$

and

$v(\nu) = E(\nu) =$ intensity spectral distribution.

With these substitutions, equation (11) may be rewritten as

$$E(x) = \int_{-\infty}^{\infty} E(\nu)[1 + \cos 2\pi\nu x]\, d\nu \tag{12}$$

$$E(x) = \int_{-\infty}^{\infty} E(\nu)d\nu + \int_{-\infty}^{\infty} E(\nu) \cos 2\pi\ x dx. \tag{13}$$

For $x = 0$

$$E(0) = 2\int_{-\infty}^{\infty} E(\nu)d\nu \tag{14}$$

and for large $x = d$

$$E(d) = \tfrac{1}{2}E(0) + \int_{-\infty}^{\infty} E(\nu) \cos 2\pi\nu d\, d\nu \tag{15}$$

The integral will vanish unless $E(\nu)$ represents strictly monochromatic radiation. In practice, the value of d required for the integral to vanish is determined by the wavelength range of the incident illumination. The broader the bandwidth, the smaller the value of d required to yield $E(d) = \frac{1}{2}E(0)$.

The difference between $E(x)$ and $\frac{1}{2}E(0)$ is analyzed and is called the "interferogram function" $F(x)$.

$$F(x) = E(x) - \tfrac{1}{2}E(0) = \int_{-\infty}^{\infty} E(\nu) \cos 2\pi\nu x d\nu \qquad (16)$$

This function is obtained from a strip chart recording of the total illumination falling upon the detector of the two-beam interferometer as the path difference is varied. The value of $\frac{1}{2}E(0)$ is determined from the asymptotic value of such a record. The total illumination approaches this value as the path difference increases.

From Fourier theory

$$E(\nu) = \int_{-\infty}^{\infty} F(x) \cos 2\pi\nu x dx \qquad (17)$$

Therefore, if we can specify $F(x)$, we can uniquely determine $E(\nu)$.

Methods of computing spectra from interferograms

For simple interferograms which can be expressed analytically, the computation can proceed directly. Two such cases are discussed.

1) Assume the interferogram can be expressed as

$$F(x) = e^{-x^2/a^2} \cos bx \qquad (18)$$

The spectrum is

$$E(\nu) = \int_{-\infty}^{\infty} F(x) \cos 2\pi\nu x dx = \int_{-\infty}^{\infty} e^{-x^2/a^2} \cos bx \cos 2\pi\nu x dx \qquad (19)$$

This may be solved with the aid of integral tables and, by neglecting constants, the result is

$$E(\nu) = e^{-a^2(\nu-b)^2/4} \tag{20}$$

This represents a line with a Gaussian frequency distribution centered at wavenumber b.

2) If the interferogram can be expressed as

$$F(x) = e^{-x^2/a^2} \cos fx \cos bx$$

where

$$b >> f, \; af >> 1 \tag{21}$$

then

$$E(\nu) = \int_{-\infty}^{\infty} F(x)\cos 2\pi\nu x \, dx = \int_{-\infty}^{\infty} e^{-x^2/a^2} \cos fx \cos bx \cos 2\pi\nu x dx \tag{22}$$

This may also be solved with the aid of integral tables and, by neglecting constants, the result is [3]

$$E(\nu) = e^{-a^2(\nu-b-f)^2/4} + e^{-a^2(\nu-b+f)^2/4} \tag{23}$$

This represents a pair of lines with Gaussian distributions centered at wavenumbers b-f and b+f. The interferograms and the corresponding spectral distributions are shown in Figure 2.

The interferogram function

$$F(x) = E(X) - \tfrac{1}{2}E(0) = \int_{-\infty}^{\infty} E(\nu) \cos 2\pi\nu x d\nu \qquad (24)$$

may be rewritten in terms of electrical engineering terminology in terms of ω, where $\omega = 2\pi f_\nu$ and is the angular frequency of the detector output. Further, $f_\nu = 2\nu v$ where v = the rate of change of groove depth or mirror position. Let $\varphi(\omega) = \frac{1}{2v} E(\nu)$ and $G(t) = F(x)$ [4]. Then

$$G(t) = \frac{1}{2\pi} \int_{-\infty}^{\infty} \varphi(\omega) \cos\omega t d\omega \qquad (25)$$

where $\varphi(\omega)$ is the frequency spectrum of the detector response and $E_1(\nu)$ is the spectrum of the radiation incident on the detector. The frequency spectrum is

$$\varphi(\omega) = \int_{-\infty}^{\infty} G(t) \cos\omega t dt \qquad (26)$$

and the problem is reduced to that of finding $\varphi(\omega)$ if given a plot of $G(t)$. Since $G(t)$ cannot generally be expressed analytically, some sort of analog or digital computer is used to obtain the Fourier transform.

SIMPLE INTERFEROGRAMS AND THEIR CORRESPONDING SPECTRA

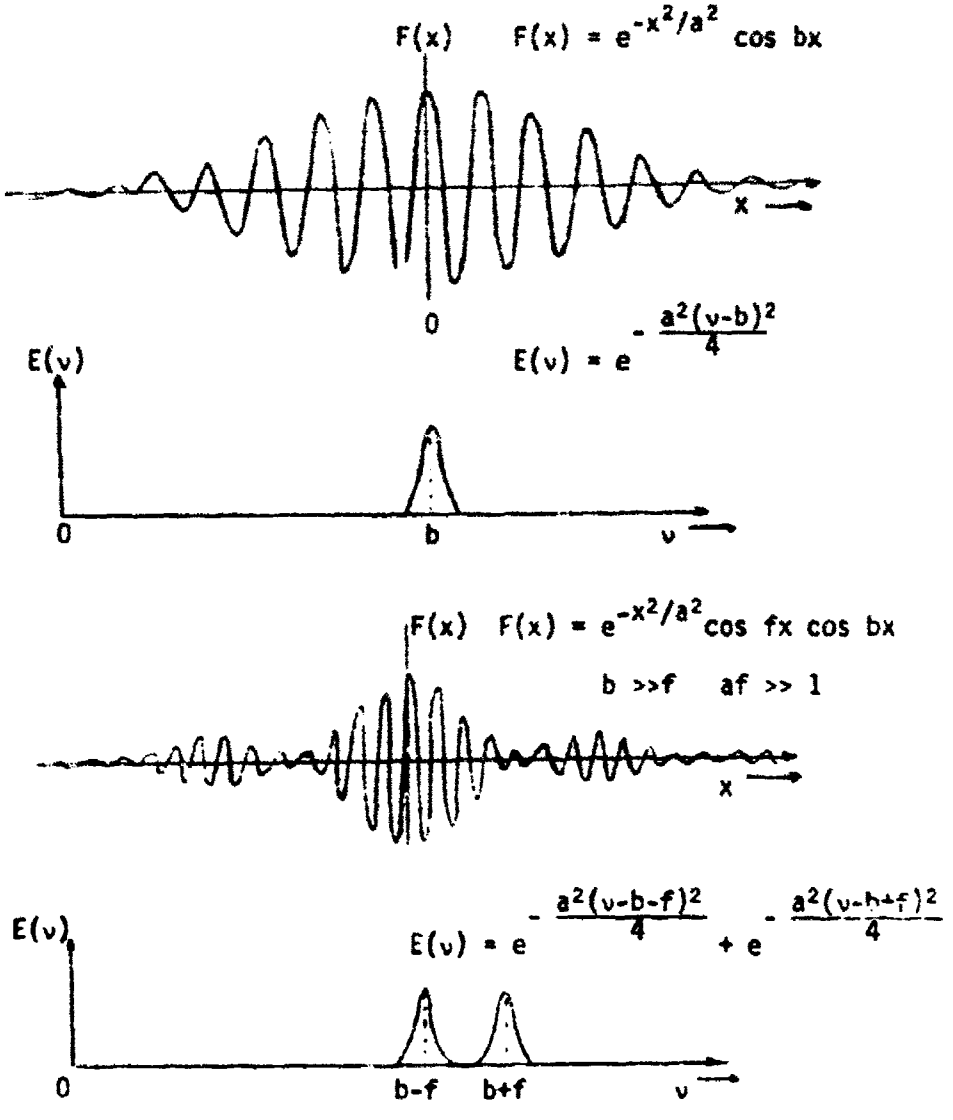

Figure 2

Analog computers have been used to compute Fourier coefficients ever since the Hendrici Analyzer was constructed in the early part of this century [5]. Many other computers were constructed, but most of them were mechanical, slow, and of limited accuracy [6, 7, 8, 9]. Several optical devices have been investigated, but they do not lend themselves to the real-time calculation of spectra from interferograms [10, 11]. One of these optical schemes is discussed in the Appendix. Firle and Staake recorded data on film or tape and played it back through a wave analyzer [12, 13].

Neither the conventional sweep analyzer nor the bank-of-filters analyzer will work in the very low frequency range of the interferogram. When these units are used, the general technique is to record the interferogram on tape and play it back at a higher speed, thus increasing all the frequencies by the speed-up ratio. Analyses by this method are either quite slow or have limited resolution.

The IFTAC [14] records the interferogram on a tape loop and actually computes one component each time the tape loop is played back. It is designed to compute the spectrum and to give 1000 output points. The SIMORAMIC Analyzer operates much faster than a conventional sweep analyzer of comparable bandwidth and resolution [15]. It has been successfully used in the range of 0-8 kc to study atmospheric whistlers [16]. Until the advent of high speed digital computers, interferometry fell into disuse, partially because of the laborious task

of analyzing the data and the inadequate computers and analyzers then available.

Only discrete values of G(t) can be utilized by a digital computer or the real-time Fourier transform synthesizer. Therefore, to compute $\varphi(\omega)$, it is necessary to sample G(t). The samples must be spaced close enough to obtain all the information, but not so close as to add complication without a gain in information. The choice of the sampling points is governed by Shannon's sampling theorem [17]. The sampling theorem in the time domain is:

> If a band limited function G(t) contains no frequencies higher than ω_o radians/second, it is completely specified by giving its ordinates at a series of points spaced π/ω_o seconds apart, the series extending throughout the time domain.

Thus, if the maximum frequency of the detector response is $\omega_o/4\pi\ v/\lambda_o$, it is sufficient to sample the interferogram at intervals $\Delta h = \lambda_o/4 = 1/4\nu_o$ seconds. The range of values which ν can assume may be selected by optical filters.

The sampling theorem in the frequency domain is important since it tells us at what interval in ω rad/sec. (or ν cm^{-1}) we must compute the spectral function $\varphi(\omega)$ (or $E_1(\nu)$) to completely specify it. The theorem is stated as follows:

> If $\varphi(\omega)$ represents the spectrum of a function G(t) which is zero everywhere except in the interval $|t| < T$, then $\varphi(\omega)$ is exactly determined for all values of ω by giving its values at series of points 1/T cycles/second apart in frequency, the series extending throughout the frequency domain [18].

No information is lost if $\varphi(\omega)$ is specified at points separated by π/T radians or 1/4D in wavenumbers where D is the maximum groove depth or mirror displacement.

The sampling theorems tell us the proper sampling interval at which we do not lose any information. It is possible to sample at faster rates, and it is generally done in practice, as signal-to-noise ratios are improved. If h is the sampling interval, the sampled spectra repeat at intervals of 1/h. Since noise is present in all practical cases, the sampling rate is increased on the order of 5 to prevent overlapping of noise in the repeating spectra [19].

When digital computers are used to calculate the Fourier transform, they are generally programmed to analyze the interferogram F(x) to obtain the spectrum E(ν). That is to say, every sample point is used to obtain information about each component of the spectrum. In the synthesis technique, used in the real-time Fourier synthesizer, each sample point gives some information about all the spectral components.

Assume the interferogram G(t) is sampled at the proper intervals from $-T < t < T$. This represents a series of impulses with amplitudes determined by the value of the interferogram at the sampling point, and the spacing is dependent on the sampling interval, Figure 3. The interferogram G(t) is then represented approximately by

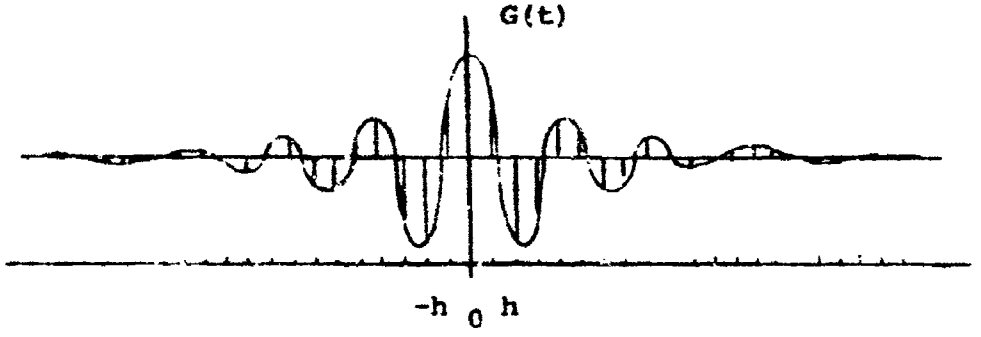

Figure 3

$$G(t) = g(0)\delta(0) + g(h)\delta(t-h) + g(-h)\delta(t+h) + g(2h)\delta(t-2h) + g(-2h)\delta(t+2h)$$

$$+ \ldots + g(nh)\delta(t-hn) + g(-nh)\delta(t+nh) \qquad (27)$$

The Fourier transform of a pair of δ functions symmetrically placed about the origin is a cosine function whose frequency depends on the distance of the pair of δ functions from the origin. Therefore, by superposition, the Fourier transform of G(t) is

$$\varphi(\omega) = g(0) + g(h)\cos\omega_h t + g(2h)\cos\omega_{2h} t + \ldots + g(nh)\cos\omega_{nh} t$$

$$\varphi(\omega) = g(0) + \sum_{n=0}^{n=N} g(nh)\cos\omega_{nh} t \qquad (28)$$

This equation states that the spectrum may be synthesized by the summation of a series of cosine functions with amplitudes dependent upon the amplitudes of the sample and frequencies dependent upon the distance of the sample point from t = 0.

Scanning function

In practice it is not possible to sample the interferogram throughout the entire time domain, and a truncation of the interferogram results The Fourier series representation of the spectrum estimate in exponential form is

$$\varphi_N(\omega) = h \sum_{n=-N}^{n=N} G(nh) e^{-jnh\omega} \tag{29}$$

This converges to the actual spectrum as $N \to \infty$, but since the interferogram is truncated, only a finite number of terms are available. This will cause the spectrum estimate to deviate from the true spectrum. The computed spectrum will be the convolution of the true spectrum with a function called the scanning function which will now be derived.

In equation (29) let

$$G(nh) = \frac{1}{2\pi} \int_{-\omega_o}^{\omega_o} \varphi(\epsilon)\, e^{jnh\epsilon}\, d\epsilon \tag{30}$$

Then, equation (29) becomes

$$\varphi_n(\omega) = h \frac{1}{2\pi} \int_{-\omega_o}^{\omega_o} \varphi(\epsilon) \sum_{-N}^{N} e^{jn(\epsilon - \omega)h} d\epsilon \tag{31}$$

Since

$$\frac{1}{2} \sum_{n=-N}^{N} e^{-jn(\epsilon-\omega)h} = \tfrac{1}{2} + \cos(\epsilon-\omega)h + \cos 2(\epsilon-\omega)h + \ldots + \cos N(\epsilon-\omega)n \tag{32}$$

the right-hand part of equation (32) is equal to [20]

$$\mu(\epsilon-\omega) = \frac{\sin(2N+1)\,\frac{(\epsilon-\omega)h}{2}}{\sin\left(\frac{\epsilon-\omega}{2}\right)h} \tag{33}$$

Substituting equation (33) into equation (31) yields

$$\varphi_n(\omega) = \frac{h}{2\pi}\int_{-\omega_o}^{\omega_o} \varphi(\epsilon)\mu(\epsilon - \omega)d\epsilon = \frac{h}{\pi}\int_{o}^{\omega_o} \varphi(\epsilon)\mu(\epsilon - \omega)d\epsilon \qquad (34)$$

For large N, the factor 1 in equation (33) is insignificant and can be dropped. Also, since the interferogram is even, only N samples are independent, so equation (33) can be rewritten

$$\mu(\epsilon - \omega) = \frac{\sin N(\epsilon - \omega)h}{\sin(\frac{\epsilon - \omega}{2})h} \qquad (35)$$

This is called the scanning function. In electrical engineering terminology, it would be called the impulse response. From equation (34), it is observed that the spectrum estimate is the convolution of the true spectrum with the scanning function as the integration is carried from 0 to ω_o, the fundamental range. The estimate $\varphi_n(\omega)$ approaches $\varphi(\omega)$ more closely as N increases. The first zero of $\mu(\epsilon - \omega)$ occurs when

$$\Delta\omega \approx \frac{2\pi}{Nh} \approx \frac{2\omega_o}{N}$$

Thus, for a monochromatic source, it is found that the computed spectral line has a width that is inversely proportional to N.

For a pair of closely spaced lines, the Rayleigh criterion gives a resolving power [21]

$$\frac{\nu_o}{\Delta\nu} \approx \frac{N}{2} \approx 2\nu_o D$$

$$\Delta\nu \approx 1/2\ D\ \text{cm}^{-1} \qquad (36)$$

It is now useful to see how the spectrum estimate approximates the true spectrum in the region of a discontinuity. In Figure 4, the true spectrum is assumed to be a square pulse and the scanning function is as shown. The computed spectrum estimates are given for two values of N.

The scanning function has a large peak and several smaller peaks on either side which decrease in amplitude. The negative peaks adjacent to the main peak have amplitudes slightly greater than one-fifth the value of the main peak, and they do not become smaller no matter how large N becomes.

The sine integral of x is shown in Figure 5. It is seen that the integral never assumes its final value but keeps continuing to approach it. The peaks occur at $x = \pi, 3\pi, 5\pi$...etc., and the valleys occur at $2\pi, 4\pi$, etc. The separation of the peaks in x is 2π. This gives a separation in ω of $\Delta\omega = \frac{2\omega_o}{N}$.

In the case where $N \to \infty$, the smaller peaks become compressed into a single vertical line at a discontinuity, but even then the Fourier series still yields a 9% overswing compared to the value of the discontinuity. Thus, to reduce this error due to the Gibbs phenomena at a discontinuity, such as a distinct spectral line, a technique called "apodization" is used. This can be seen more clearly by the following derivation.

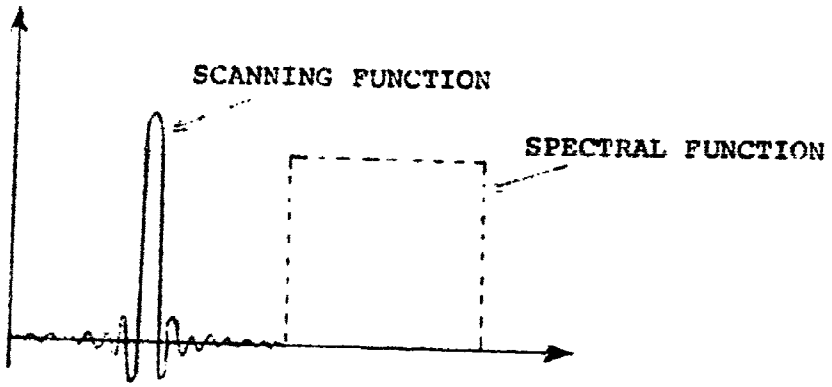

SPECTRUM ESTIMATES

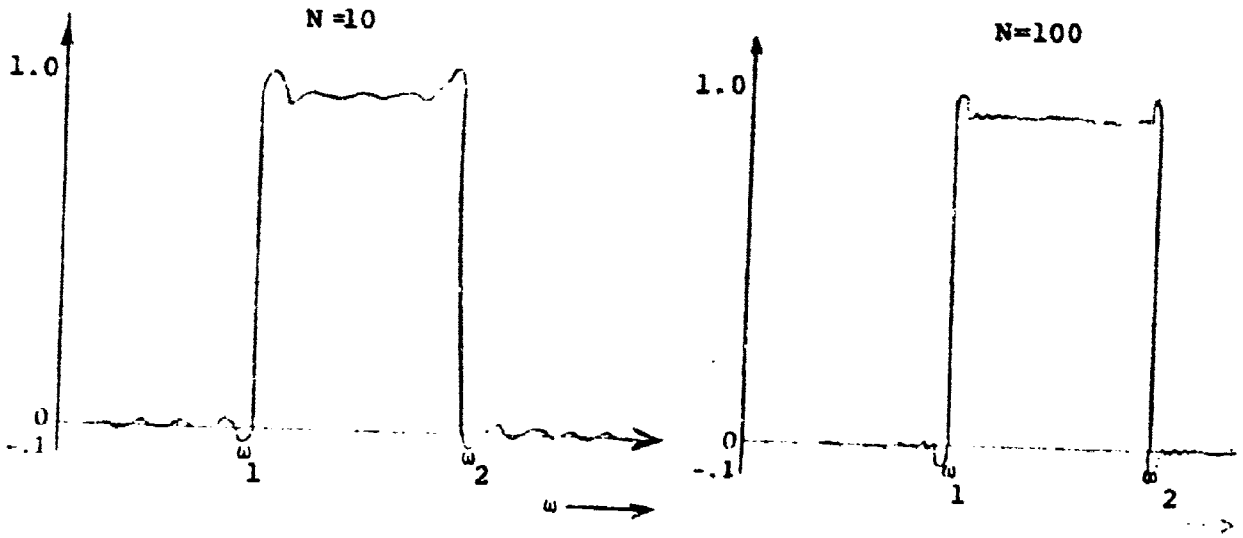

Figure 4

$$\mathrm{Si}(x) = \int_0^x \frac{\sin u}{u}\, du$$

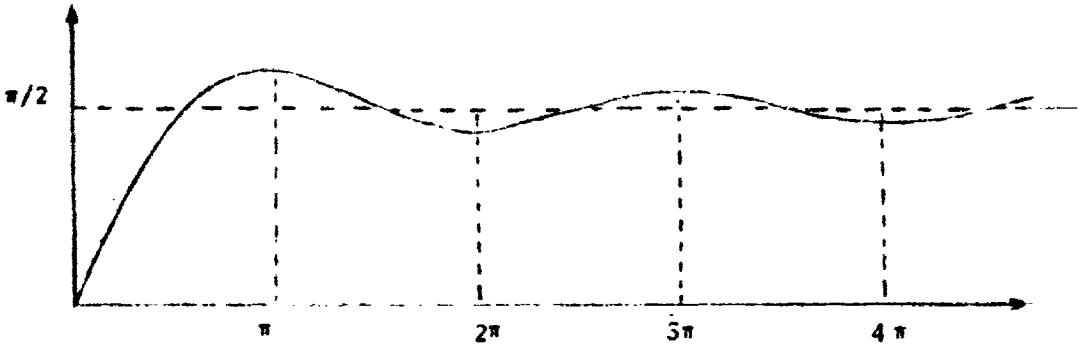

Figure 5

The true spectrum, in terms of wavenumbers, is given by

$$E(\nu) = \int_{-\infty}^{\infty} F(x) \cos 2\pi\nu x \, dx \qquad (37)$$

The maximum path difference is finite, and this causes truncation of the interferogram function F(x). Equation (37) may now be expressed as

$$E_n(\nu) = \int_{-\infty}^{\infty} F(x) \, C(x) \cos 2\pi\nu x \, dx \qquad (38)$$

where

$$C(x) = 1 \quad \text{for } -D < x < +D$$

$$C(x) = 0 \quad \text{for } x < -D \text{ and } x > +D$$

and

$$D = \text{maximum path difference.}$$

The cosine transform of the product of two even functions is the convolution of the cosine transforms of each of the two functions. Therefore,

$$E_n(\nu) = [\text{cosine transform of } F(x)] * [\text{cosine transform of } C(x)].$$

The cosine transform of F(x) is the true spectrum, while the cosine transform of C(x) is the scanning function. The scanning function has the

dimension of 1/length when $E(\nu)$ is computed and 1/time when $P(\omega)$ is computed. Now define the cosine transform of $C(x) = \mu(\epsilon - x)$. This gives the same result as previously obtained.

If the interferogram function is multiplied by a function $A(x)$ other than $C(x)$, equation (38) becomes

$$E_n(\nu) = \int_{-\infty}^{\infty} F(x)\, A(x) \cos n\nu x dx \qquad (40)$$

$A(x)$ is called an apodizing function and is chosen to possess the property of having low-side lobes. A commonly used function is the triangle shown in Figure 6.

$$A_1(x) = 1 - x/d \qquad \text{for } -D < x < D$$

$$A(x) = 0 \qquad \text{for } x < -D \text{ and } x > D$$

The Fourier transform of this function is of the form

$$\mu(\epsilon - x) = D \left(\sin \frac{n\nu D}{n\nu D}\right)^2$$

It has no negative ripples and much smaller side lobes than the sinc function obtained for square pulse apodization.

Another useful apodizing function is of the form

$$A_2(x) = [1 - x^2/D^2]^2 \qquad \text{for } -D < x < D$$

$$= 0 \qquad \text{for } x < -D \text{ and } x > D$$

APODIZING FUNCTIONS AND THEIR CORRESPONDING SCANNING FUNCTIONS

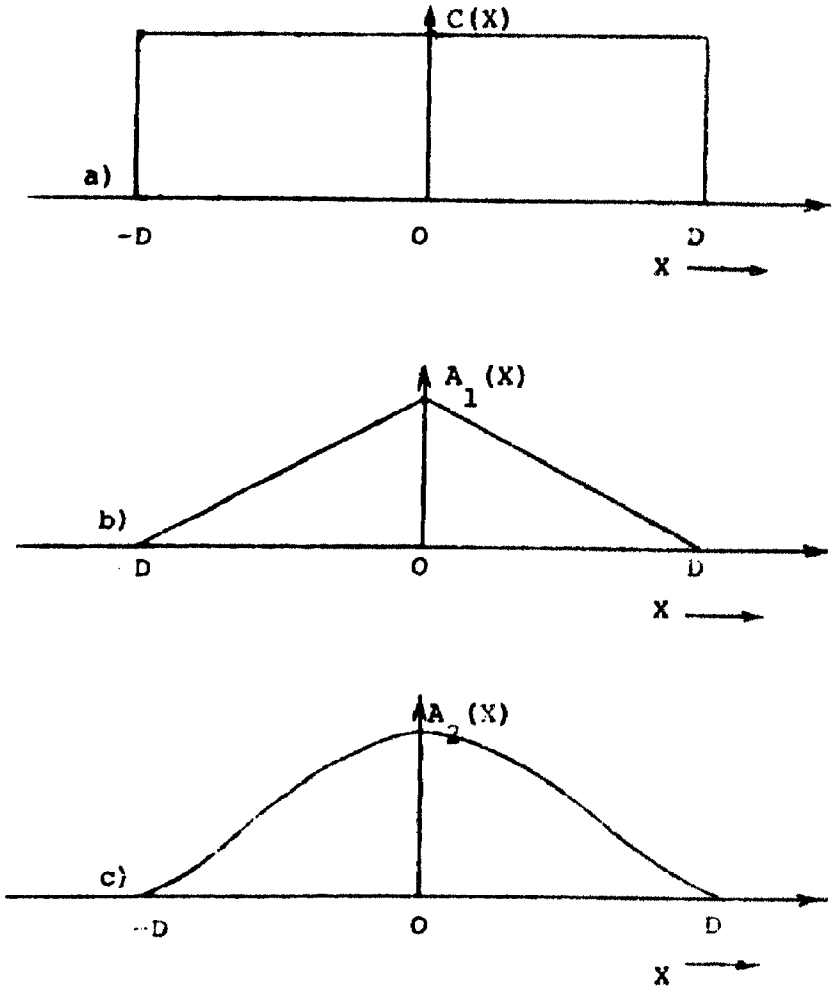

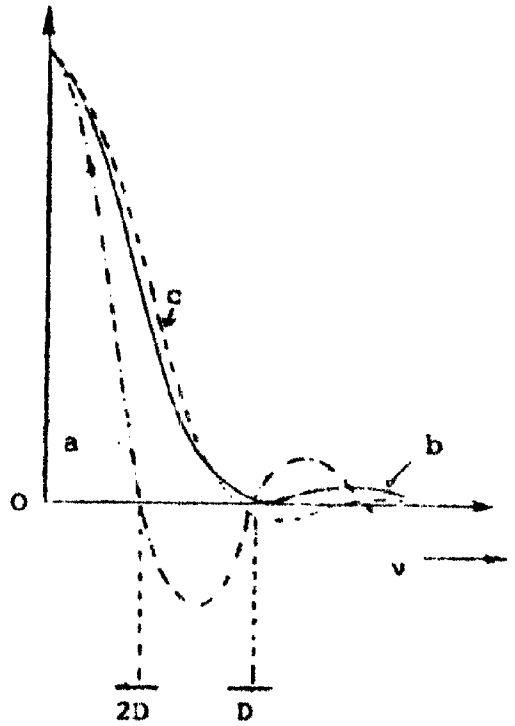

Figure 6

For this case, the Fourier transform is of the form [23]

$$\mu(\epsilon - x) = (2\pi D\nu)^{-5/2} \; J_{5/2}(2\pi D\nu)$$

Figure 6 shows this function and the effective scanning function.

Resolving power

The terms "spectral element" and "resolution" have been used. Let us now examine their meaning. The resolution or resolving power of a system is a measure of how close two adjacent lines or sources can be before they are no longer sufficiently separated so as to be identified. Assume a pair of lines of arbitrary intensity and separated by $\Delta\nu$ cm^{-1}. The lines will be considered to be resolved if the difference between the intensity of the weaker line and the intensity where it overlaps the stronger line is at least twenty per cent of the intensity of the weaker line. For two lines which can be considered as delta functions, the overlap is produced by the scanning function of a spectrometer, or the scanning function due to apodization for the case of an interferometer. For triangular apodization, this is equivalent to the Rayleigh criterion. This means that the scanning function for a line at ν cm^{-1} has a maximum while the scanning functions for lines at $\nu \pm \Delta\nu$ cm^{-1} have zeros at ν cm^{-1}, Figure 7.

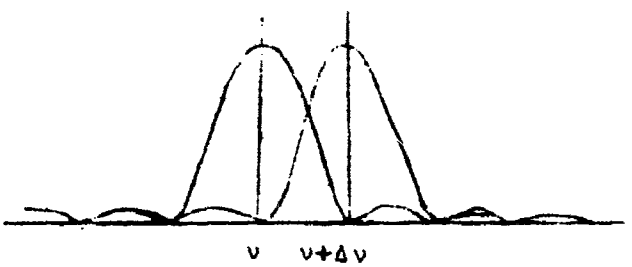

Figure 7

For a triangular apodizing function of length D, its Fourier transform (the scanning function) is $\text{sinc}^2(\pi\nu D)$. Two adjacent lines scanned by this function overlap at a point midway between them, where the value is approximately 0.8.

Figure 6 shows several apodizing functions and their corresponding scanning functions. The first zero of the scanning function for rectangular truncation (no apodization) occurs at half the frequency of the first zero of the scanning function for triangular apodization. That is, the resolving power is increased by a factor of two when no apodization is used. The spectrum in this case will have spurious oscillations due to the oscillations of the scanning function. The Fourier transform of a function gets narrower as the function gets wider, and one can see immediately that the limit of resolution varies inversely with the maximum path difference. The exact variation is determined by the particular case. The limit of resolution will be called a spectral element. That is, it is the smallest value of $\Delta\nu$ by which two lines can differ and still be resolved.

REAL-TIME FOURIER COSINE TRANSFORM SYNTHESIZER

Principles of Operation

The interferogram is represented by

$$F(x) = \int_{\nu_m}^{\nu_M} E(\nu) \cos 2\pi\nu x \, d\nu \qquad (41)$$

where ν_m and ν_M are the minimum and maximum wavenumbers in the spectral distribution. It is evident from equation (41) and from the discussion in the preceding chapter, that the interferometer has synthesized the interferogram by a superposition of trigonometric functions with amplitudes determined by the spectral distribution. Each point on the interferogram may be represented by a finite polynomial, the number of terms being limited by the upper frequency limit of the radiation. This polynomial is a partial sum of a Fourier series [24].

The spectral distribution is related to the interferogram by

$$E(\nu) = \int_{-\infty}^{\infty} F(x) \cos 2\pi\nu x dx \qquad (42)$$

It is reasonable then to obtain the spectral distribution by the inverse process; i.e., by a superposition of trigonometric functions with amplitudes determined by the interferogram. A synthesis of the spectral function is thus obtained. This synthesis is the Fourier series approximation to the spectrum.

The interferogram function F(x) is sampled at intervals determined by the sampling theorem. F(x) may then be expressed as F'(x), where

$$F'(x) = \sum_{n=-\infty}^{\infty} F(x_{nh})\, \Delta(x-nh) \qquad (43)$$

The expression $\sum_{n=-\infty}^{\infty} \Delta(x-nh)$ is a Dirac comb of periodicity h. It has the property that it picks up values of F(x) at equal intervals h of x, where h is the spacing between sample points. Its Fourier transform is also a Dirac comb, but of periodicity 1/h. Further, $F(x_{nh})$ is the value of F(x) at sample point nh, see Figure 8 .

Equation (42) may now be written as a summation instead of an integral.

$$E(\nu) = \sum_{n=-\infty}^{\infty} F(x_{nh}) \cos 2\pi\nu x_{nh} \qquad (44)$$

Since the interferogram has been sampled, the synthesized spectrum is the convolution of the true spectrum with the Dirac comb; thus, the synthesized spectrum repeats at intervals of 1/h.

Equation (44) requires an infinite number of samples, which is clearly a practical impossibility. Path differences are governed by the physical limitations of the instrument and only a finite number of samples are obtained. This limits the resolution of the instrument, but it may still be very large because the path difference can be made much larger than

$$\sum_{n=-\infty}^{\infty} \Delta(n - nh) = III(x)$$

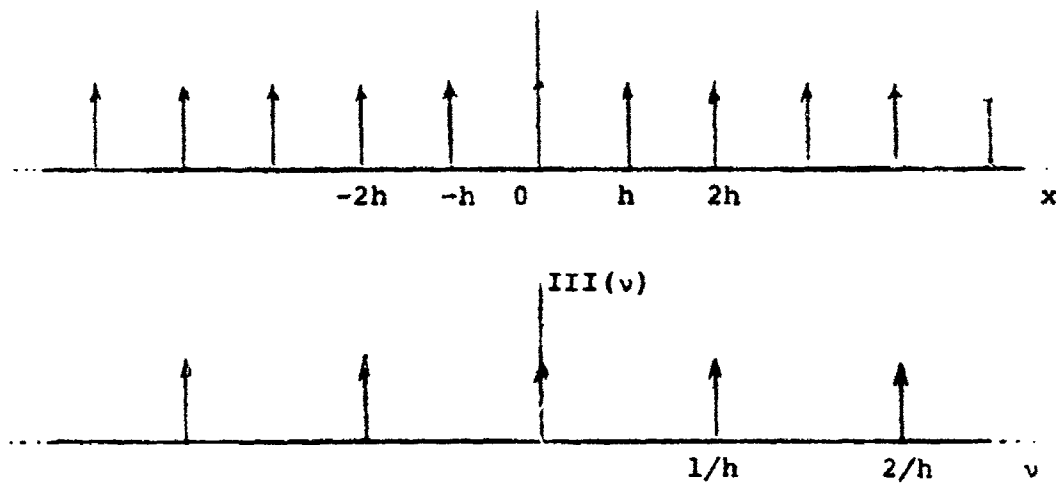

Figure 8

the longest wavelength. The interferogram is an even function so only those sample points from n = 0 to N need be used, where N is the last sample point and is governed by the maximum path difference. With these stipulations, equation (44) may be written

$$E(\nu) = \sum_{n=0}^{N} F(x_{nh}) \cos 2\pi\nu x_{nh} \tag{45}$$

The relationship between the functions $E(\nu)$ and $\varphi(\omega)$ and between $F(x)$ and $G(t)$ have been discussed previously. Equation (45) may be rewritten in terms of these parameters as

$$\varphi(\omega) = \sum_{n=0}^{N} G(t_{nh}) \cos\omega_n t \tag{46}$$

where $\varphi(\omega)$ is the spectrum of the detector response, and $G(t_{nh})$ is the amplitude of the detector response at the sample point nh. The angular frequency of the cosine functions is given by

$$\omega_n = 2\pi f_n = 2\pi \left(\frac{n}{2\Delta\nu}\right) \tag{47}$$

where $\Delta\nu$ is the bandwidth of the incident radiation and the running variable t is equivalent to the parameter ν. Each sample point of the interferogram is used to generate a cosine function with an amplitude determined by the sample value and a frequency determined by the path difference.

Equation (46) forms the basis of the real-time Fourier synthesizer. The sample value $G(t_{nh})$ is held while it is multiplied by a cosine function of the proper frequency. Each succeeding product is put into the memory and is added to the preceding data. A summation of $G(t_{nh})\cos\omega_n t$ terms is thus obtained.

A photographic summation technique was investigated. It has some severe disadvantages which limit its usefulness. A discussion of the technique and the results of the experiments are given in the Appendix. As a result of this investigation, the technique was abandoned in favor of a fully electronic system.

A photograph of the real-time Fourier transform synthesizer is shown in Figure 9 and an elementary block diagram is presented in Figure 10. Four signals are required to synthesize the spectral distribution. Three of these are inputs to the transform synthesizer. They are: the output of the lamellar grating, the reference signal from the Michelson, and the initiating pulse from the zero path difference detector. The cosine functions are generated within the instrument.

The relationship between the lamellar grating and the Michelson is shown schematically in Figure 33, while Figure 11 is a photograph of the two interferometers and the driving system. The movable facets of the lamellar grating are designated by the letter "D" while the fixed facets are designated "E." Mirror M_1, of the Michelson, is mounted on the

REAL TIME FOURIER SYNTHESIZER

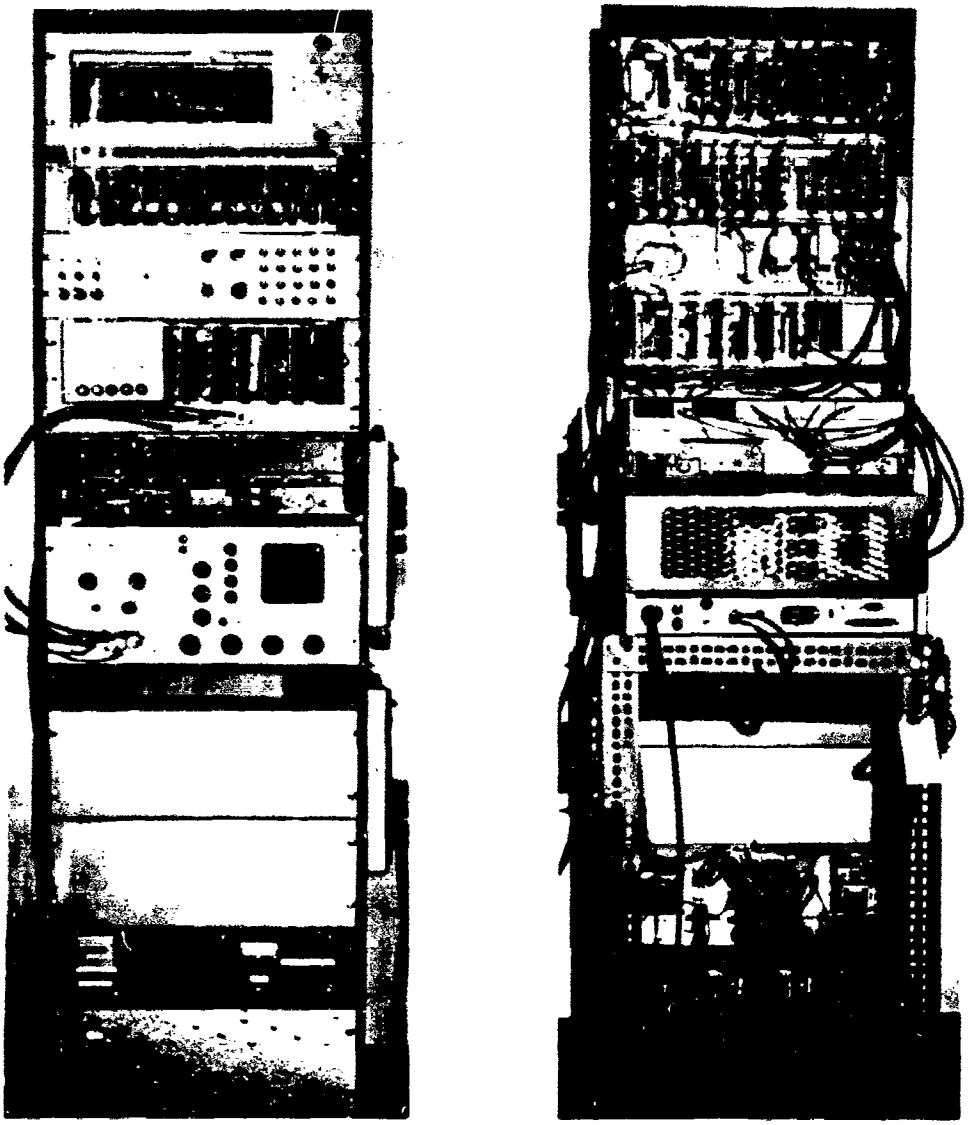

FRONT REAR

Figure 9

REAL TIME FOURIER SYNTHESIZER
BASIC BLOCK DIAGRAM

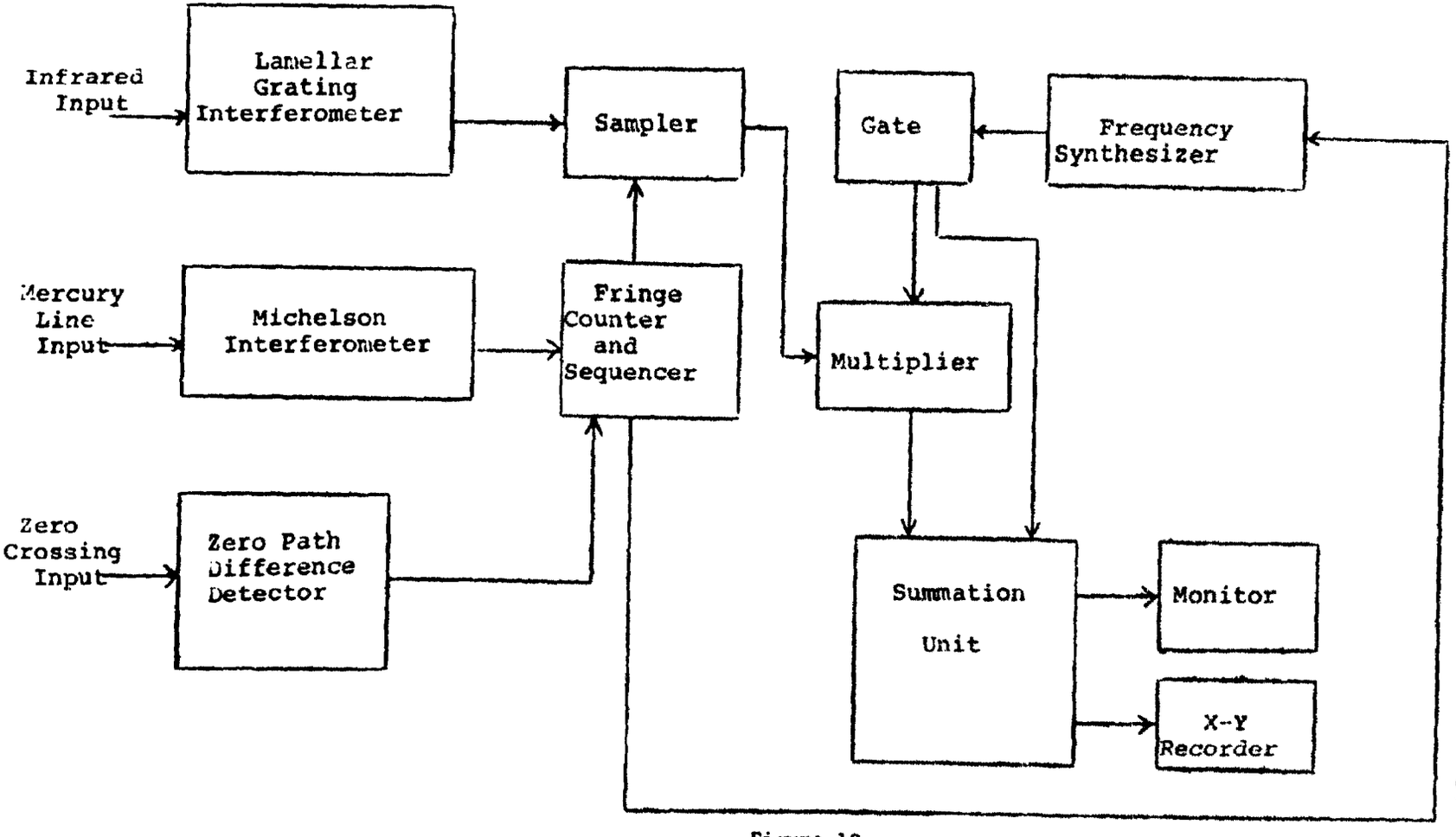

Figure 10

LAMELLAR GRATING AND MICHELSON INTERFEROMETERS

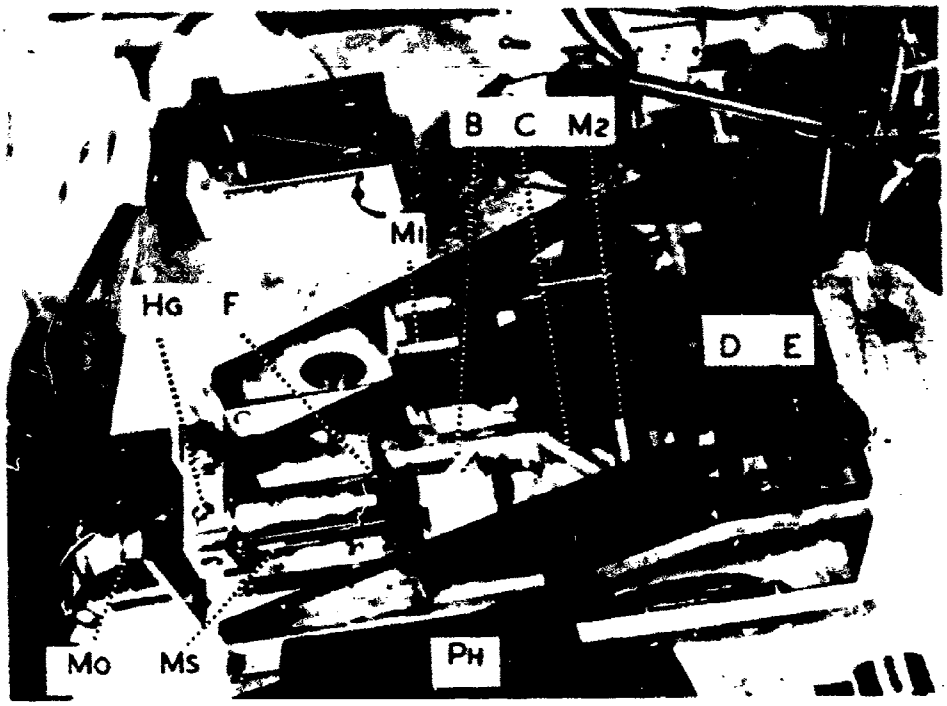

D = MOVABLE FACETS
E = FIXED FACETS
M1 = FIXED MIRROR
M2 = MOVABLE MIRROR
B = BEAMSPLITTER
C = COMPENSATOR

Hg = MERCURY LAMP
F = 5461Å FILTER
Mo = MOTOR
Ms = MICROMETER SCREW
PH = PHOTOMULTIPLIER

Figure 11

baseplate while M_2 is mounted on the slide which carries the movable facets. Items "B" and "C" are the beamsplitter and compensator, respectively. A mercury lamp and filter are the source of a 5461 Å radiation which is detected by a photomultiplier. A 1/10 rpm synchronous motor and micrometer screw are used to drive the interferometers.

The output of the photomultiplier varies sinusoidally as a function of mirror displacement. Each cycle indicates a change in displacement of $\lambda/2$, or 0.27305 microns. This signal is used to measure displacements, and its accuracy is independent of any imperfections in the driving system. This reference signal is used to control the sampling intervals and the frequency of the cosine functions.

In order to synthesize the Fourier cosine transform of the interferogram, it is necessary to know when the path difference between the two beams is zero. This information is supplied by the zero path difference detector. A novel approach is used to generate a pulse when the groove depth of the lamellar grating passes through zero. The approach and the results are explained more fully in a section devoted to this particular circuit. The pulse initiates the automatic operation of the transform synthesizer.

There are four main signal paths in the instrument. Two of these initially end at an open relay while the others are complete but inactive. The zero path difference detector generates a pulse which closes the relay.

This completes the paths taken by the outputs of the two interferometers and initiates the sampling of the interferogram.

With reference to Figure 10, the first path begins at the output of the lamellar grating, extends through the sample and hold circuit and ends in the multiplier. The sampler takes a sample of the interferometer signal and holds it during the interval between successive samples. During this period, the sample value is multiplied with the output of the second path in an analog multiplier.

The proper cosine functions are generated in the second signal path. This begins at the frequency synthesizer, extends through the gate circuit and ends in the multiplier. The frequency synthesizer generates a sinusoidal signal of known frequency. It is remotely programmed and automatically changes frequency according to a pre-set program. The gate opens at the proper instant and cosine functions enter the multiplier.

The first two signal paths are joined in the analog multiplier to form the third. The sample values $G(t_{nh})$ are multiplied by the proper cosine functions to produce a series of terms of the form $G(t_{nh}) \cos\omega_n t$. These terms follow the third path to the summation unit.

Figure 12 is a diagram which shows the waveforms in these first three signal paths. The input and output of the sample and hold circuit are shown. The two inputs to the multiplier and the output of it are also presented. Figure 13 shows the result of the summation of these first

WAVE FORM DIAGRAM

Interferogram

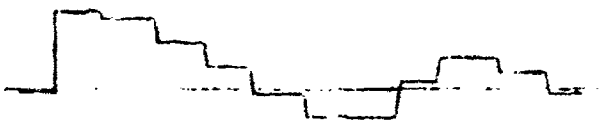

Output of the Sample and Hold Circuit

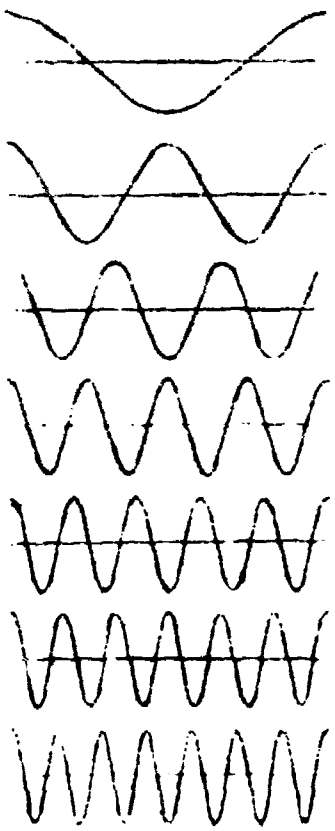

First Seven Frequencies Entering the Multiplier

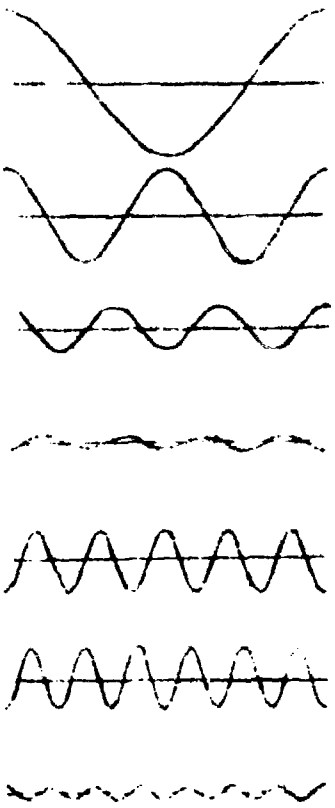

First Seven Frequencies Entering the Summation Unit

Figure 12

SUMMATION OF THE FIRST SEVEN FREQUENCIES

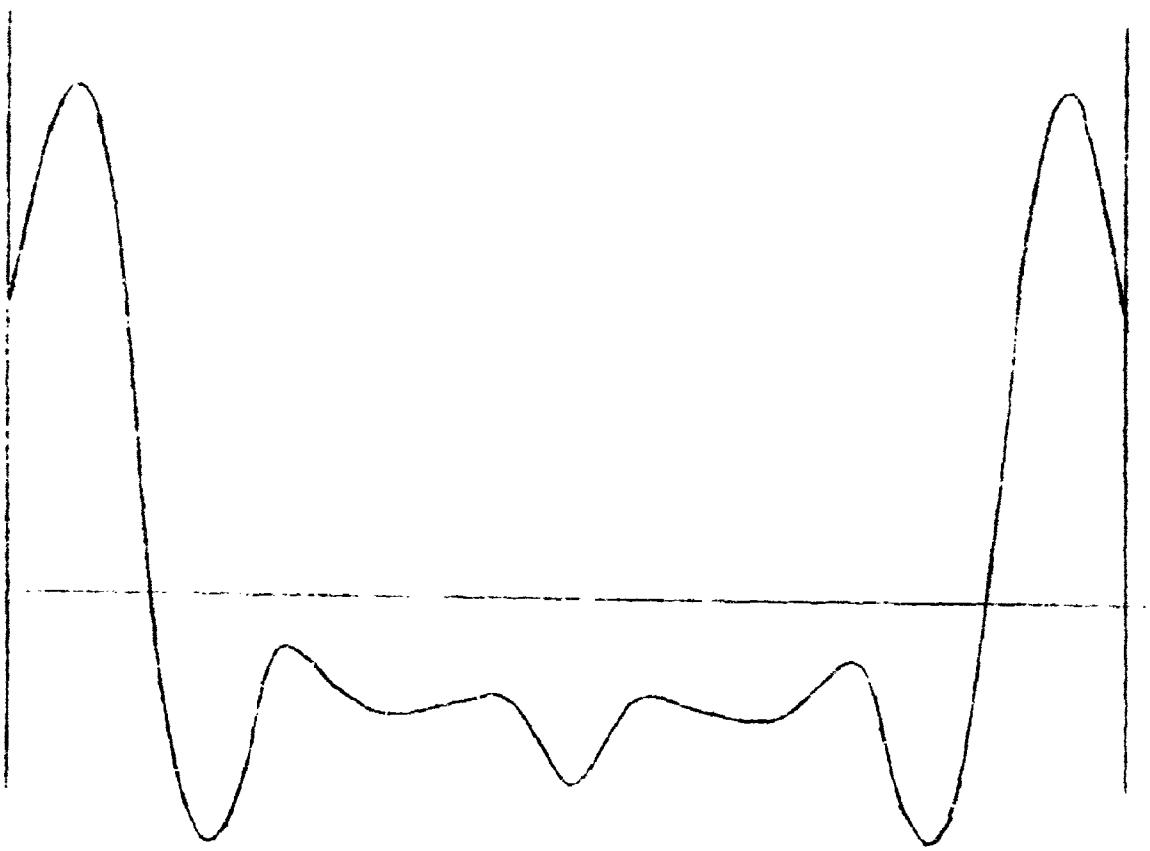

Figure 13

few terms. The synthesized spectrum, represented by the summation, is seen to repeat, as would be expected from a consideration of the sampling process.

The fourth signal path in Figure 10 is the one taken by the reference signal. It extends from the detector of the Michelson interferometer to the fringe counter. At this point, it splits into two branches. One branch goes to the sampler where the signal controls the sampling interval. The second branch goes to the sequencer where the signal controls the frequency of the cosine functions.

The summation expressed by equation (46) is performed in a digital averager or summation unit. Signals of the form $G(t_{nh})\cos\omega_n t$ are digitized at 1024 ordinates, and each of these values is stored in an address of the memory. When the mth sample point is taken from the interferogram, the term $G(t_{mh})\cos\omega_m t$ is produced by the multiplier. This is digitized and added to

$$\sum_{n=1}^{n=m-1} G(t_{nh})\cos\omega_n t$$

which is already stored in the memory. The previous data are read out on each address, modified by the new data, and the result is rewritten into the address. When this has been done for all the addresses, the summation

$$\sum_{n=1}^{n=m} G(t_{nh}) \cos\omega_n t$$

is stored in the memory. Corresponding ordinates of the successive signals are stored in the same address. One additional signal per second may be added to the memory. An external trigger initiates the digitization-storage cycle, and an external signal advances the memory from one address to the next.

The data in the memory are monitored on an oscilloscope and may be plotted on an X-Y recorder as soon as the interferogram is obtained. As additional terms are added to the synthesized spectrum, greater detail appears and the resolution increases. Figures 37 and 38 show the effect of additional terms on the synthesized spectra.

The synthesized spectra repeat at intervals of 1/h. The external advance is adjusted to limit the repeating spectra to the last 24 addresses of the memory. The non-repeating spectra are contained in the first 1000 address points.

Description of the Individual Circuits

The foregoing section discussed the operation of the complete instrument while this section is devoted to a detailed description of some of the more important components and circuits. The first of these is the zero path difference detector which initiates the automatic operation of the system.

Zero path difference detector

It has been shown that the spectrum may be obtained by synthesizing the cosine transform of the interferogram. This requires an accurate knowledge of the point $x = 0$ or $t = 0$, depending upon which function, $F(x)$ or $G(t)$, is being transformed. Errors in the location of this point perturb the shape of the scanning function, which becomes asymmetrical and has important negative minima. Part of a typical interferogram and the effect of errors in the determination of the zero point are shown in Figure 14. Figure 15 shows the effect of a small error on the shape of the scanning function. The term ϵ/λ is a measure of the phase error where ϵ is the error and λ is the wavelength of the radiation [25]. If the error is small with respect to the shortest wavelength, the scanning function changes only slightly as a function of wavelength.

When broad spectra are studied, the interferogram in the region of zero path difference contains only a few fringes of rapidly decreasing

EFFECT OF AN ERROR IN THE CHOICE OF THE ZERO POINT ON THE INTERFEROGRAM
(a) $\epsilon = 0$ (b) $\epsilon > 0$ (c) $\epsilon < 0$

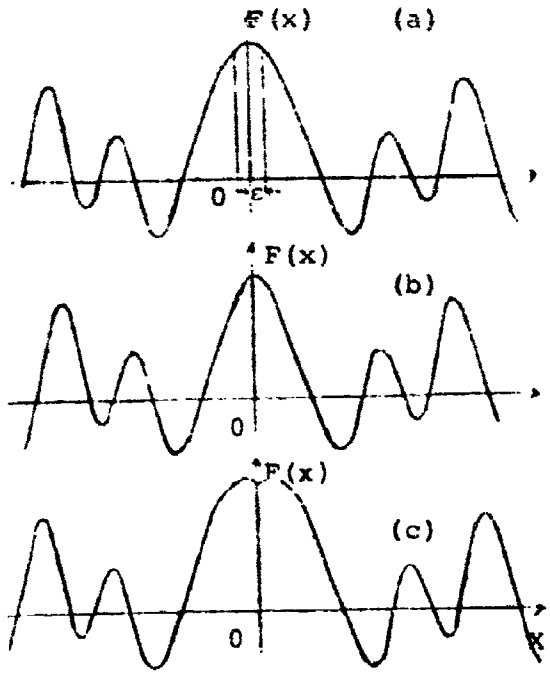

Figure 14

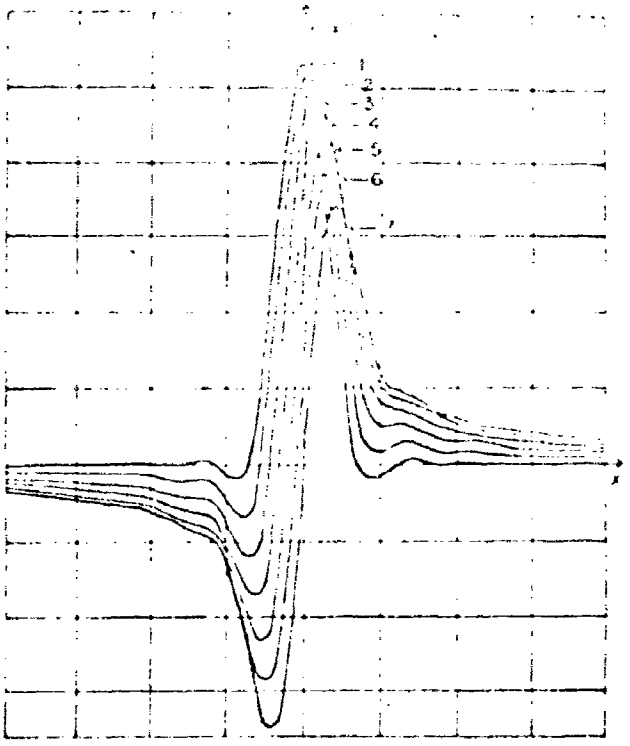

DIFFERENT FORMS OF THE SCANNING FUNCTION FOR DIFFERENT VALUES OF THE PHASE DISPLACEMENT: CURVE 1, $\epsilon/\lambda = 0$;

CURVE 2, $\epsilon/\lambda = 0.042$; CURVE 3, $\epsilon/\lambda = 0.084$;

CURVE 4, $\epsilon/\lambda = 0.126$; CURVE 5, $\epsilon/\lambda = 0.168$;

CURVE 6, $\epsilon/\lambda = 0.210$; CURVE 7, $\epsilon/\lambda = 0.250$.

Figure 15

intensity. The location of the point of zero path difference can be determined with precision. An electronic circuit could select this point by properly operating upon the interferogram signal. However, for narrow band spectra, the region near zero path difference has many fringes of nearly constant intensity. In this case, an uncertainty of several fringes may exist and an electronic circuit is not able to select the proper point. Examples of typical interferograms are presented in Figure 16 .

The zero path difference detector consists of an additional optical system and the associated electronics. The optical system is clamped to the sides of the lamellar grating. A lamp and collimator produce a narrow beam of light which strikes the grating at near grazing incidence and covers a narrow section of all the facets. Stops isolate the zeroth order interference pattern, and a lens focuses it onto the detector. The optical system and the mounting details are shown in Figure 34 . In the figure, K indicates the light source and collimator while L is the detector.

Figure 17 shows the configuration of the lamellar grating for the general case and for the case of zero path difference. As a result of constructive interference between rays 1 and 2, the output of the detector is a maximum when the groove depth is zero. The grating then behaves like a plane mirror. The angle of incidence of the light beam is critical and must be carefully adjusted to obtain the response shown in Figure 18 .

INTERFEROGRAMS OBTAINED FOR NARROW AND BROAD BAND SOURCES

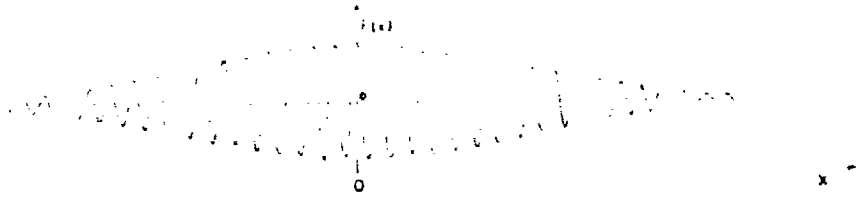

NARROW BAND SOURCE

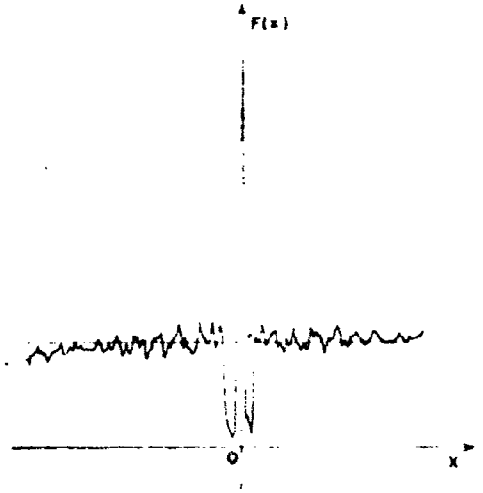

BROAD BAND SOURCE

Figure 16

OPTICAL SYSTEM FOR THE ZERO PATH

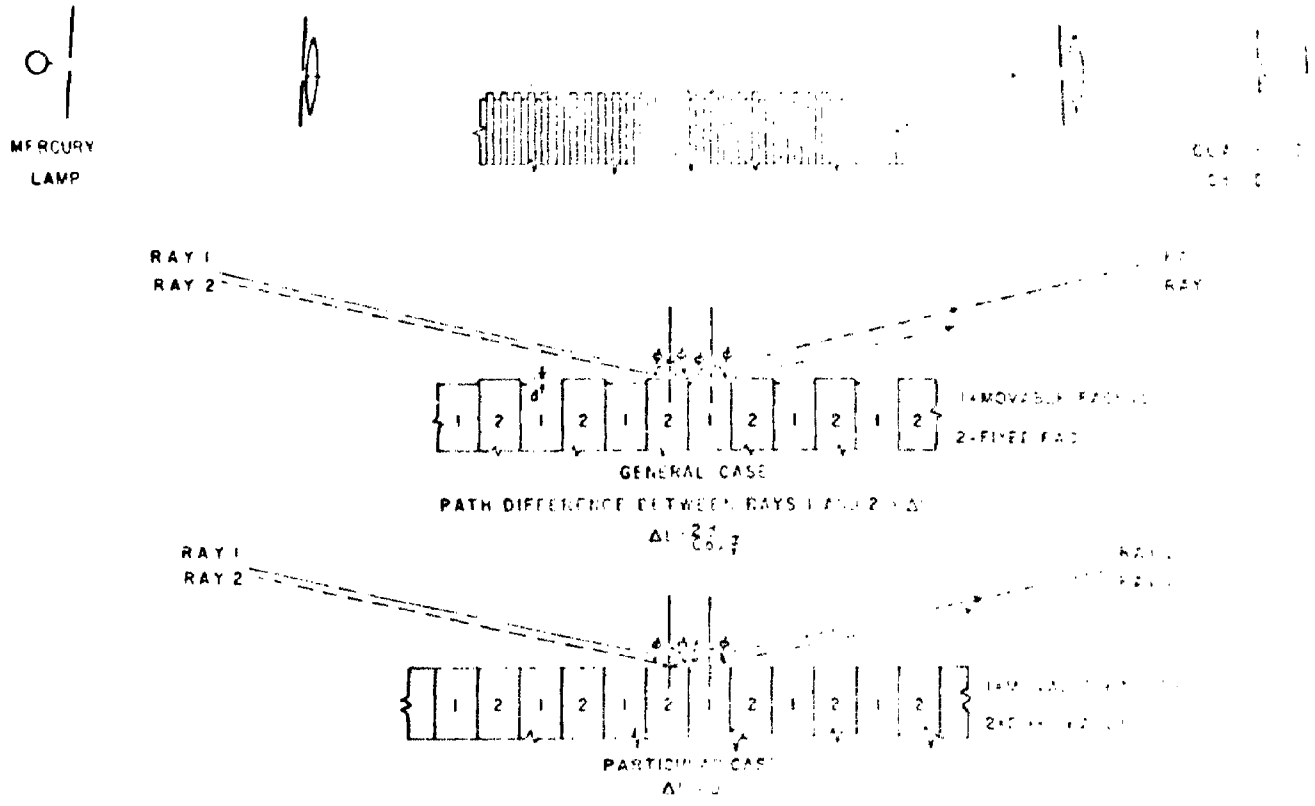

Figure 17

WAVEFORMS FOR THE ZERO PATH DETECTOR

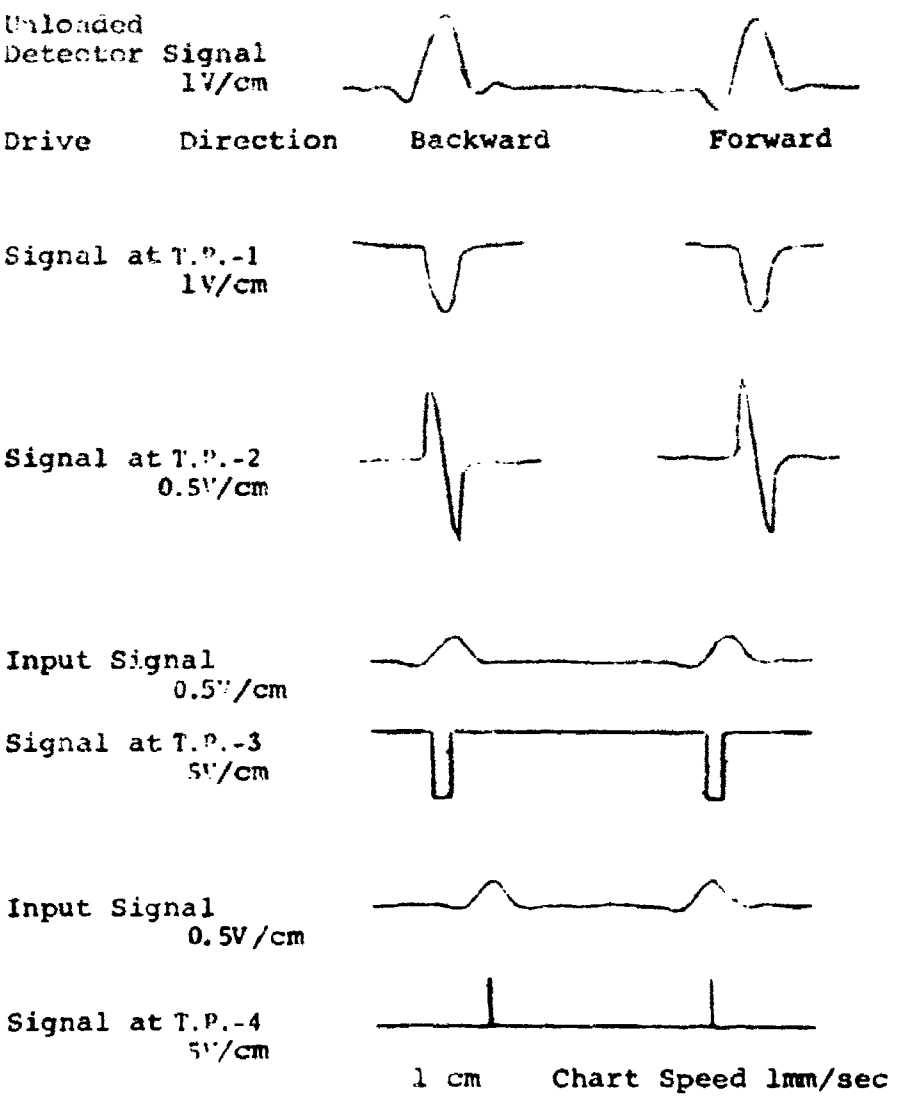

Figure 18

This figure shows the detector response in the region of zero path difference as the movable facets are driven in both directions.

A block diagram and schematic of the electronic system is shown in Figure 19. The triangle with an "A" is used to designate an operational amplifier, and this notation will be used whenever operational amplifiers are employed.

Input, output and intermediate waveforms are shown in Figure 18. The input is amplified and clipped to isolate the peak which is then differentiated with the resulting signal passing through zero when the input signal reaches the peak. An amplifier and clipper circuit are used to shape the differentiated input signal into a rectangular pulse. The trailing edge of this pulse corresponds, in time, to the peak of the detector response. A narrow voltage spike is generated by differentiating the rectangular pulse. The spike triggers a circuit which closes the relay. This completes the signal paths used by the outputs of the two interferometers. The spike may be advanced or retarded slightly, with respect to the peak of the detector signal. This permits a fine adjustment of the detected point of zero path difference. The detected point of zero path difference is compared to the actual value in Figure 20. The coincidence of the actual and detected points of zero path difference is repeatable if the grating is driven in one direction. The two points do not coincide when the grating is driven in the opposite direction. This is not a

BLOCK DIAGRAM FOR THE ZERO PATH DETECTOR

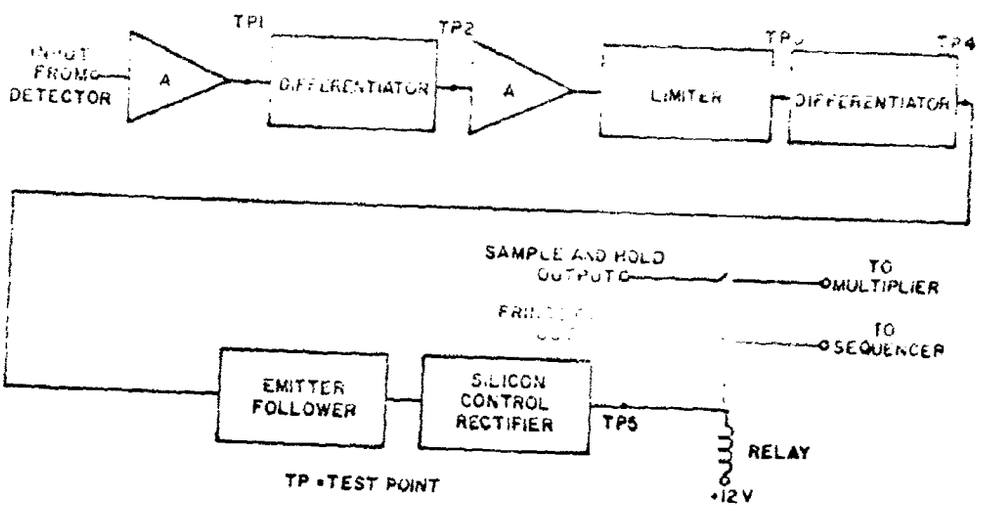

ZERO PATH DETECTOR

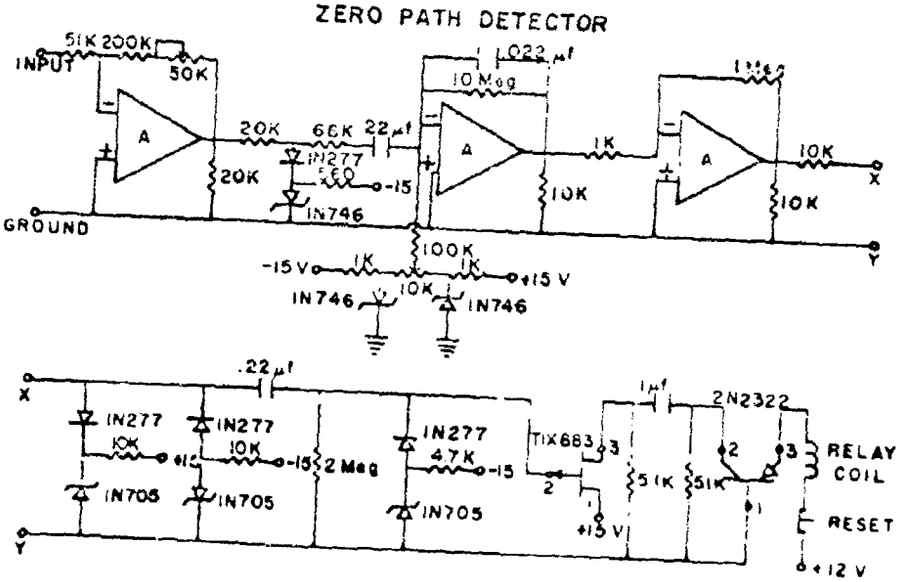

Figure 19

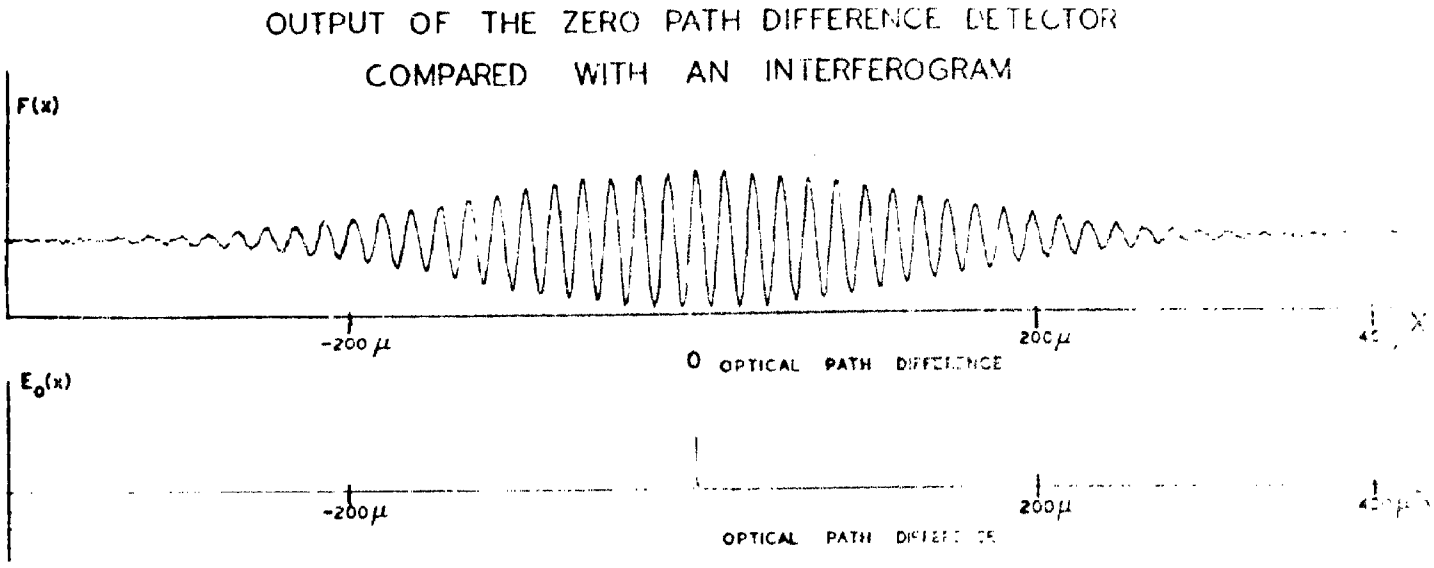
OUTPUT OF THE ZERO PATH DIFFERENCE DETECTOR
COMPARED WITH AN INTERFEROGRAM
F(x)
-200 μ
0 OPTICAL PATH DIFFERENCE
200 μ
E₀(x)
-200μ
200μ

Figure 20

limitation to the system performance since it is only necessary to take data from x = 0 to x = D, where D is the maximum path difference.

Input amplifier and sample and hold circuit

The interferogram function was defined in equation (16) as

$$F(x) = E(x) - \tfrac{1}{2}E(0) = \int_{-\infty}^{\infty} E(\nu) \cos 2\pi\nu x d\nu \qquad (48)$$

The expression $\frac{1}{2}E(0)$ is the asymptotic value approached by E(x) as the path difference becomes large. It is a dc value which must be removed or an error will be produced in the synthesized spectrum. A network is connected to the input amplifier to cancel this dc value. The cancellation is done experimentally by adjusting the dc level of the input to the sample and hold circuit to zero. A standard analog sample and hold circuit is used in the system. This supplies the dc input to the multiplier, Figure 21 .

Multiplier

The system uses a quarter square analog multiplier. This type was chosen because it exhibits superior phase and frequency response in the region of interest, <2500 cps. It uses biased diode squaring networks and these are the cause of moderate waveform distortion when the dc input becomes less than 1 volt. Compensation is accomplished

BLOCK DIAGRAM
REAL TIME FOURIER SYNTHESIZER

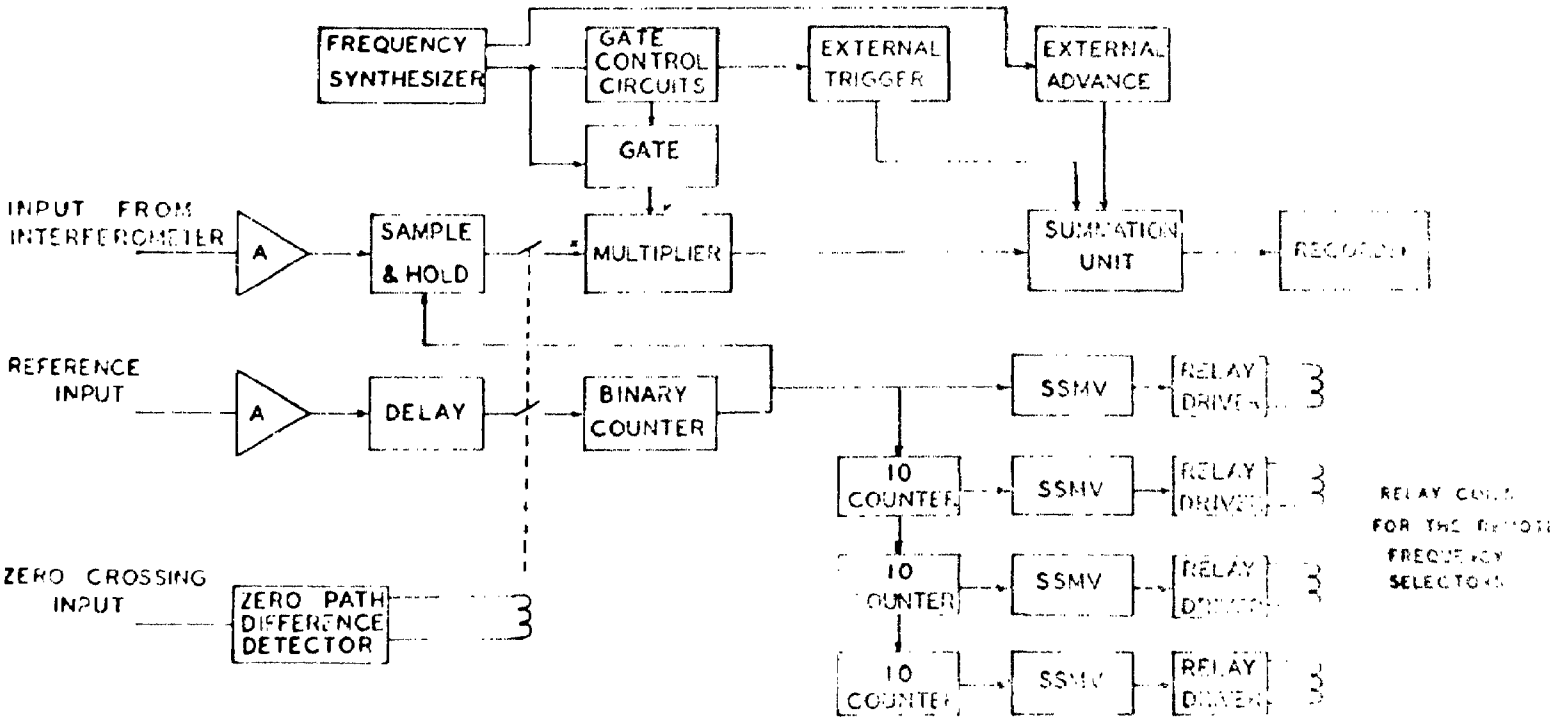

Figure 21

by means of a level detector and a pair of amplifiers. One of these increases the dc level by a factor of 10 while the other alternates the output of the multiplier by the same factor. The multiplier then operates over a more linear portion of its characteristic. An absolute value circuit and level detector switches these amplifiers in and out of the signal path as required. The multiplier and its compensation system are shown in the complete system diagram, Figure 27.

Frequency synthesizer and gate

The frequency synthesizer, gate, and gate control circuitry are used to generate cosine functions of the proper frequency. The frequency synthesizer is a standard unit with provision for remotely controlling the frequency. The frequencies are synthesized by the combination of various frequencies which are derived from a crystal controlled master oscillator. Thus, the accuracy of these frequencies is precisely controlled. The proper frequency is selected by a switching network consisting of four 10-contact rotary step switches. These are driven by the sequencer. Frequencies may be selected in 1 cycle steps from 1 cps to 9999 cps. The frequency response of the synthesizer is flat over the range of interest, < 2.5 kc, and varies only 0.5% from 0 to 10 kc. Harmonics are down at least 40 db.

A standard type of gate circuit is used. It is operated by a pulse generator which is triggered by the output of the 90° detector.

90-degree detector

Cosine functions are obtained from the frequency synthesizer by means of a 90-degree detector and a gate circuit. The 90° detector opens the gate at the peak of the sinusoidal signals. This permits a cosine function to pass through the gate. The gate automatically closes after a one-second time delay. The 90-degree detector should meet the following specifications:

1. It should be able to detect the 90° point of a sine wave while operating over a frequency range of more than 3 decades, from 1 cps to 2500 cps.

2. It should not require tuning or readjustment as the frequency is varied.

3. The output of the frequency synthesizer should be the only input signal required.

Many standard techniques are available for triggering circuits at perpendicular points on a wave form. These generally use a level detector and some phase shifting scheme. None of these will operate satisfactorily for this particular application. Level detectors themselves are unstable in the region of the peak of a sine wave. Phase shifters used in conjunction with level detectors do not have the desired bandwidth. Phase splitters, such as are used in single sideband equipment, have neither the required bandwidth nor the proper amplitude response. The

heterodyne and phase shifting technique has also proven unsatisfactory for this application. Shifting phase by differentiation or integration is not practical when the bandwidth extends over three decades.

The technique that was developed is to utilize the sinusoidal output of the frequency synthesizer and shape it into a series of very narrow pulses. It is important to maintain coincidence between the peak of the input and the peak of the pulse. The pulse shaping is done with non-linear circuits. Each stage generates a narrower pulse. The last stage of the shaping circuitry drives a level detector. Its output is now stable in the region of the peak of the input, since it is operating on a narrow pulse which has a rapid rise and fall. The wave-shaping circuits are the key to the successful operation of the 90-degree detector.

A diagram of the shaping circuit is presented in Figure 22. A schematic of two of the shaping networks and their amplifiers is shown in Figure 23. The output of the frequency synthesizer is amplified, and the resulting signal goes to the gate circuit and also to the first stage of the shaping circuit. This is a non-linear, biased-diode network. The component values have been chosen to produce an approximately quartic characteristic. Thus, the output current is related to the input voltage by

$$i_o \approx k E_{in}^4$$

SYNTHESIZER AMPLIFIER AND SHAPING NETWORK

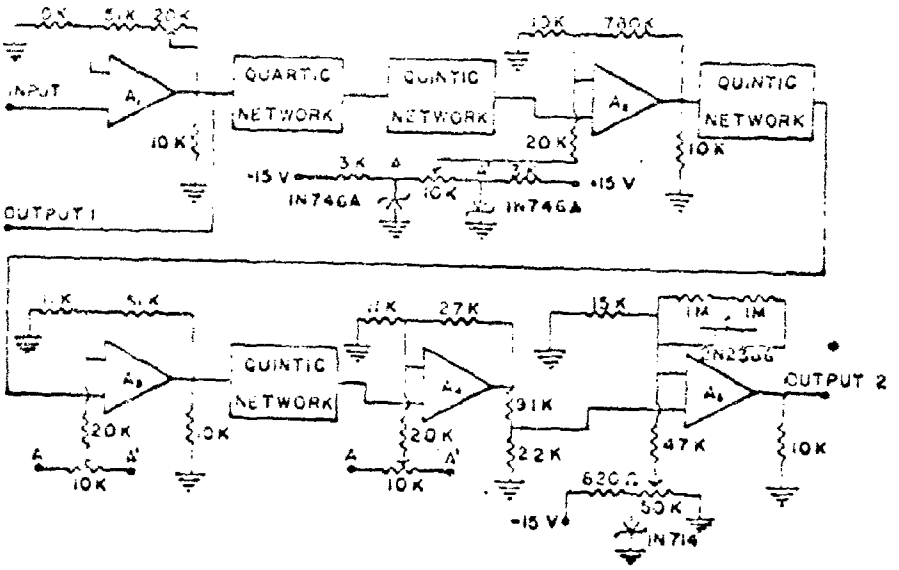

Figure 22

SHAPING NETWORK

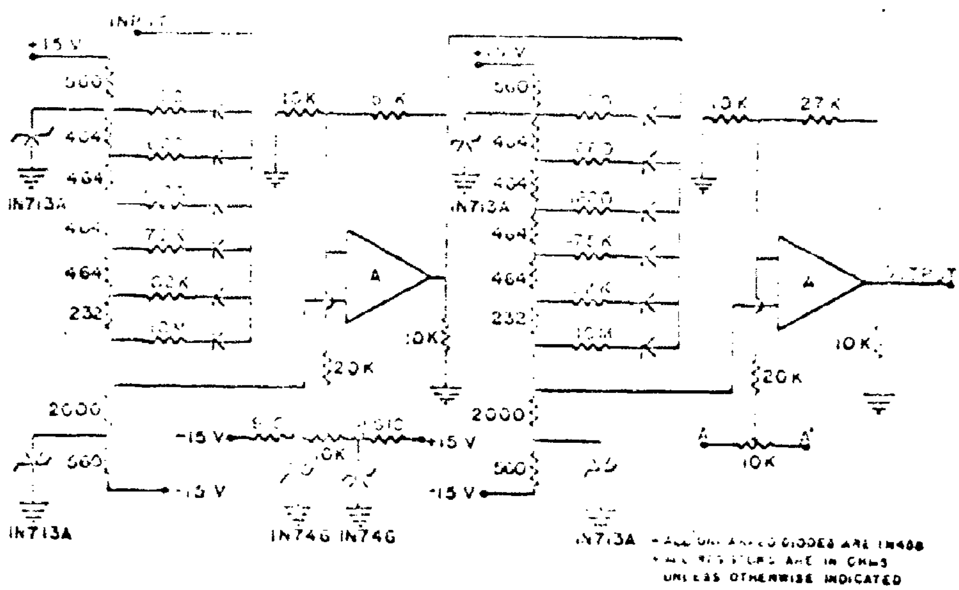

Figure 23

where k is a constant chosen to give the components reasonable values. Six line segments are used in the approximation.

The output of the first shaping network drives the second one directly. This has an approximate quintic characteristic, $i_o \approx k E_{in}^5$, as have all the remaining networks.

With reference to Figure 23, the output current of the biased diode network flows through the 2 K resistor and develops a voltage which is then amplified. The amplifier also serves two additional functions. It is a buffer between the networks to prevent loading effects, and it permits adjustment of the dc level. The ability to adjust the dc level is important to the proper operation of the circuit, and each stage is provided with a network by which a dc voltage may be added to or subtracted from the signal.

The final shaping circuit is a non-linear amplifier. A field effect transistor is used in the feedback loop of an operational amplifier to provide the effect of a voltage variable resistor. The connection of the field effect transistor is shown in Figure 22. In this case, the effective resistance of the transistor increases as the output voltage increases. Since the transfer function of the amplifier is

$$\frac{e_o}{e_{in}} = \left(1 + \frac{R_{feedback}}{R_{input}}\right)$$

the gain increases nonlinearly. The net effect of this circuit is to produce very narrow pulses which occur at the peaks of the original input waveform. The output of the nonlinear amplifier drives a level detector, which is now stable in the region of the peak of the input sinusoid, since it operates on a narrow pulse.

Figure 24 shows the waveforms obtained at various points in the circuit. It is observed that each succeeding stage generates a narrower pulse. The output of the level detector is shown for two values of the sweep speed. In this case, the level detector is triggered 1.44° before the 90° point is reached. The original circuit design did not include the nonlinear amplifier and, in this case, the stable triggering point was 6° before the peak. Since the pulse is very narrow but has a finite width, the triggering point will be slightly ahead of the 90° point unless phase shift elsewhere in the circuitry causes a delay.

The accuracy of the circuit is dependent upon the initial adjustment, the amplitude stability of the various signals, phase shift, and power supply fluctuations. Gain controls and a dc balancing network are provided for each stage. The initial adjustment of these controls is critical because of the nonlinear circuits, high amplification, and the saturation characteristics of the amplifiers. Once the circuit has been properly adjusted, no further adjustments are required as the frequency changes.

Waveforms for the 90 Degree Detector

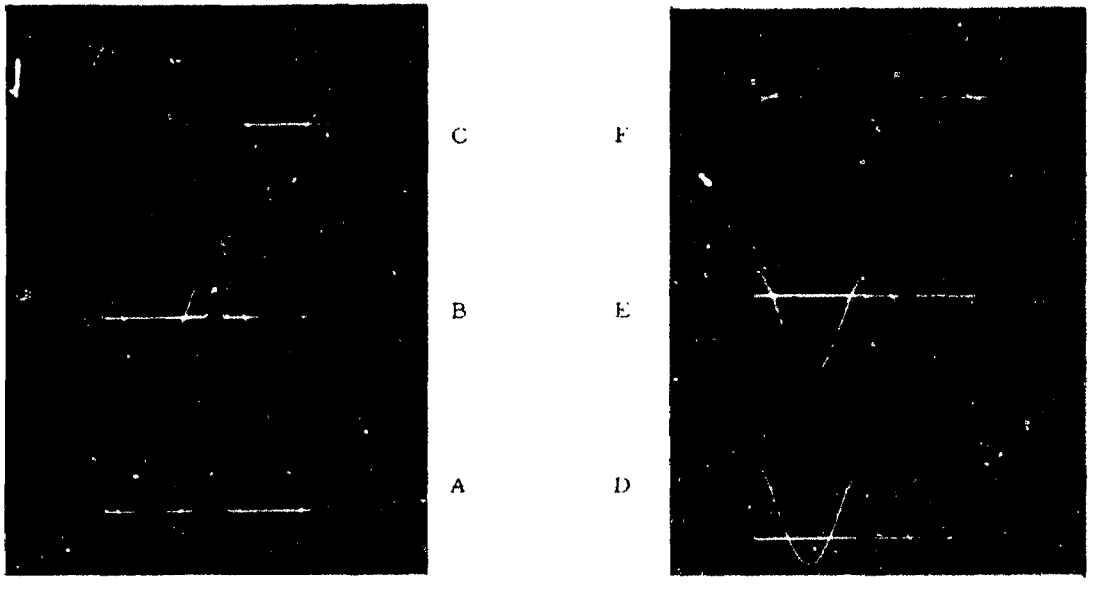

Sine Wave = Output of Amplifier A_1

A. Output of Amplifier A_2

B. Output of Amplifier A_3

C. Output of Amplifier A_4

D. Output of Amplifier A_5

E. Output of the Level Detector

F. Output of the Level Detector
Horizontal Sensitivity: 0.4 msec/cm

Vertical Sensitivity: 5 volts/cm

Horizontal Sensitivity: 2 msec/cm

Figure 24

The biasing networks employ zener diodes to stabilize the operation of the shaping networks. A stable power supply with low ripple voltage is very important to the proper operation of the circuits.

A combination of phase shift in the shaping networks and lack of sufficient high frequency response in the amplifiers causes the operation of the circuit to deteriorate beyond 2500 cps. This range of operation is adequate for the present system.

Figure 25 shows a plot of the measured triggering points for the level detector as a function of frequency. Triggering error is less than 2 degrees in the range from 2 cps to 3 kc. This is a considerable improvement over several other methods. Level detectors become unstable at about 15 degrees from the peak of a sinusoid. Single sideband phase splitters generate 2 signals $90^{\circ} \pm 1.5^{\circ}$ out of phase with each other over a bandwidth of 1 decade, 300-3000 cps, and the amplitude response is not flat. Figure 25 also shows the phase shift at the output of the fourth amplifier as compared to the input, as a function of frequency.

Summation unit

A standard digital summation unit is used to sum the $G(t_{nh}) \cos\omega_n t$ terms as they are produced in the multiplier. The output of the multiplier is digitized at 1024 ordinates, and each of these values is stored in a separate address of the memory. Two external control signals are used. The first is derived from the gating circuit which produces a pulse at the

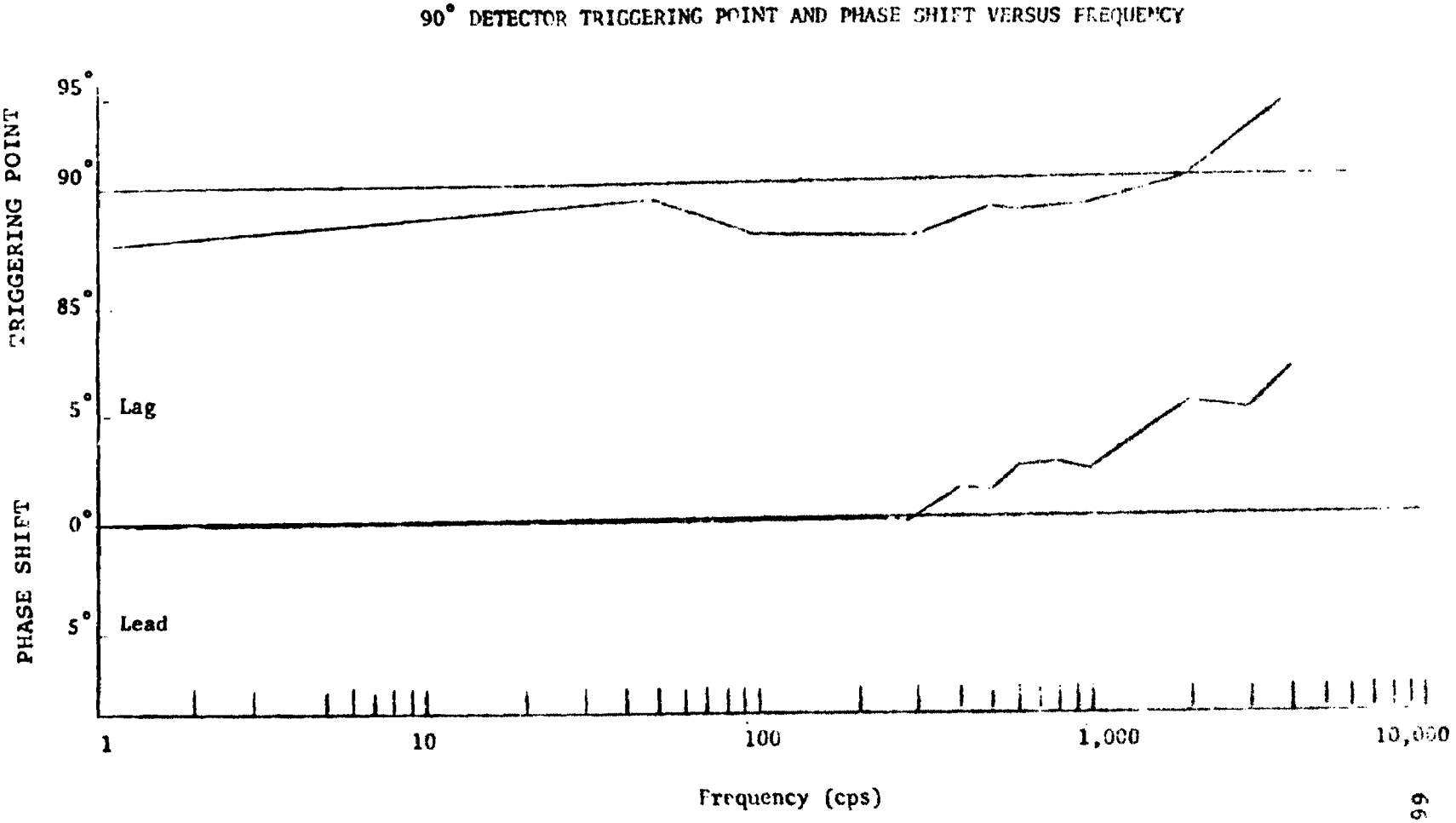
90° DETECTOR TRIGGERING POINT AND PHASE SHIFT VERSUS FREQUENCY
TRIGGERING POINT
95°
90°
85°
PHASE SHIFT
5°
Lag
0°
5°
Lead
1
10
100
1,000
10,000
Frequency (cps)
99

Figure 25

instant the gate opens. This pulse initiates the digitization and sweep cycle in the memory. The second control signal is derived from a fixed frequency output of the frequency synthesizer. It is used to externally advance the memory from one address to the next. These two control signals ensure that the digitizer begins operation at the same point (the peak) of each succeeding cosine function, and that data for corresponding ordinates are stored in the same address. The synthesized spectrum will repeat at intervals of 1/h. The highest frequency in the synthesized spectrum is 1/2h, and the repetition rate of the external advance signal is adjusted to scale this frequency to the 1000^{th} address. The last 24 addresses then carry part of the repeated spectrum. It is important to properly choose the sampling intervals to reduce the effect of overlap of noise frequencies. The techniques for this are discussed in the first section of this report.

Fringe counter

The sinusoidal reference signal is derived from the Michelson interferometer and is used to control the sampling interval and the frequency of the cosine functions. The zero crossings are used as the reference points, and each cycle indicates a 0.27305 micron additional displacement of the movable facets. The sampling theorems do not require that samples be taken this closely, if the shortest wavelength is

10 microns. Therefore, a counter is used which enables samples to be taken at each, every other, every 4^{th}, 8^{th} or 16^{th} cycle.

The sinusoidal reference signal is converted to pulses and delayed in a variable delay circuit. The delay circuit consists of a single-shot pulse generator with a variable pulse width. The delay is incorporated to ensure that beginning of the sampling interval and the output of the zero path detector coincide. As a result of mechanical imperfections in the system, and vibration, the coincidence cannot be repeated more than a few times before an adjustment is required. The maximum error introduced if the delay is not used, or if it is misadjusted, is half a mercury fringe or .136525 microns. If the infrared radiation is 10 microns, the phase error is $\epsilon/\lambda = .0136525$. With reference to Figure 16 the scanning function is only slightly altered and no appreciable error results.

Sequencer

The fringe counter provides the "command" signal for the sample and hold circuit and the sequencer. The sequencer consists of counters, pulse generators, transistor driving circuits and four rotary step switches. A block diagram of the sequencer is shown in the lower right-hand part of Figures 21 and 27. The block marked "SSMV" contains the pulse generator. The leads which control the frequency generated by the frequency synthesizer are connected to the 10 contact step switches.

Each time a pulse enters the sequencer, the "units" step switch advances one contact and the frequency of the synthesizer advances one cycle per second. The remaining switches operate in the proper counting sequence, and the frequencies can be advanced from 1 cps to 9999 cps in steps of one cps. All the step switches may be reset to zero by means of a "homing" switch.

The coils of the step switches are energized by the application of a pulse from the transistor driving circuits. No switching takes place, however, until the coils are de-energized. This introduces a delay of approximately 40 milliseconds between the application of the switching pulse and a change in the frequency of the frequency synthesizer.

A 70 millisecond delay is introduced into the gate control circuitry to ensure that the gate opens after the proper frequency has been established and the switching transients have died out.

Control circuitry

Figure 26 presents a timing diagram which shows the important relationships between the several inputs, outputs and control signals. A complete block diagram of the electronic system is shown in Figure 27. This shows the control circuits in detail.

The counter signal comes from the fringe counter and is derived from the reference input. Each time a negative transition occurs, the sampler takes a new sample and the output of the frequency synthesizer

TIMING DIAGRAM

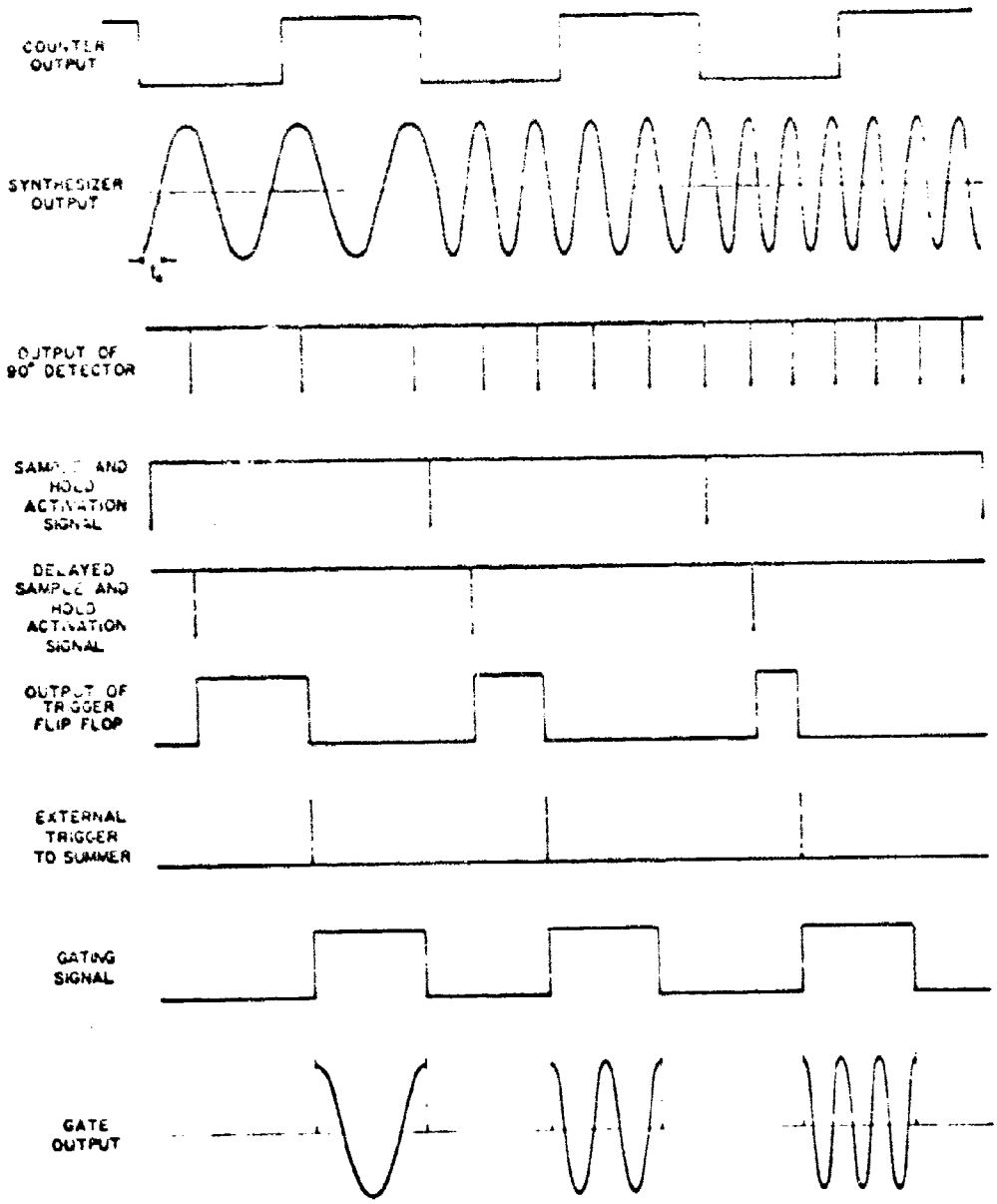

Figure 26

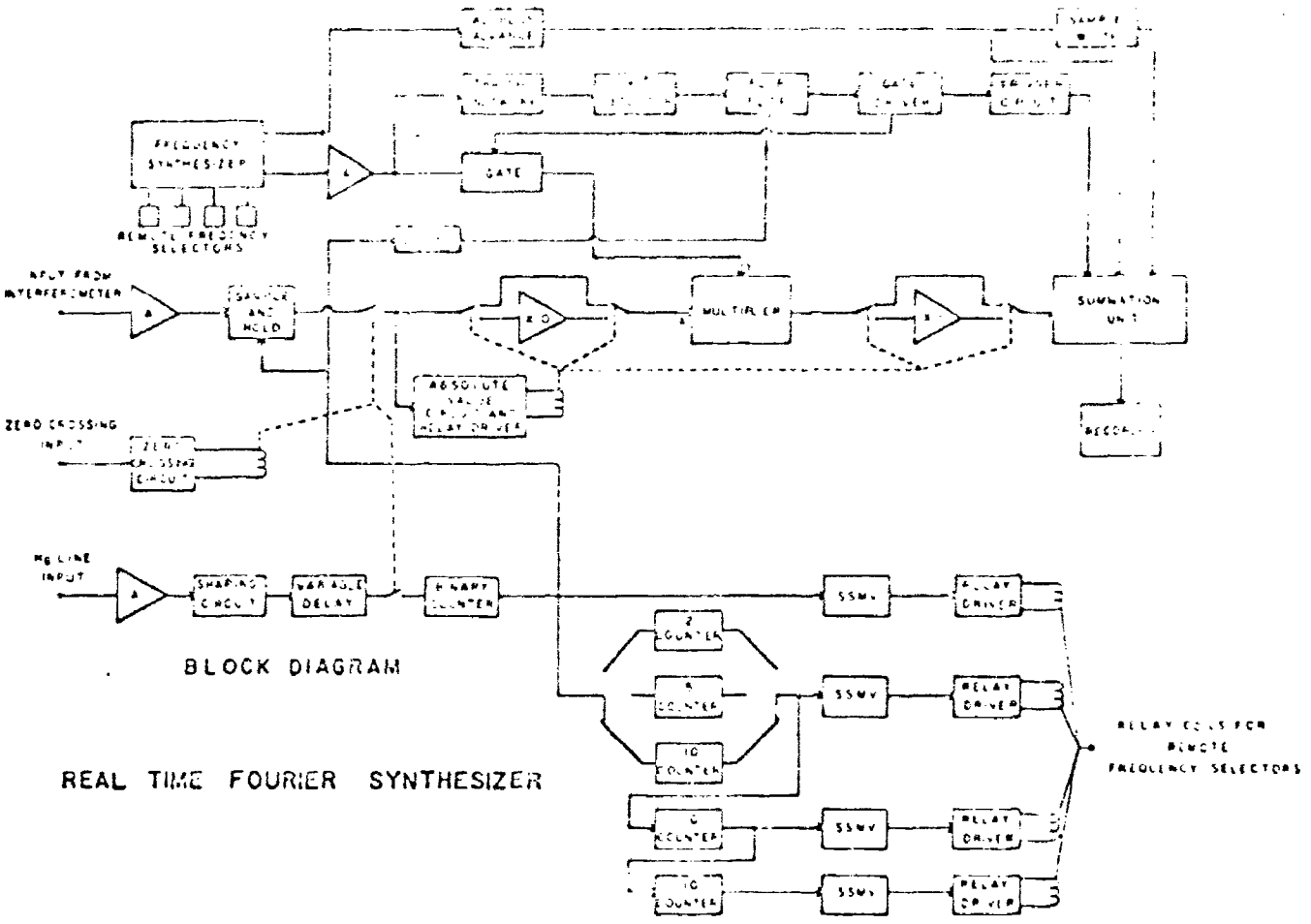
FREQUENCY SYNTHESIZER
GATE
SAMPLE AND HOLD
MULTIPLIER
SUMMATION UNIT
ZERO CROSSING
ABSOLUTE VALUE
MC LINE INPUT
SHAPING CIRCUIT
VARIABLE DELAY
BINARY COUNTER
SSMV
RELAY DRIVER
BLOCK DIAGRAM
REAL TIME FOURIER SYNTHESIZER

Figure 27

is advanced one cycle per second. The delay, t_o, is the 40-millisecond switching delay between the application of the switching pulse and the actual switch closure. The 90-degree detector generates a pulse each time the output of the frequency synthesizer passes through a maximum. The signal which controls the sampling in the sample and hold circuit is also available as an output of that circuit. This signal is delayed 70 milliseconds and fed to one input of a bistable circuit. The signal from the 90-degree detector is fed to the other input. The sample and hold activation signal sets the output transistor to the "off" state. The 90-degree detector resets it to the "on" state. This creates a negative voltage transition which operates the gate-driver circuit and opens the gate. It also produces a trigger signal which begins the digitizing sequence in the summation unit. The gate is closed after a predetermined time delay by the gate driving circuit. When the output of the gate enters the multiplier, it is multiplied with the value of the interferogram sample and is immediately digitized and stored in the summation unit.

TEST RESULTS AND THE SYNTHESIZED SPECTRA OBTAINED WITH THE INSTRUMENT

Experimental Procedure

The completed real-time Fourier transform synthesizer was subjected to a series of tests designed to evaluate its performance. Since it will be used to synthesize the spectra produced by both broad and narrow spectral band sources, known functions with these types of spectra were used. The entire system was not operated during those initial tests. The zero path difference detector was disconnected, and the relay it controls was manually operated.

The performance in the synthesis of continuous spectra was investigated by utilizing single pulses of various widths. Rectangular, triangular and cosine pulses were used. They were derived from a low frequency signal generator, and an identical generator supplied the reference signal. These signals were inserted into the normal data input and their amplitudes were adjusted to simulate the normal input levels. The signals were monitored on a strip chart recorder, and the sampling sequence was manually initiated at the proper instant. The summation of $f(t_{nh}) \cos\omega_n t$ terms was stopped at the proper time by switching the summation unit from the "count" mode to the "display" mode.

The test functions will be discussed mathematically using Bracewell's [26] notation. This notation is now defined.

The rectangular function of unit height, area, and base is defined as $\Pi(x)$.

$$\Pi(x) = \begin{cases} 0 \text{ for } |x| > \frac{1}{2} \\ 1 \text{ for } |x| < \frac{1}{2} \\ \frac{1}{2} \text{ for } |x| = \frac{1}{2} \end{cases}$$

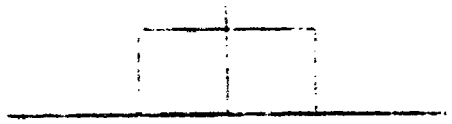

The triangular function of unit height and area is defined as $\Delta(x)$.

$$\Delta(x) = \begin{cases} 0 \text{ for } |x| > 1 \\ 1 - |x| \text{ for } |x| < 1 \end{cases}$$

This function is also the self-convolution of $\Pi(x)$.

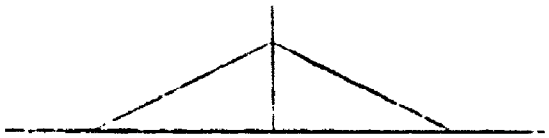

The sampling or replicating symbol $\text{Ш}(x)$ is defined as

$$\text{Ш}(x) = \sum_{n=-\infty}^{\infty} \Delta(x-n)$$

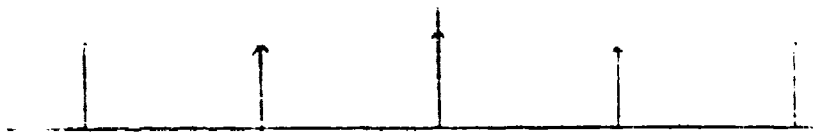

The rectangular functions of unit height may be represented mathematically as $\Pi(t/b)$, where t is time and b is width. In a similar manner, the triangular functions become $(t/b/2)$ and the cosine pulses are expressed as $\Pi(t/b)\cos\pi(t/b)$. Figure 28 shows the rectangular functions and both their synthesized and theoretical spectra. Figures 29 and 30 show similar data for the triangular and cosine pulses, respectively. The fluctuations in the synthesized data are due to digitization error and recorder jitter. Figure 31 shows a set of normalized error curves for the preceding data. The error is normalized to the amplitude of the dc component of the spectrum, and its absolute value is plotted. The greatest error occurs for shorter pulses. This is so for two reasons: First, only a few terms make up the synthesized spectrum and an insufficient number are used to obtain good convergence to the true spectrum. Second, because of the sampling rate limitations imposed by the components of the system, the fastest allowable sampling rate is insufficient to allow sampling at twice the highest frequency of the spectrum. The spectra of these signals theoretically extends to infinity, but amplitudes soon become negligible for all practical purposes. The region of the spectrum in which the amplitudes are non-negligible is wider for short pulses than it is for long ones. Thus, the allowable sampling rate is not fast enough to prevent overlap of spectral components with non-negligible amplitudes.

FREQUENCY SPECTRA FOR RECTANGULAR PULSES

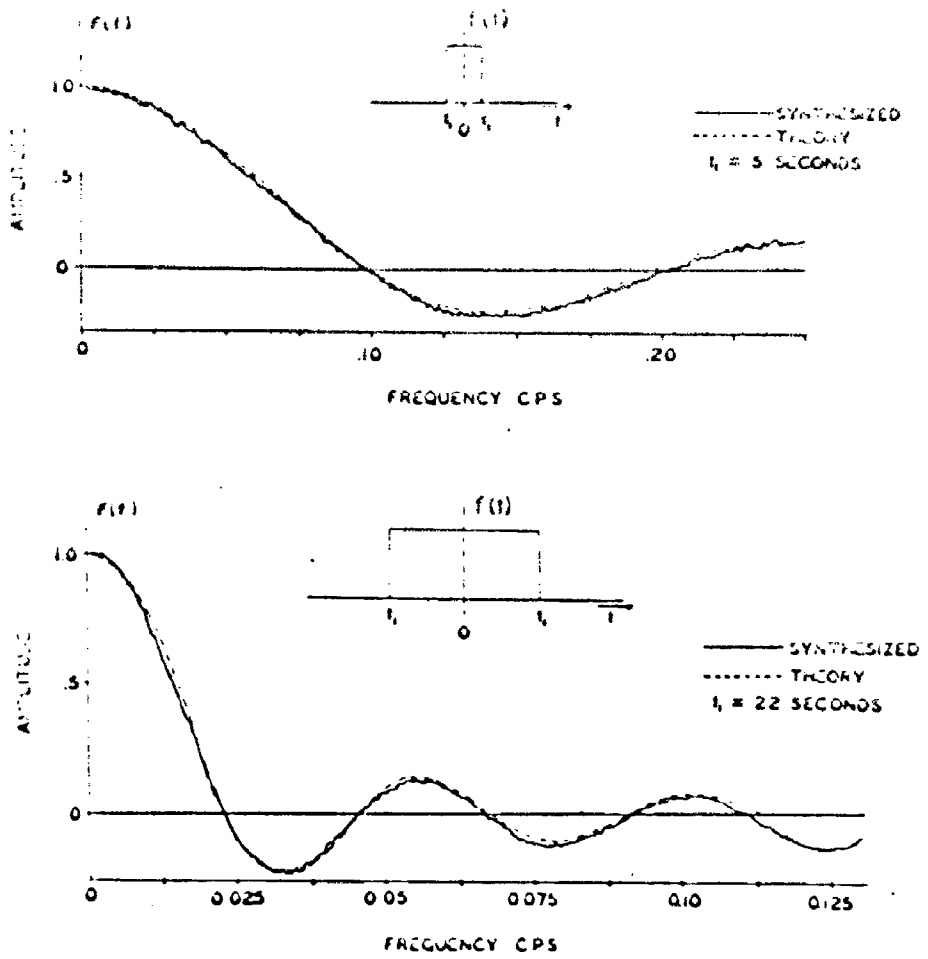

Figure 28

FREQUENCY SPECTRA FOR TRIANGULAR PULSES

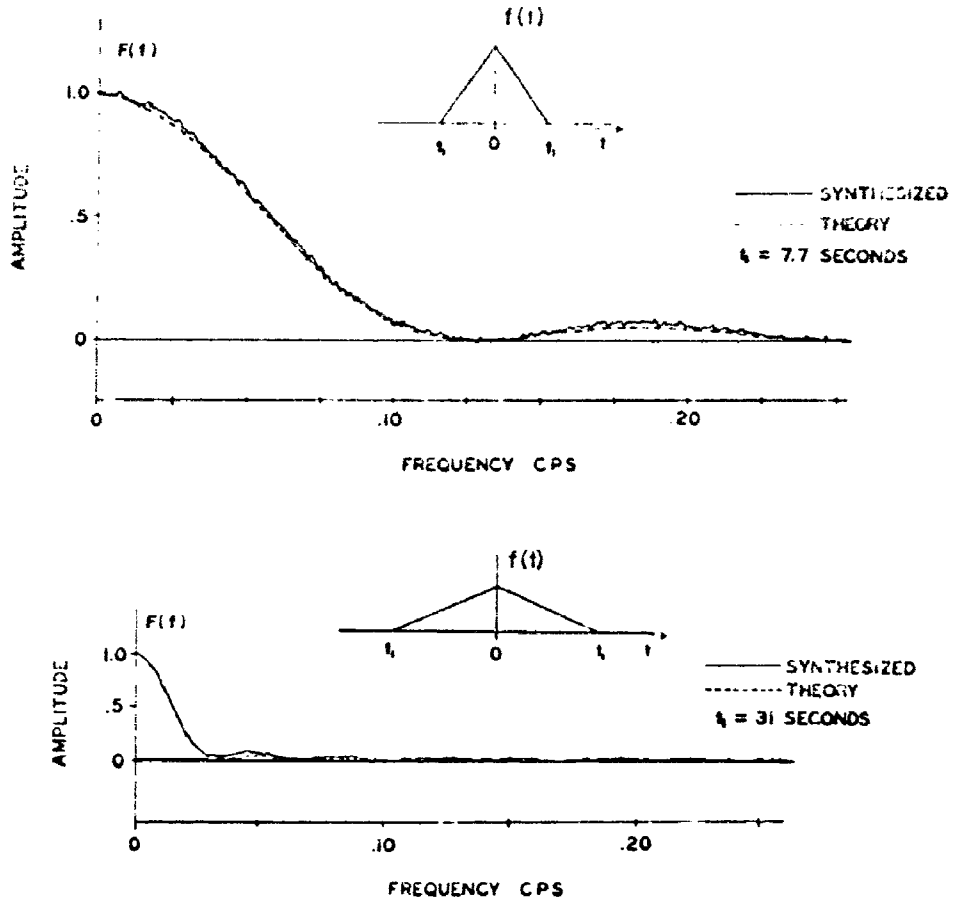

Figure 29

FREQUENCY SPECTRA FOR COSINE PULSES

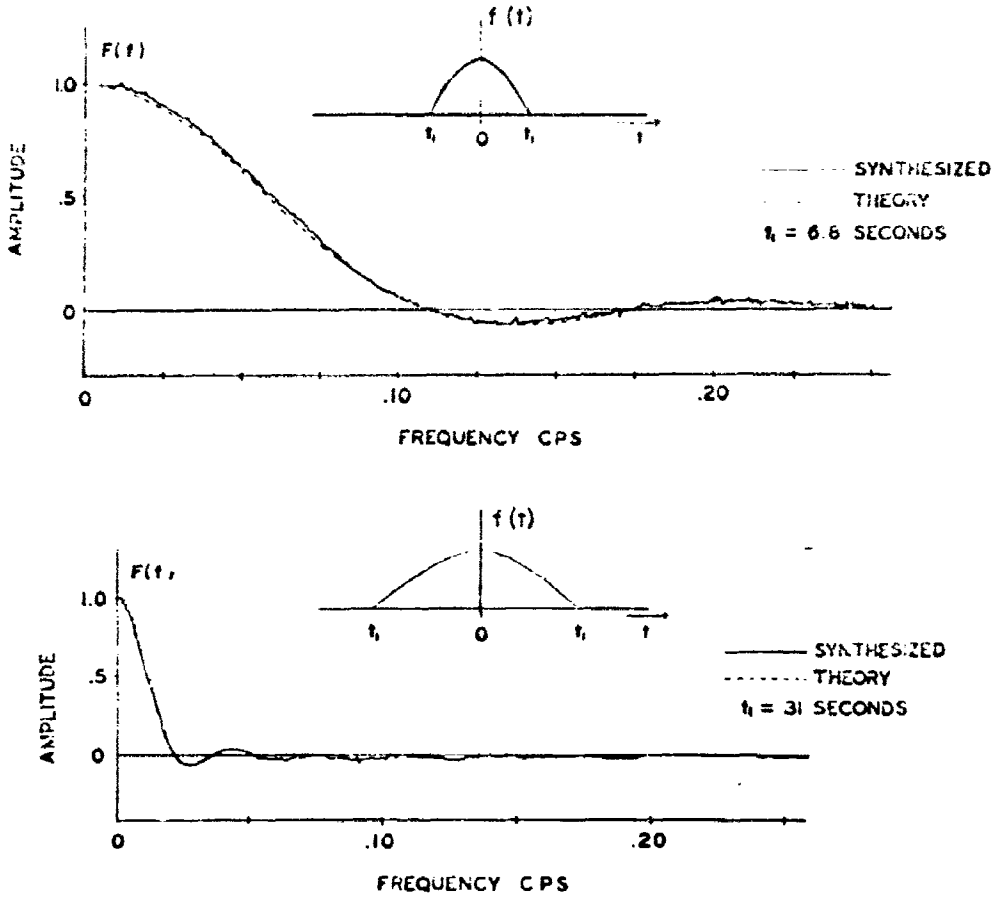

Figure 30

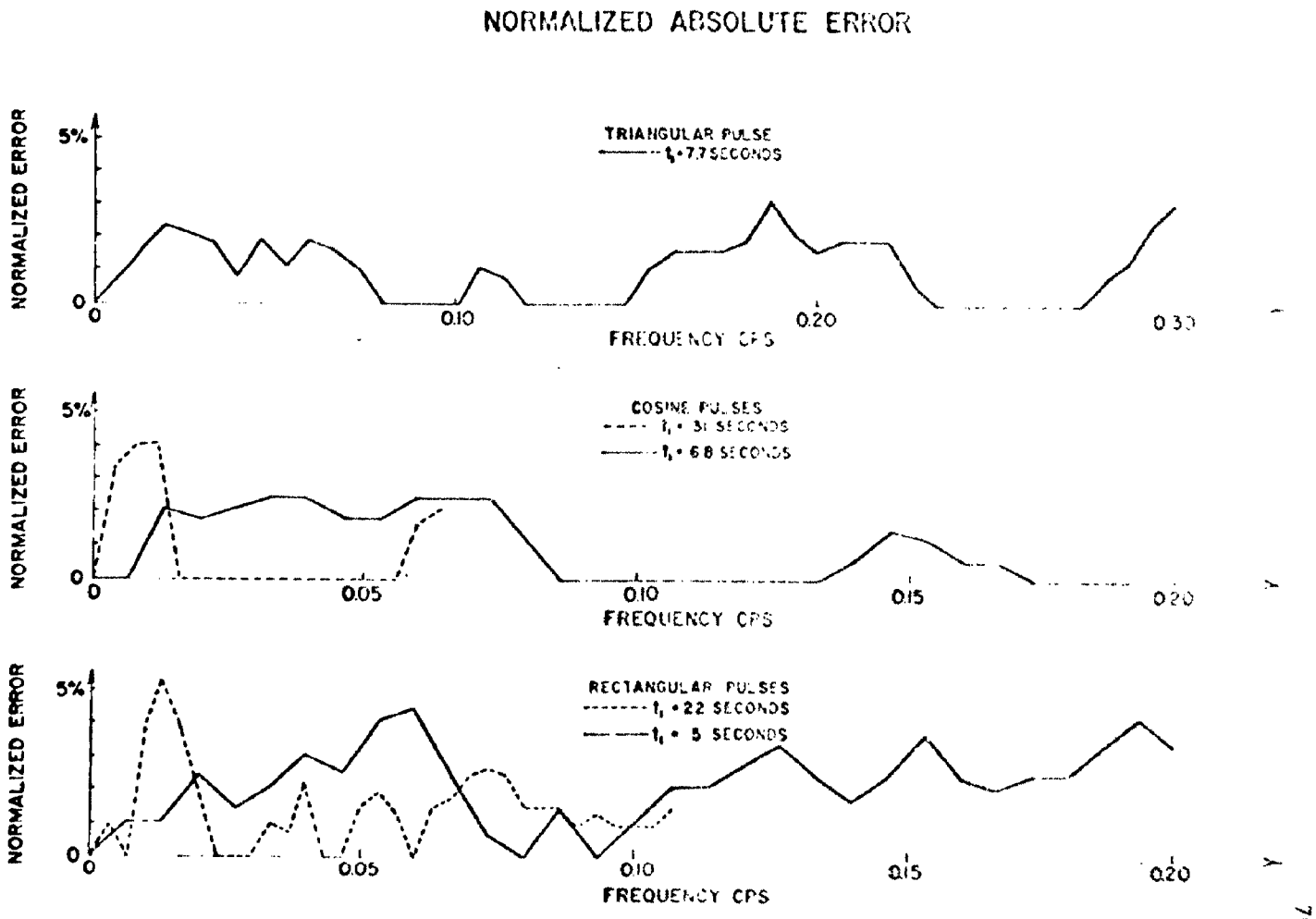
NORMALIZED ABSOLUTE ERROR
NORMALIZED ERROR
5%
0
TRIANGULAR PULSE
t_1 = 7.7 SECONDS
0
0.10
0.20
0.30
FREQUENCY CPS
NORMALIZED ERROR
5%
0
COSINE PULSES
t_1 = 31 SECONDS
t_1 = 6.8 SECONDS
0
0.05
0.10
0.15
0.20
FREQUENCY CPS
NORMALIZED ERROR
5%
0
RECTANGULAR PULSES
t_1 = 22 SECONDS
t_1 = 5 SECONDS
0
0.05
0.10
0.15
0.20
FREQUENCY CPS

Figure 31

The accuracy improves for long pulses because a greater number of samples produces a larger number of terms. The spectrum estimate, therefore, more closely approaches the true spectra. Also, the non-negligible portion of the spectrum is narrower and the overlap of repeated spectra occurs for components with much smaller amplitudes.

The spectrum for a short rectangular pulse was synthesized from only three samples while the short cosine and triangular pulses were synthesized from only four samples. Sampling rate limitations are discussed further in the next section.

The preceding functions have continuous spectra which contain no rapid variations or discontinuities. It is therefore possible to synthesize the spectra with a finite number of terms and obtain good accuracy, provided the number of terms is sufficient. This is not the case when the spectrum is discontinuous, since Gibbs phenomenon occurs. An infinite number of terms produces a synthesized spectrum which exhibits "ringing" at the discontinuities.

Let us now investigate the synthesized spectrum estimate when functions having discontinuous spectra are involved. For this purpose, finite trains of rectangular and triangular pulses, and a truncated cosine wave, were used.

Mathematically, the rectangular pulse train can be represented as

$$f(t) = \Pi(t/b)[\{\mathrm{III}(t/c)*2\Pi(t/a)\} - 1]$$

where * denotes convolution and the parameters are defined by the following diagram.

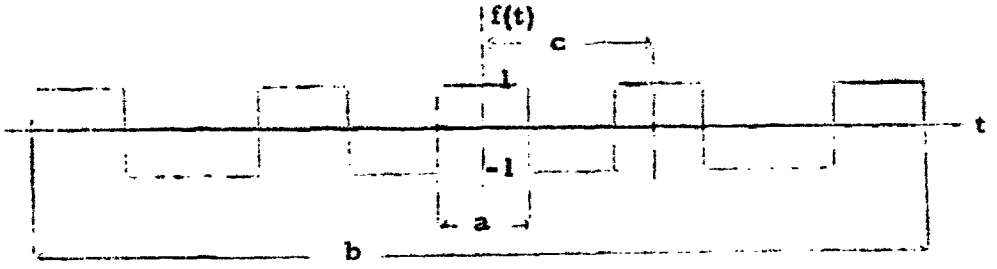

The rectangular pulse, convolved with the replicating function produces a pulse train. The dc value is removed and the result is truncated by a second rectangular function. In the frequency domain, the spectrum is the spectrum of the rectangular pulse, multiplied by the sampling function, which is then convolved with the scanning function. In this case, the scanning function is the Fourier transform of the truncating function. Thus, the line spectrum of an infinite pulse train is convolved with a scanning function of the form $\frac{\sin \pi t}{\pi t}$ = sinc t. The synthesized spectrum will be a series of sinc functions located at the harmonics of the fundamental frequency.

The truncated cosine wave is represented by

$$f(t) = \Pi(t/b) \cos \omega t.$$

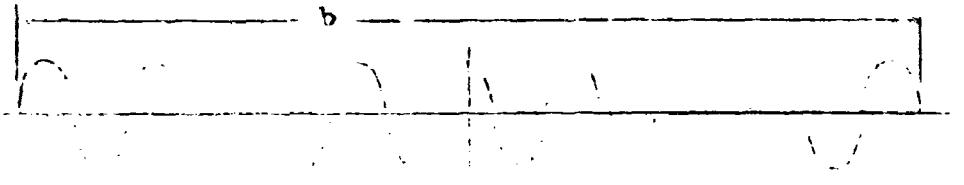

The spectrum is simply a pair of impulse functions convolved with the scanning function. In this case, one of the impulse functions occurs for negative frequencies which have no meaning.

The triangular function may be represented in the general case as

$$f(t) = \Pi(t/b)[\{\mathrm{III}(t/c) * 2(t/a)\} - 1]$$

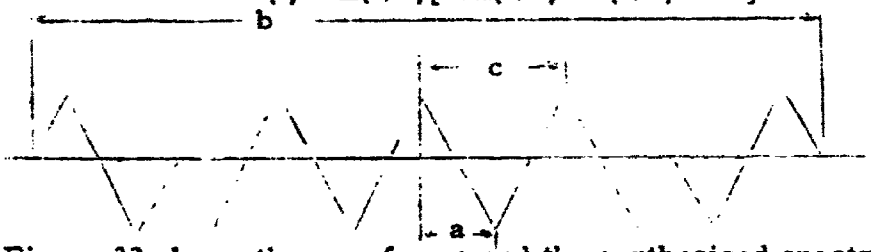

Figure 32 shows the waveforms and the synthesized spectra. Each waveform was sampled at 2-second intervals, and 500 samples were obtained. Table 1 shows the measured and theoretical values for the spectral components.

Frequencies may be determined with an error of less than 2%. The accurate determination of amplitudes is somewhat more difficult. This is due to the fact that there are only a finite number of addresses in which data are stored. The resolution of the system improves, and the peak of the synthesized harmonic may actually fall between two address points when many samples are taken. In this case, the true peak will not be recorded. This is true of any system which utilizes a finite number of input or output points. The oscilloscope display was expanded, and the main peak was found to be stored in only four addresses. The peak was

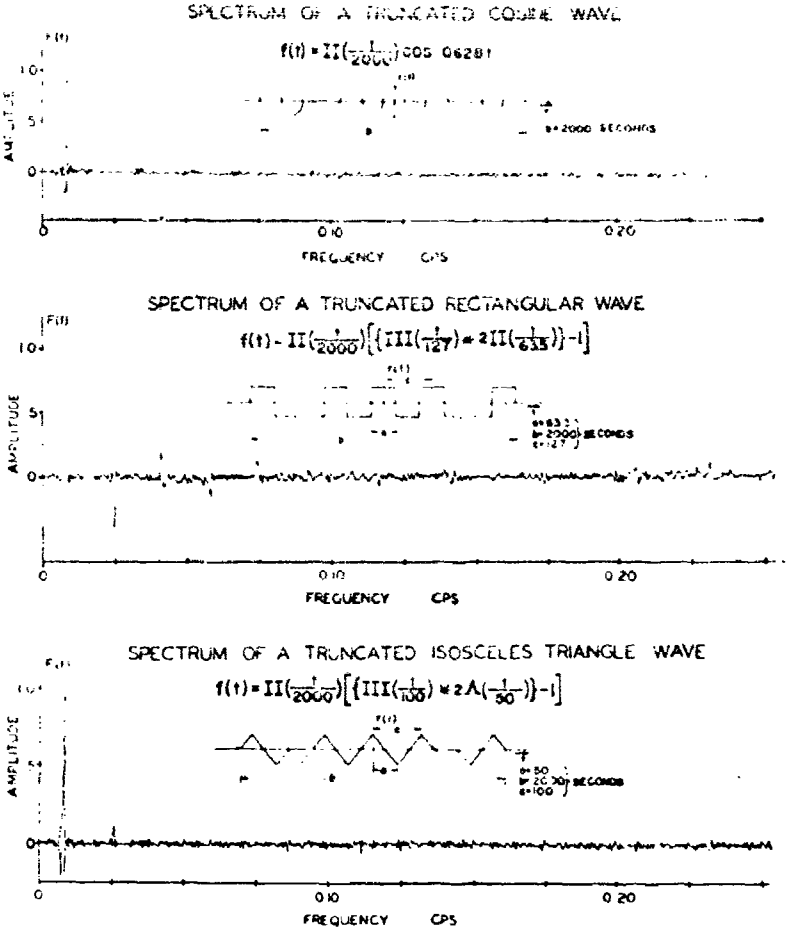
SPECTRUM OF A TRUNCATED COSINE WAVE
f(t) = Π(t/2000) cos 0.628t
AMPLITUDE
a = 2000 SECONDS
0
0.10
0.20
FREQUENCY CPS
SPECTRUM OF A TRUNCATED RECTANGULAR WAVE
f(t) = Π(t/2000)[{III(t/127) * 2Π(t/63.5)} - 1]
AMPLITUDE
10
5
0
0.10
0.20
FREQUENCY CPS
SPECTRUM OF A TRUNCATED ISOSCELES TRIANGLE WAVE
f(t) = Π(t/2000)[{III(t/100) * 2Λ(t/50)} - 1]
AMPLITUDE
0
0.10
0.20
FREQUENCY CPS

Figure 32

Table 1. Results of the synthesis of the spectra of truncated waveforms.*

Cosine Wave					
Harmonic	1	3	5	7	9
Amplitude					
Theoretical	1	0	0	0	0
Synthesized	1	0	0	0	0
|Error|	0	0	0	0	0
Frequency					
Theoretical	1	0	0	0	0
Synthesized	1	0	0	0	0
|Error|	0	0	0	0	0
Triangular Wave					
Harmonic	1	3	5	7	9
Amplitude					
Theoretical	1.0	0.111	.04000	.021	.01235
Synthesized	1.0	0.1094	.01885	---	---
|Error|	0	1.45%	52.8%		
Frequency					
Theoretical	1.0	3.00	5.00	7.00	9.00
Synthesized	1.0	3.05	5.10	---	---
|Error|	0	1.6%	2.0%		

Table 1. (Continued).

Rectangular Wave					
Harmonic	1	3	5	7	9
Amplitude					
Theoretical	1	-0.333	0.200	-0.1428	0.111
Synthesized	1	-0.391	0.221	-0.1465	0.129
|Error|	0	18.5%	10.5%	2.6%	16.4%
Frequency					
Theoretical	1	3.00	5.00	7.00	9.00
Synthesized	1	3.00	5.00	7.10	9.04
Error	0	0	0	1.428%	0.445%

*All the data are normalized to the amplitude and frequency of the fundamental.

not stored. This causes an amplitude error in the synthesized harmonic. Methods of reducing this error are discussed in the following section.

A test of the resolution of the system was made with these signals. The theoretical resolution is .0005 cps while the measured resolution is approximately the same. Another rest was made with a triangular waveform and 61 samples were taken. The measured and theoretical resolutions were nearly the same again, but the amplitudes of the harmonic components were more nearly equal to the theoretical values. The peaks, representing harmonics, were stored in more addresses, and the actual location of the peak was more closely determined.

The real-time Fourier transform synthesizer was evaluated under actual operating conditions. The experimental apparatus is shown in Figure 33. Figure 34 is a photograph of the optical system while Figure 35 is a photograph of the equipment. In Figure 34, E is the lamellar grating, K and L are the optics for the zero path difference detector, G is the globar, P is the monochromator, and PM is the parabolic mirror.

The lamellar grating was illuminated with parallel radiation produced by the globar which is at the focal point of the parabolic mirror. After reflection from the face of the grating, this radiation is focused by the optical system into the monochromator. This was used as both an optical filter and a detector. The output of the monochromator was amplified and

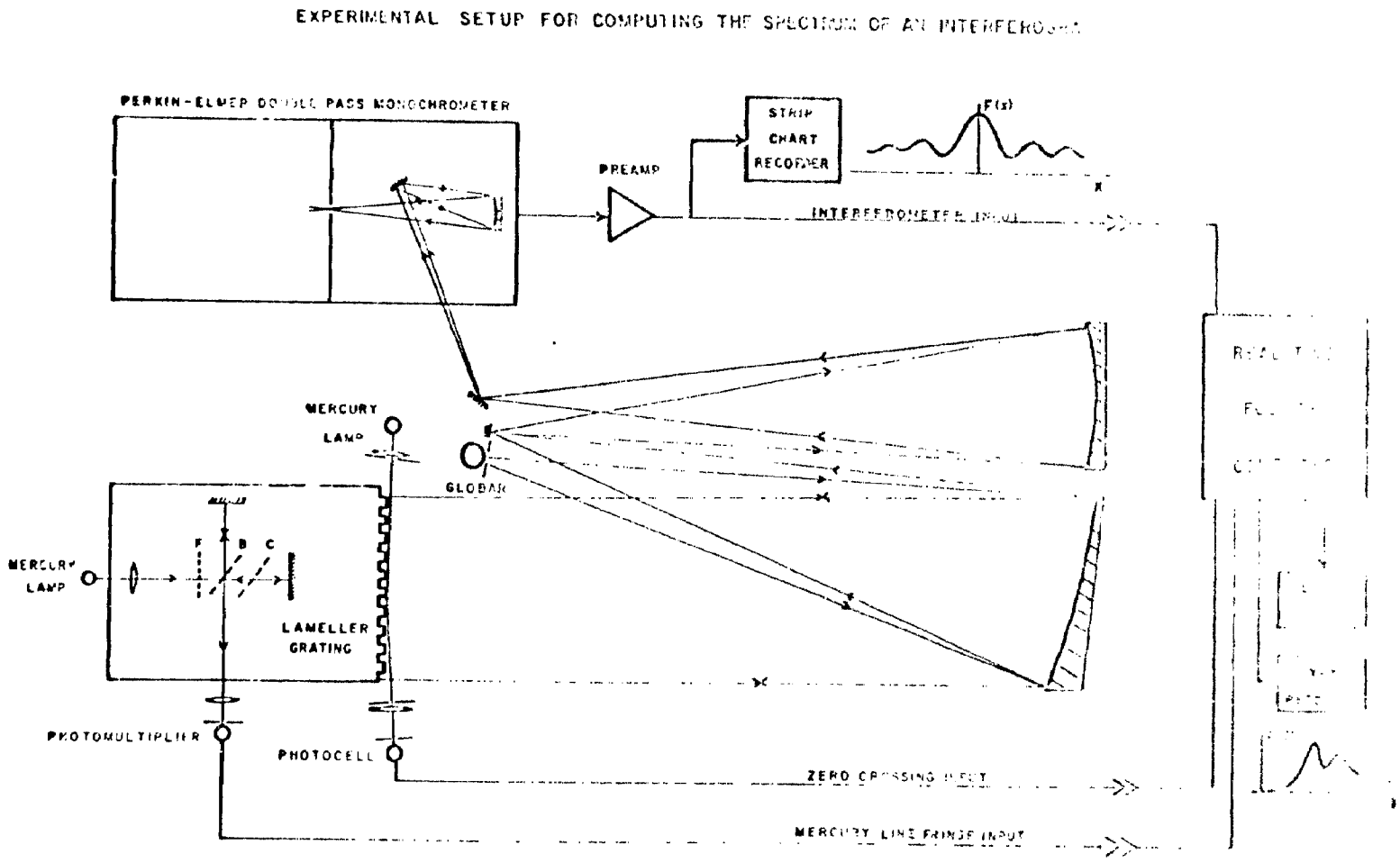
PERKIN-ELMER DOUBLE PASS MONOCHROMETER
PREAMP
STRIP CHART RECORDER
F(x)
x
INTERFEROMETER INPUT
MERCURY LAMP
GLOBAR
MERCURY LAMP
F
B
C
LAMELLER GRATING
PHOTOMULTIPLIER
PHOTOCELL
ZERO CROSSING PULSE
MERCURY LINE FRINGE INPUT

Figure 33

OPTICAL SYSTEM

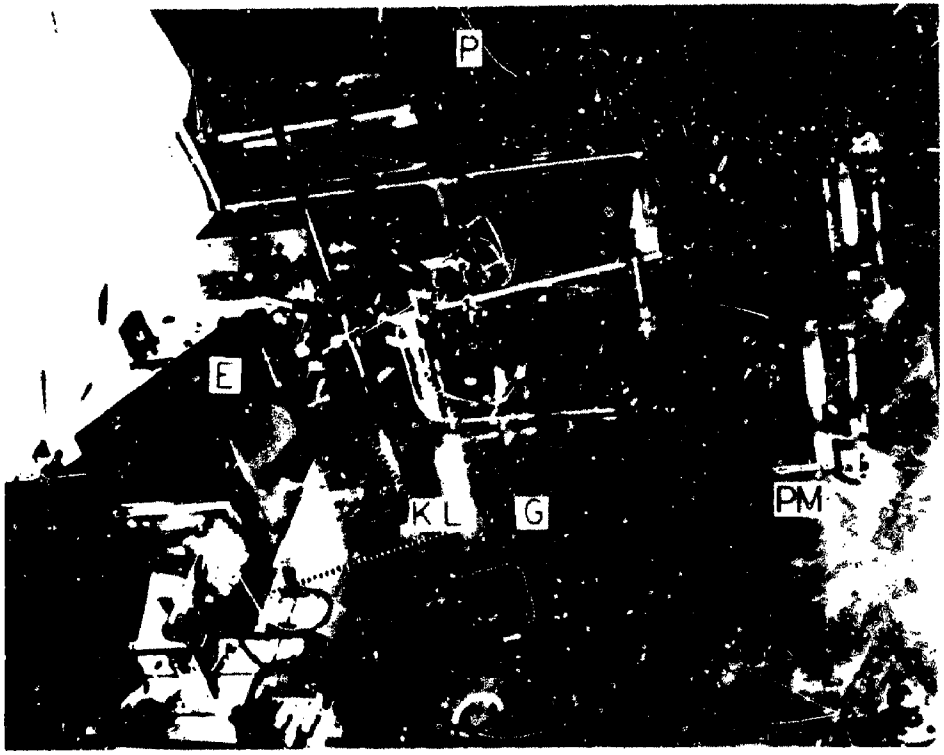

E = LAMELLAR GRATING
G = GLOBAR
K = LIGHT SOURCE AND COLLIMATOR
L = DETECTOR
P = MONOCHROMATOR
PM = PARABOLIC MIRROR

Figure 34

EXPERIMENTAL SET-UP

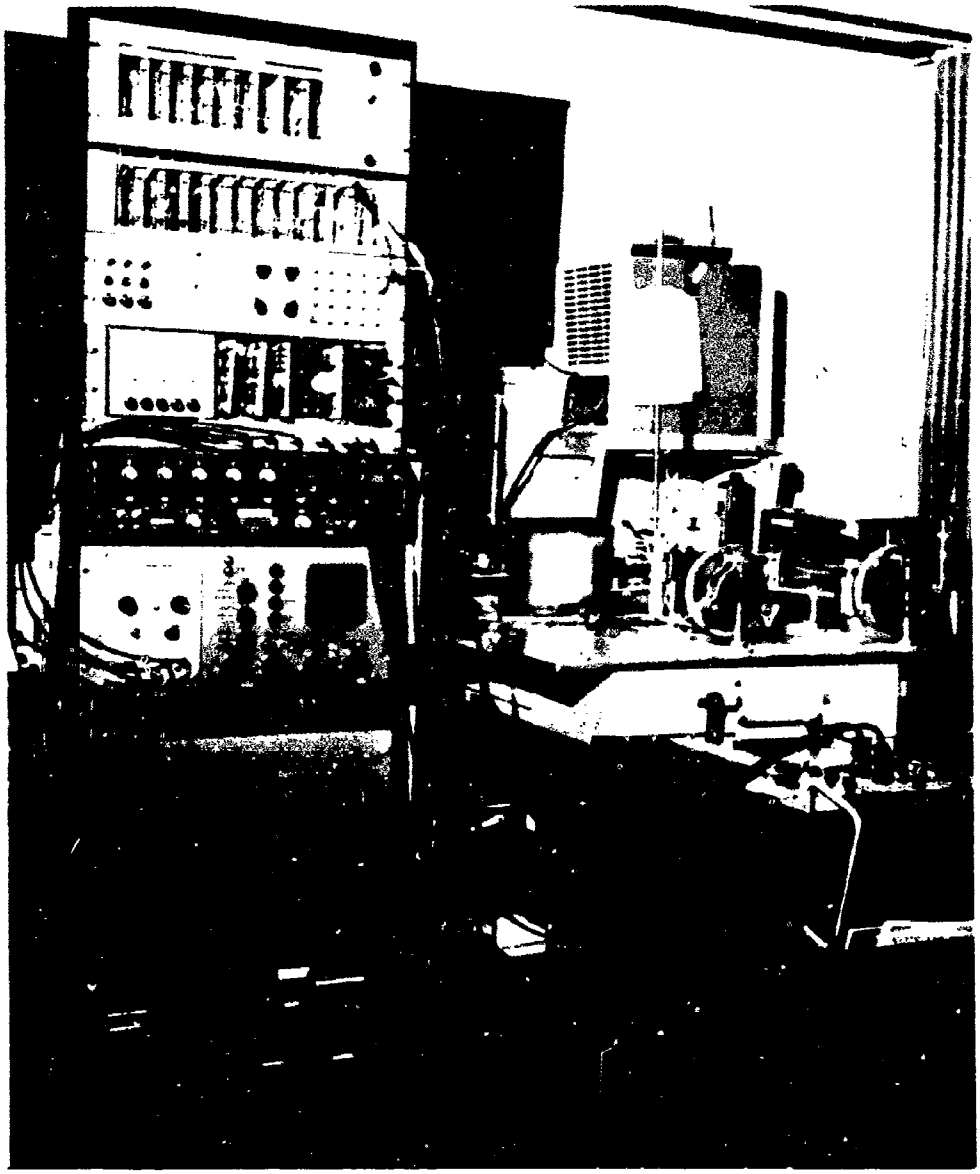

FIGURE 35

connected to the input of the Fourier transform synthesizer. The interferogram was recorded on a strip chart recorder. The reference signal was obtained from the Michelson interferometer, and the zero path difference detector supplied the initiating pulse.

Figure 36 shows the interferogram and the corresponding synthesized spectrum. The optical path difference was varied from -400 to +400 microns. The samples were taken over the 0 to 400 micron region. It required approximately 200 seconds to obtain the data. The synthesized spectrum is always monitored, and Figure 37 shows the increase in detail as the path difference is increased.

The interferogram is produced by a narrow band of radiation with a central wavenumber of approximately 605 cm^{-1}. This corresponds to a wavelength of $1/\nu_o$, or approximately 16.5 microns. The halfwidth of the synthesized spectral line is $\Delta\nu_L = 30.5\ cm^{-1}$ and the theoretical resolution of the instrument is $\Delta L_i = 25\ cm^{-1}$ for the path difference utilized.

Figure 38 shows the result of synthesizing the spectrum produced by the interference of two electrical signals of slightly different frequencies. This also shows the increase in detail and resolution as the number of samples (and hence terms) increases.

INTERFEROGRAM AND THE SYNTHESIZED SPECTRUM

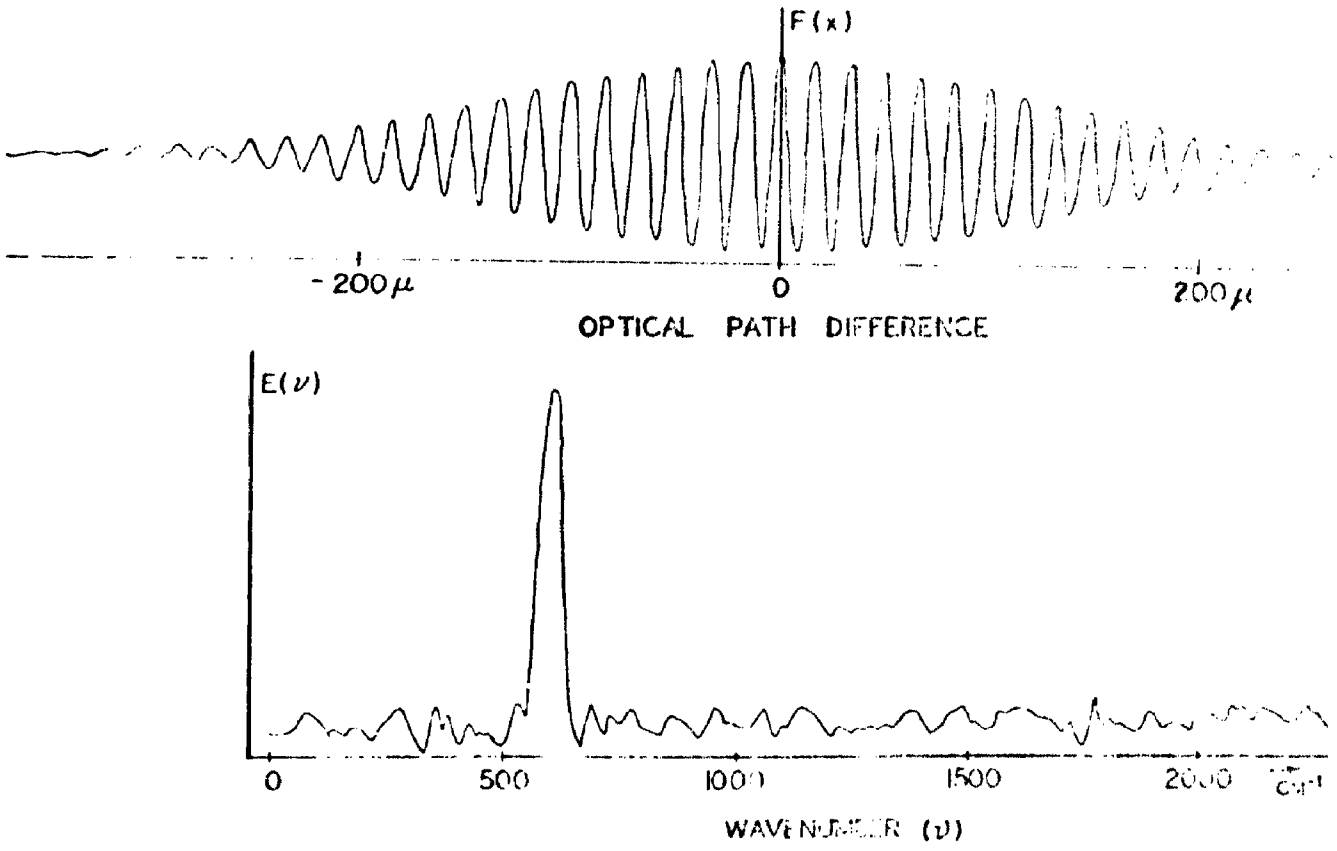

Figure 36

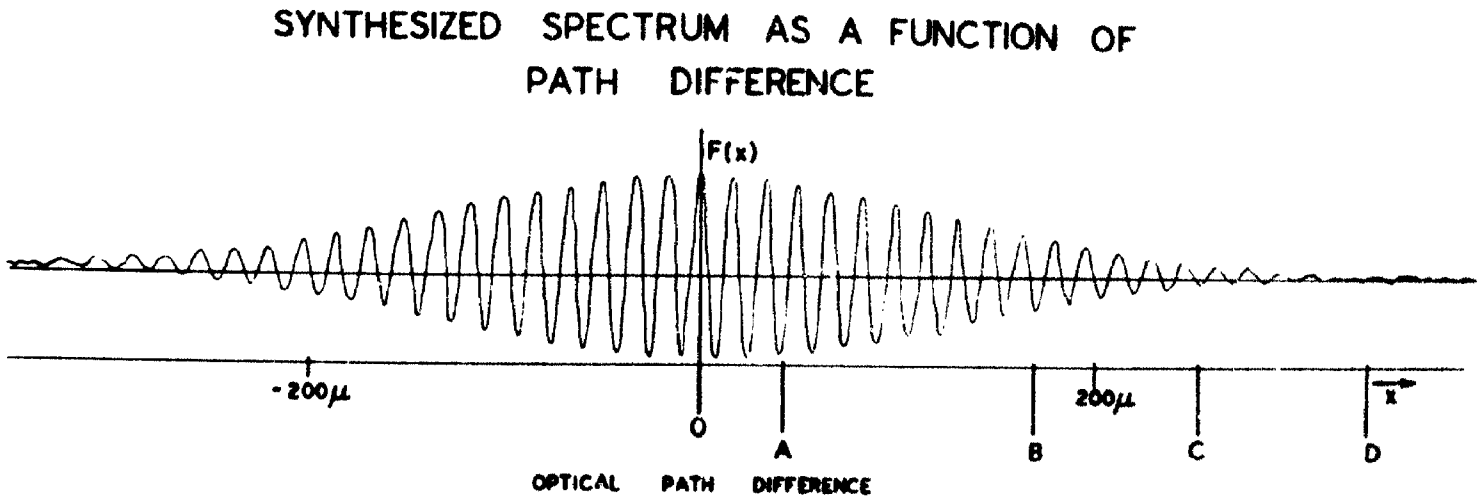
SYNTHESIZED SPECTRUM AS A FUNCTION OF PATH DIFFERENCE
F(x)
-200μ
0
A
B
200μ
C
D
x
OPTICAL PATH DIFFERENCE
A
C
B
D
WAVENUMBER
WAVENUMBER

Figure 37

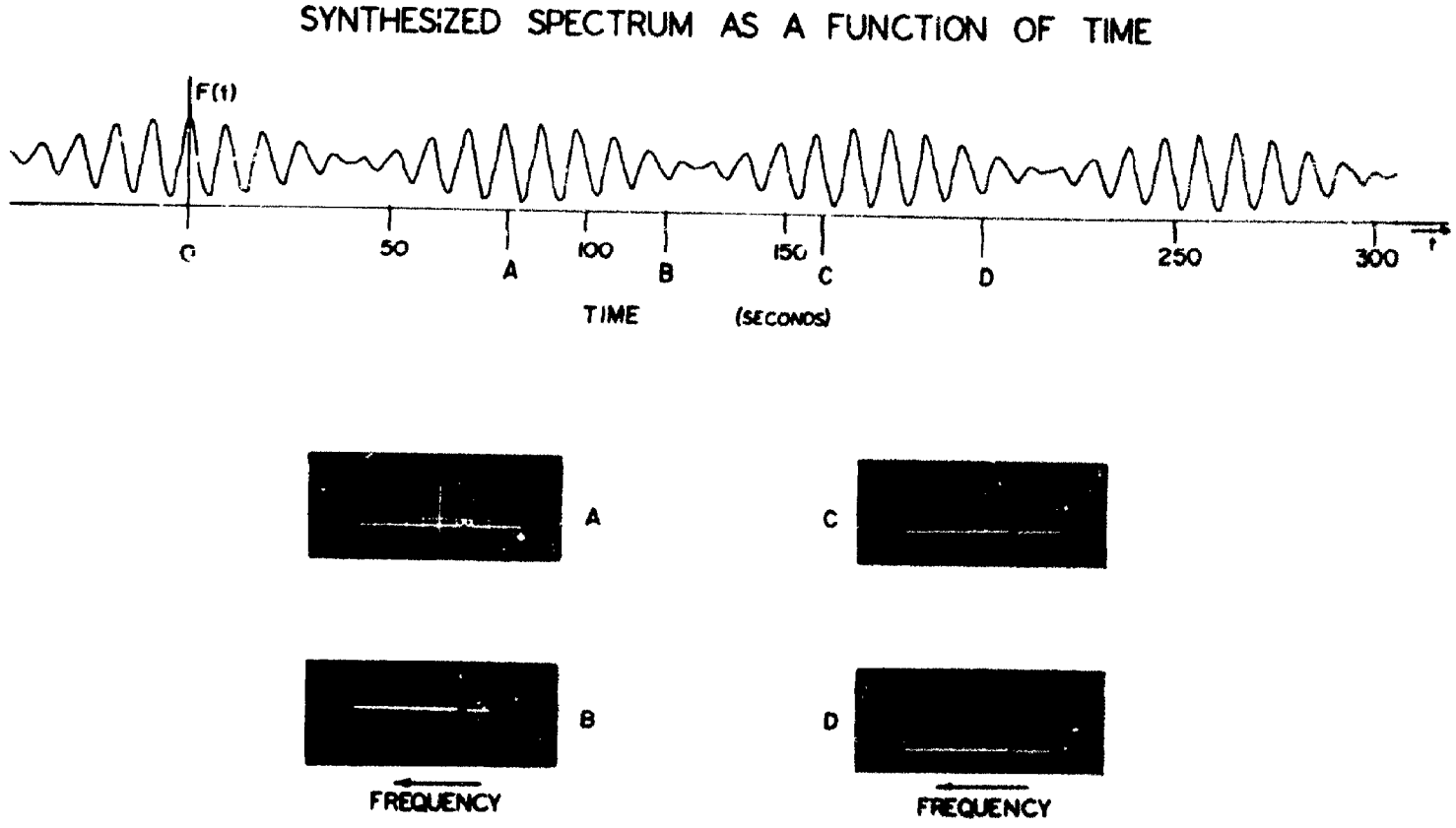
SYNTHESIZED SPECTRUM AS A FUNCTION OF TIME
F(t)
0
50
A
100
B
150
C
D
250
300
t
TIME (SECONDS)
A
C
B
D
FREQUENCY
FREQUENCY

Figure 38

Summary of the data

The real-time Fourier synthesizer has been tested under actual operating conditions. It is able to synthesize continuous and discrete spectra. It is limited in the maximum frequency at which samples can be obtained. Thus, greater error occurs when it is called upon to synthesize short pulses with broad spectra. Accuracy improves as the pulses become wider and the spectra narrower. The theoretical and measured resolutions were approximately the same. Accuracy was satisfactory when it was used to synthesize a spectrum from the corresponding interferogram.

A DISCUSSION OF ERRORS AND RECOMMENDED SYSTEM IMPROVEMENTS

The synthesized estimate of the spectrum will deviate slightly from the true spectrum because of the following:

1. Errors in obtaining the interferograms are unavoidable.

2. Errors are introduced in the insertion of the data into the computer.

3. Errors arise in the technique of computing the spectrum.

4. Errors arise due to limitations of the component parts of the Fourier synthesizer.

It is impossible to allow the path difference, when taking the interferogram, to vary from $-\infty$ to $+\infty$. The maximum path difference is determined by the limitations of the interferometer. The interferogram is therefore truncated, which causes an unavoidable error and limits the resolution. The spectrum estimate is, therefore, the true spectrum convolved with the scanning function of the instrument.

Let us now investigate the error in the spectrum when an improper interferogram function is used. We will assume a noise-free interferogram. The interferogram function has been defined as

$$F(x) = E(x) = \tfrac{1}{2}E(0)$$

where E(x) is the detector response and $\frac{1}{2}E(0)$ is its asymptotic value as the path difference is made large. An error in F(x) is made if $\frac{1}{2}E(0)$ is improperly removed from E(x). For an error of ΔE, the error in the spectrum will be

$$E(\nu)_{\Delta E} = 4D\Delta E \left(\sin \frac{4\pi\nu D}{4\pi\nu D}\right)$$

where D is the maximum groove depth of the grating. This is the same as the Fourier transform of a rectangular pulse of amplitude ΔE and width 4D. The error adds a decaying oscillation with a period $\frac{1}{2D}$, in ν, to the spectrum. This error is ignored in several digital computation schemes since it only occurs near $\nu = 0$ [22]. It cannot be ignored here, for all wavenumbers are present from $\nu = 0$ to $\nu = \nu_M$ where ν_M is the maximum wavenumber. Since the error cannot be ignored, it must be removed. The input amplifier contains a balancing network to remove $\frac{1}{2}E(0)$ from E(x). The adjustment is made experimentally by taking the same interferogram several times and adjusting the dc level at the input of the sample and hold circuit to zero. Several sets of data are usually required to reduce ΔE to zero. The synthesized spectrum may be monitored, and it is not usually necessary to obtain the entire interferogram. The error begins to appear after only a few terms in the synthesis have been obtained. This fact saves considerable time in making the adjustment.

The spectrum estimate converges to the true spectrum as the number of terms in the Fourier series expansion becomes very large, provided the spectrum is continuous. A finite series expansion, produced by an interferogram of finite length, shows spurious oscillations in the spectrum in the region of a discontinuity. The amplitude of these oscillations remains constant as the number of terms increases, but the spurious peaks crowd toward the discontinuity [23]. The peak separation is given by

$$\Delta\nu = \frac{1}{2D}$$

This is the Gibbs phenomenon.

As discussed in section 1, Gibbs phenomenon may be removed by a process known as "apodization," in which the interferogram is truncated by some non-rectangular function. The function is chosen so that its Fourier transform (the scanning function) has a main lobe and low side lobes. A common apodizing function is the triangle shown in Figure 5. This produces a scanning function of the form $(\frac{\sin\eta}{\eta})^2$ while rectangular truncation produces a $(\frac{\sin\xi}{\xi})$ scanning function. The $(\frac{\sin\eta}{\eta})^2$ function has a half width, for the same number of terms, which is twice as wide as $\frac{\sin\xi}{\xi}$. Thus, for triangular apodization, the resolving power is decreased by a factor of two. However, the scanning function for triangular apodization has adjacent side lobes which have amplitudes about 4.5% of the main peak and they do not oscillate. The expression $\frac{\sin\xi}{\xi}$ has

adjacent maximum with amplitudes more than 10% of the main peak. It also has negative values, and the first minimum has an absolute value of approximately 20% of the main peak. Other apodizing functions can be used, and the choice depends on the characteristics of the spectrum. The present system does not contain an apodizing system since an additional multiplier is not available. This feature will be added to the system as soon as one is obtained.

The accuracy of the real-time Fourier transform synthesizer may be improved by changing several of its present components. Provision has been made, in the design of the system, to install a more accurate analog multiplier. The static accuracy of the present unit is 1% while the new one will have a specified accuracy of 0.2%. The installation of the new unit will free the present one so it may be used in the apodization system.

The summation unit contains an analog to digital converter. It is an F" system, and its linearity is specified as .5%. It digitizes the average value of the signal during the digitizing interval. This causes the frequency response to begin decreasing for frequencies in excess of 200 cps. This problem could be solved with the addition of a separate, high speed analog to digital converter, with provision of holding the signal value during the digitizing interval. A high speed unit would require less digitizing time, and these facts would improve the frequency response of

the converter-summation unit combination. The accuracy of digitization could be improved by using a converter which can digitize 10 or 12 bits. This gives an accuracy of 0.1% or 0.025% respectively. The summation unit can accept a pulse input so the output of the additional converter can be fed into the summation unit with a minimum of interfacing.

In section 3, it was mentioned that the point where the peak occurs in the discrete line spectra may not be recorded due to a finite number of channels. This is a limit to the accuracy of resolving amplitude differences. This is present in any system in which only a finite number of points are recorded, in this case 1024. The number of recorded points can be increased by the addition of a larger memory with 2048 or 4096 available addresses. A solution to this problem involved both the addition of more memory addresses and an interpolating scheme to obtain information located between address points.

The maximum allowable sampling rate is limited by several factors. First, there is an unavoidable delay in switching the frequency synthesizer with stepping switches. Second, it is required that at least a half cycle of the lowest frequency generated by the frequency synthesizer be stored in the memory. The lowest frequency is presently one cycle per second. The maximum sampling rate can be increased about five times. This requires a new switching scheme and increased frequency response

capabilities of the memory unit. This feature will be added as soon as an additional A-D converter becomes available. The counting circuits for this scheme are already included in the sequencer.

CONCLUSION

Various techniques for obtaining the Fourier transform have been studied. A technique was developed to determine the transform in real time. A Fourier transform synthesizer has been designed, constructed and evaluated. It is designed to synthesize the spectrum of any low-frequency even function, but it could easily be modified to synthesize the spectra of odd functions. The principles are also applicable to a design which could synthesize the spectrum of a general function. In the latter case, either a two-channel memory or a pair of memories is required, and the synthesizer becomes considerably more complex.

The Fourier synthesizer operates upon signals with frequencies which range from dc to an upper limit that is imposed by the allowable sampling rate. The present upper limit is 0.5 cps. An improvement by a factor of five is expected as soon as several components in the system are replaced.

The system has been designed for use in Fourier spectroscopy to synthesize the spectral distribution from the corresponding interferogram. It has been tested in this application, and the performance is satisfactory. It was used with a lamellar grating interferometer, but it could also be used with a well-compensated Michelson interferometer.

Additional work is required to reduce the errors to a minimum. This may be accomplished by adding an apodization system and by changing several of the components in the synthesizer. A more accurate multiplier, a better analog to digital converter, and a larger memory with more addresses will improve the accuracy. A system to interpolate the data which is in the memory will also improve the performance.

A secondary design criterion has been met. This was to design a system that would be portable and one that could also be used outside a laboratory. The present synthesizer can meet this requirement by being packaged into a more compact form. The choice of the type of summation unit and the decision to use a crystal-controlled frequency synthesizer and special gating circuitry instead of a phase locked oscillator chain permitted the construction of a fairly compact system. The exclusive use of solid state circuits also made this small size possible.

APPENDIXES

APPENDIX I

Design Equations and Data for the Non-Linear Shaping Networks

The 90-degree detector used several non-linear networks to shape a sinewave into a series of narrow pulses. Biased diode networks are used, and the components are chosen to give a network with an approximate quartic or quintic transfer characteristic. Thus,

$$i_{out} \cong k E_{in}^4 \quad \text{or} \quad i_{out} \cong k E_{in}^5$$

where k is chosen to give the components reasonable values. Six line segments are used to approximate the characteristic, and the breakpoints are chosen at e = 1, 3, 5, 7, and 9 volts. Figure 39 shows part of the characteristic and the first few line segments of the approximation.

Let the voltages at the breakpoints be E_1, E_2, E_3, E_4, E_5, and E_6, respectively. Conductances will be used in the equations as it simplifies the calculations. The values will then be converted to resistances, which are shown in Figure 23 . At the first breakpoint, E_1, the current for the quintic network is

$$i = G_o E_1 = k E_1^5$$

When $e = E_2$, it is

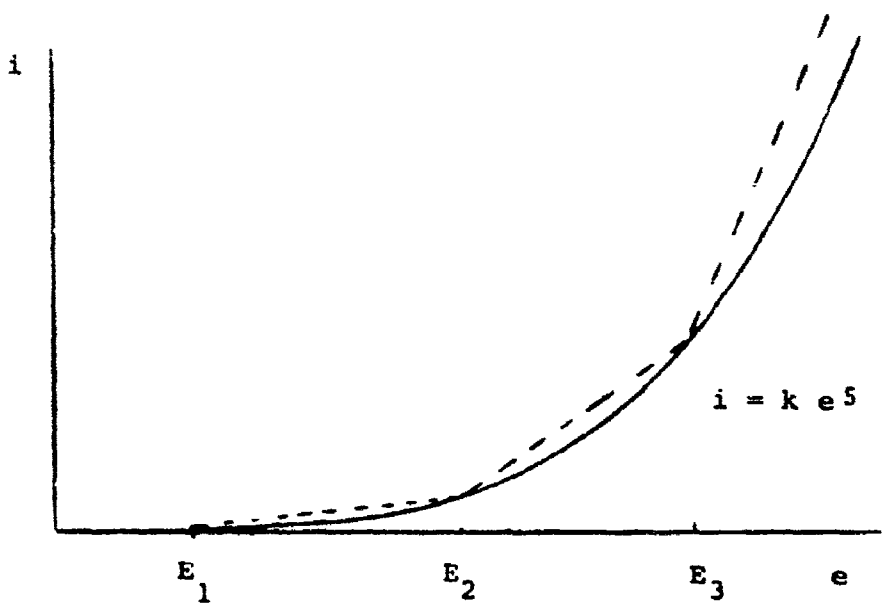

Figure 39

$$i = G_o E_2 + G_1(E_2 - E_1) = k E_2^5$$

Likewise, at $e = E_3$

$$i = G_o E_3 + G_1(E_3 - E_1) + G_2(E_3 - E_2) = k E_3$$

Similarly, at $e = E_4$

$$i = G_o E_4 + G_1(E_4 - E_1) + G_2(E_4 - E_2) + G_3(E_4 - E_3) = k E_4$$

Also, at $e = E_5$

$$i = G_o E_5 + G_1(E_5 - E_1) + G_2(E_5 - E_2) + G_3(E_5 - E_3)$$

$$+ G_4(E_5 - E_4) = k E_4$$

Finally, at $e = E_6$

$$i = G_o E_6 + G_1(E_6 - E_1) + G_2(E_6 - E_2) + G_3(E_6 - E_3)$$

$$+ G_4(E_6 - E_4) + G_5(E_6 - E_5) = k E_6$$

The equations are solved in turn, and the conductances (resistances) are determined. The value of k is chosen such that the largest resistance is less than 10^7 ohms.

A basic diagram of a non-linear network is shown in Figure 40 while Figure 41 shows a practical network that has been used. The breakpoint voltages are determined with the aid of a resistance voltage divider. One percent precision resistors are employed and zener diodes are used to control the voltages at the ends of the divider. The resistors in the divider have low values, compared to the ones in the shaping network. This is necessary if the breakpoint voltages are to remain nearly constant as the input voltage varies.

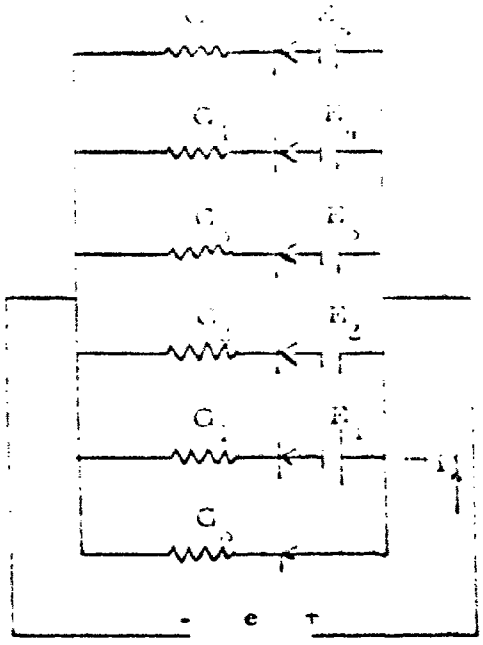

Figure 40

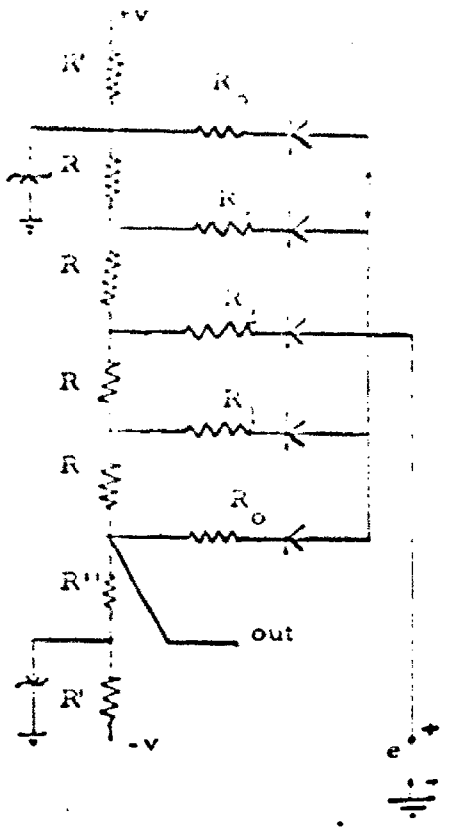

Figure 41

APPENDIX 2

Analysis and Performance of Two Preliminary Methods for Obtaining Fourier Transforms

Electro-Optical Spectrum Analyzer

An electro-optical computer, somewhat similar to Montgomery's [10], was constructed. In this case, an oscilloscope was used to furnish both the light source and the harmonic functions. Montgomery used a projector lamp and sine-cosine masks of different frequencies.

A periodic function can be expanded in a Fourier series of the form

$$f(t) = \frac{a_o}{2} + \sum_{n=1}^{\infty} (a_n \cos\omega_n t + b_n \sin\omega_n t)$$

where

$$a_n = \frac{1}{T} \int_{-T/2}^{T/2} f(t) \cos\omega_n t \, dt$$

and

$$b_n = \frac{1}{T} \int_{-T/2}^{T/2} f(t) \sin\omega_n t \, dt$$

For a non-periodic function, the Fourier transform is

$$F(\omega) = \int_{-\infty}^{\infty} F(t) e^{-j\omega t} dt$$

The functions to be examined are either even or odd. Then only one type of terms, cosine or sine, is needed in the series expansion. For non-periodic functions, only the cosine or the sine transform is required.

The multiplication and integration may be performed optically. In the following diagram, light entering from the left is modified by passing through a mask whose transmission function is T. The light between the masks can be represented as $I_o T_1$ while to the right of the second mask it is $I_o T_1 T_2$. Thus, the light output is the product of the two transmission functions.

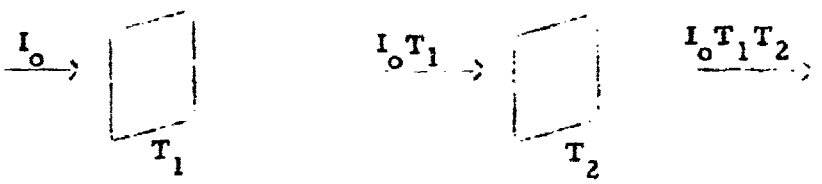

The transmission functions are masks of variable density or variable width. Two variable density, or one variable density, and one variable width function may be multiplied.

If the transmission function of one of the masks is f(x) and the other mask carries the sine or cosine function, the integral is obtained by focusing the emerging light onto a photocell. The output of the photocell is a constant times the integral

$$\int f(x) \cos\omega x dx \qquad \text{or} \qquad \int f(x) \sin\omega x dx.$$

Several Fourier coefficients may be obtained by the use of several slides, each with a cosine or sine function of a different "spatial" frequency.

The experimental system is shown in Figure 42a . The 100 kc oscillator, operating in conjunction with a slow sweep speed, produces a band of light on the screen. The vertical gain is adjusted so only the most uniform central region of the pattern is used. The variable frequency oscillator (VFO) is connected to a motor which drives the tuning mechanism. The frequency is varied from 100 cps to 20 kc in a period of several minutes. This oscillator is used to intensity modulate the scope in a sinusoidal manner. A trigger circuit produces synchronizing pulses to start successive sweeps at the same point with respect to the intensity modulating signal. As the frequency increases, fringes of increasing spatial frequency move across the screen.

The mask carries the f(x) function. The light emerging from the mask is focused onto a photocell. The cell output is amplified and recorded on a strip chart recorder.

Several test functions were evaluated to determine the system performance. Variable width and variable density functions were used. Variable width masks were made by modulating a carrier with the desired function and photographing the amplitude modulated wave from a scope, using Polaroid transparency film. Variable density masks were made by projecting a Ronchi Ruling onto photographic film with an enlarger

OPTICAL FOURIER ANALYSIS SYSTEM

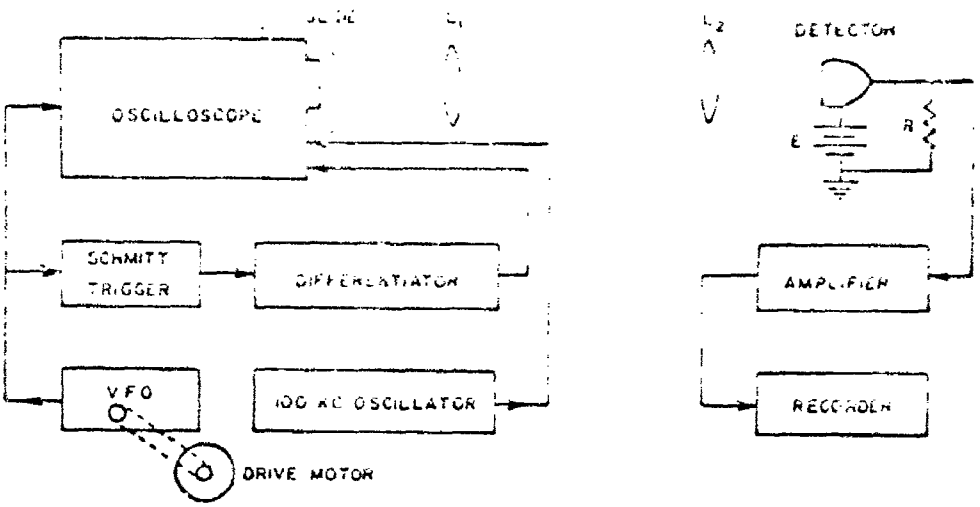

(a)

PHOTOGRAPHIC SPECTRUM SYNTHESIS SYSTEM

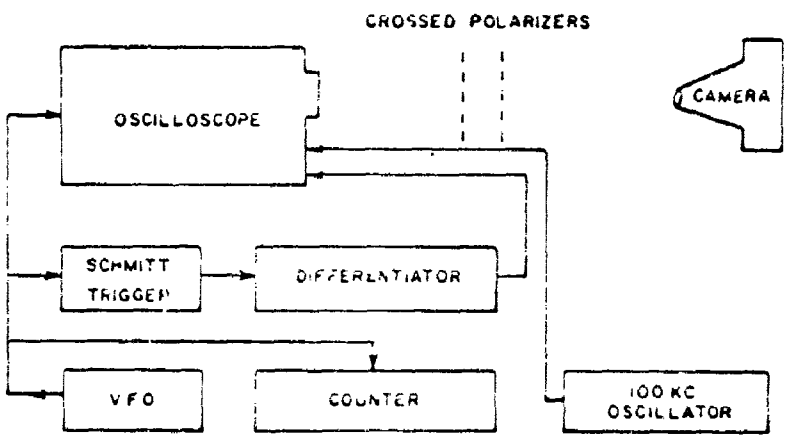

(b)

Figure 42

and developing the film. A sample of the analysis of the Ronchi Ruling data is shown in Figure 43a , and a sample of the variable width data is shown in Figure 43b .

This system has many disadvantages which render it unfeasible for an accurate high speed Fourier analysis technique:

1. The number of fringes that can be placed on the cathode ray tube is limited by resolution and defocusing effects. With 100 fringes on the screen, defocusing at the edges is very noticeable while the central region is still in good focus.

2. The intensity is not uniform and varies across the face of the scope. This is called the "shading" characteristic.

3. A very high noise level exists due to the continuously varying pattern. As each new fringe comes on the screen, the total light intensity varies. This is especially evident when only a few fringes are present and causes very large variations in the detected signal.

4. Higher harmonics in the spectrum are lost as a result of the combined effects of noise and defocusing.

5. Because of the high noise level, amplitude comparison between different frequency components is difficult.

6. The intensity modulation is not uniform as a function of frequency and good cosinusoidal intensity distributions are difficult to obtain.

TRANSPARENCIES AND THEIR SPATIAL FREQUENCY SPECTRA

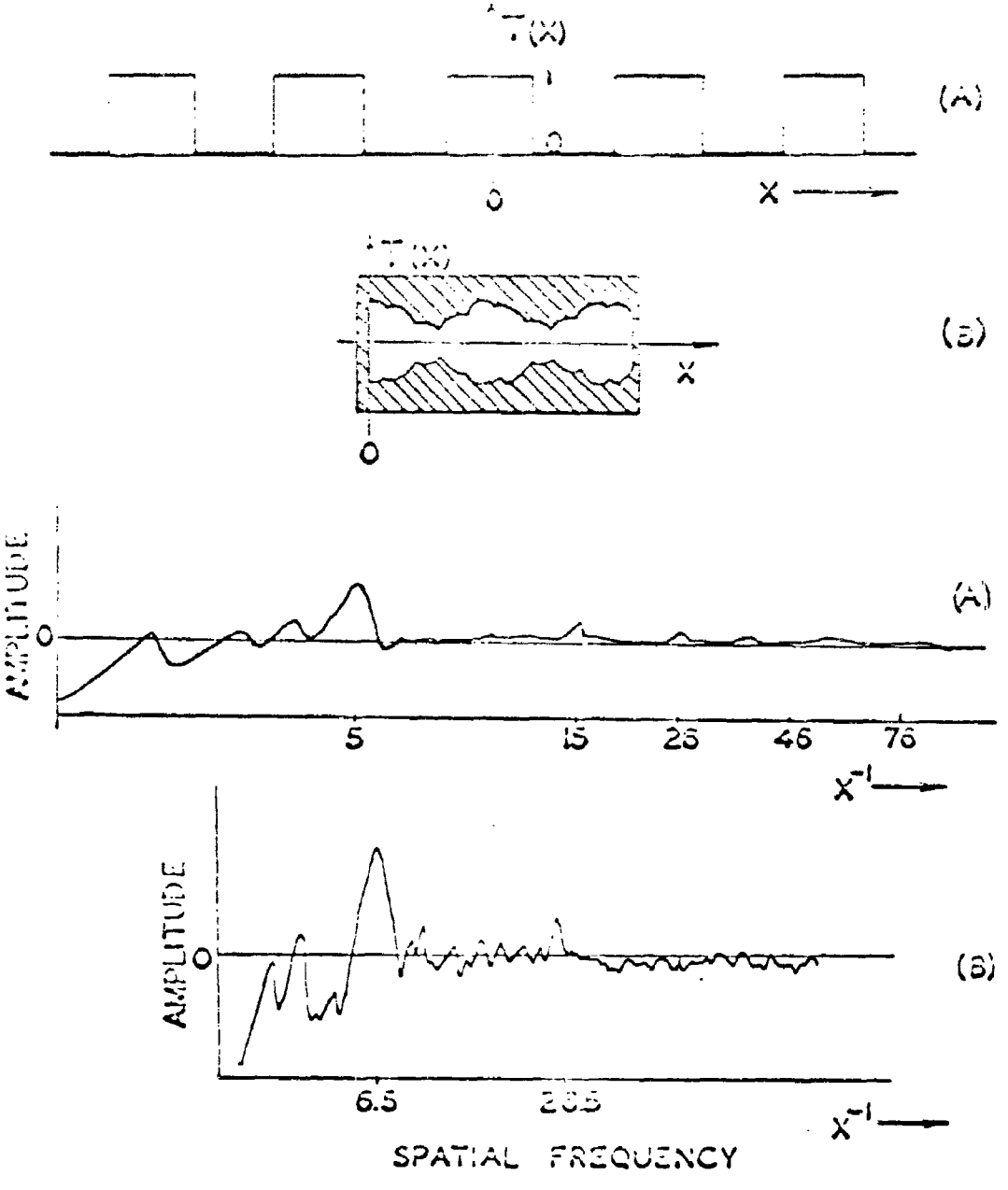

Figure 43

7. Two closely-spaced frequencies in a width modulated pattern are not accurately resolved.

8. Initial phasing of the scope pattern and the mask is done by eye and is not sufficiently accurate. Errors cause the sinc function, representing a harmonic, to be asymmetrical.

9. The method is not suited for the real-time analysis of an electrical signal.

A Photographic Spectrum Synthesizer

Experiments were performed to determine the feasibility of using photographic techniques to compute Fourier transforms. A diagram of the system is shown in Figure 42b . The VFO is manually controlled, and a counter is used to determine the discrete frequencies required in the synthesis. A set of polarizers controls the intensity of the light which reaches the film. The camera photographs each succeeding pattern as a multiple exposure on the same frame.

The function under investigation is even and is represented in Figure 44 . It is properly sampled, and the sampled function is also shown. The sampled function may be represented as

$$f(t) = f_o(0) + f_1(t_1) + f_2(t_2) + f_3(t_3) + \ldots f_2(t_n)$$

It is possible to obtain the Fourier transform of F(t) by superposition.

INTERFEROGRAM AND THE SAMPLE POINTS

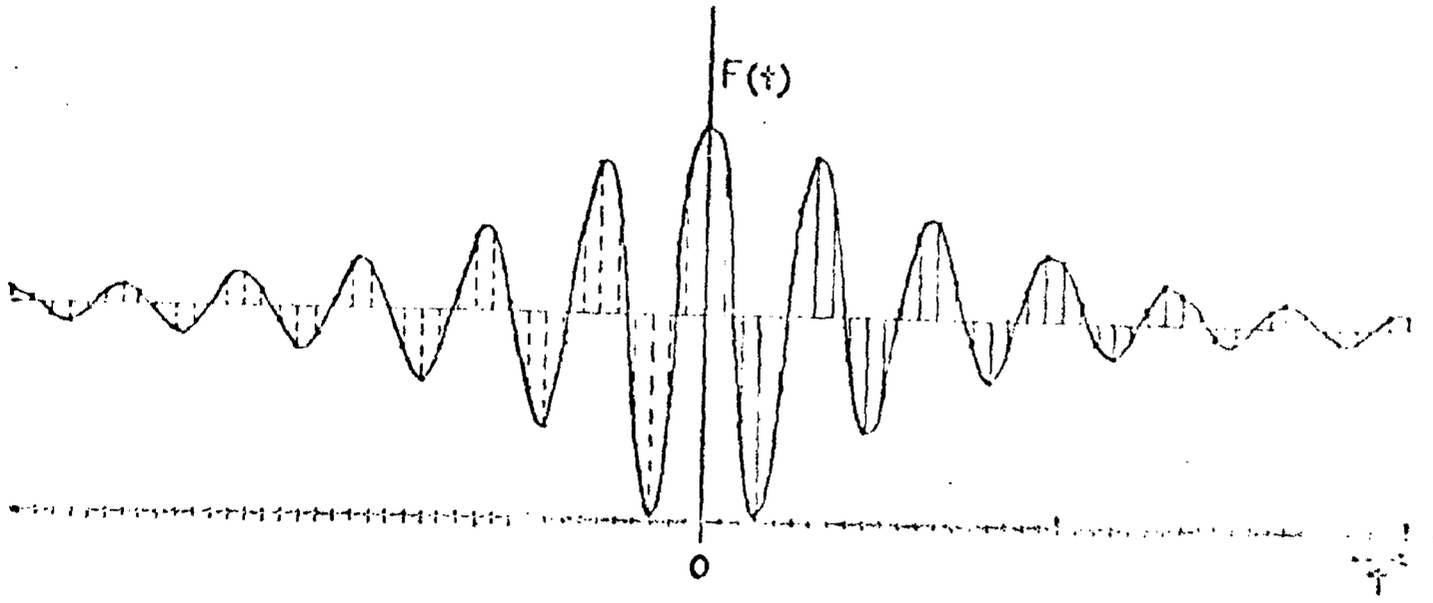

Figure 44

$$f_o(0) + f_1(t_1) + f_2(t_2) + \ldots f_n(t_n) = \int_{-\infty}^{\infty} F_o(0)e^{j\omega t}d\omega + \int_{-\infty}^{\infty} F_1(t)e^{j\omega t}d\omega$$

$$+ \ldots + \int_{-\infty}^{\infty} F_n(\omega)e^{j\omega t}d\omega$$

where $F_n(\omega)$ is the Fourier transform of $F_n(t)$. Conversely

$$F_o(\omega) + F_1(\omega) + F_2(\omega) + \ldots F_n(\omega) = \int_{-\infty}^{\infty} F_o(t)e^{-j\omega t}dt + \ldots$$

$$\ldots + \int_{-\infty}^{\infty} F_n(t)e^{-j\omega_n t}\,dt$$

Thus

$$F(\omega) = \sum_{n=0}^{\infty} F_n(\omega)$$

The function has been reduced, by sampling, to a set of delta functions, and the total transform is a summation of the transforms of the delta functions.

The Fourier transform of a δ function at $t = 0$ is of constant amplitude and extends to ∞ in both directions in the frequency domain. The Fourier transform of a pair of delta functions, symmetrically placed about $t = 0$, is a cosine wave whose frequency depends on the location of the δ functions from $t = 0$.

The function to be analyzed is manually sampled, and the sample amplitudes are recorded. These are then converted into the angles at which the crossed polarizers must be set when the photographic data are taken. These control the intensity of the light reaching the film, and each sample corresponds to a different intensity and spatial frequency. The film is developed, dried, and processed with a micro-densitometer which plots the density of the negative versus position. The more dense portions are points where the fringes have added in phase and represent harmonics of the original function.

Several simple functions were analyzed. Data are presented in Figures 45 and 46 which show the results of analyzing a $\left|\frac{\sin \pi t}{\pi t}\right|^2$ pulse, a finite cosine wave and a simple interferogram. The system has disadvantages which render it unacceptable for a real-time synthesizer:

1. The samples are manually obtained and converted to polarizer angles.

2. The system is feasible for only even or odd functions.

3. Film grain adds greatly to the noise level.

4. It is difficult to maintain the shape of the cosinusoidal fringes as the frequency is altered.

5. The pattern does not have uniform focus.

6. There is a non-uniform shading characteristic that cannot be exactly compensated.

WAVEFORMS AND THEIR SYNTHESIZED SPECTRA

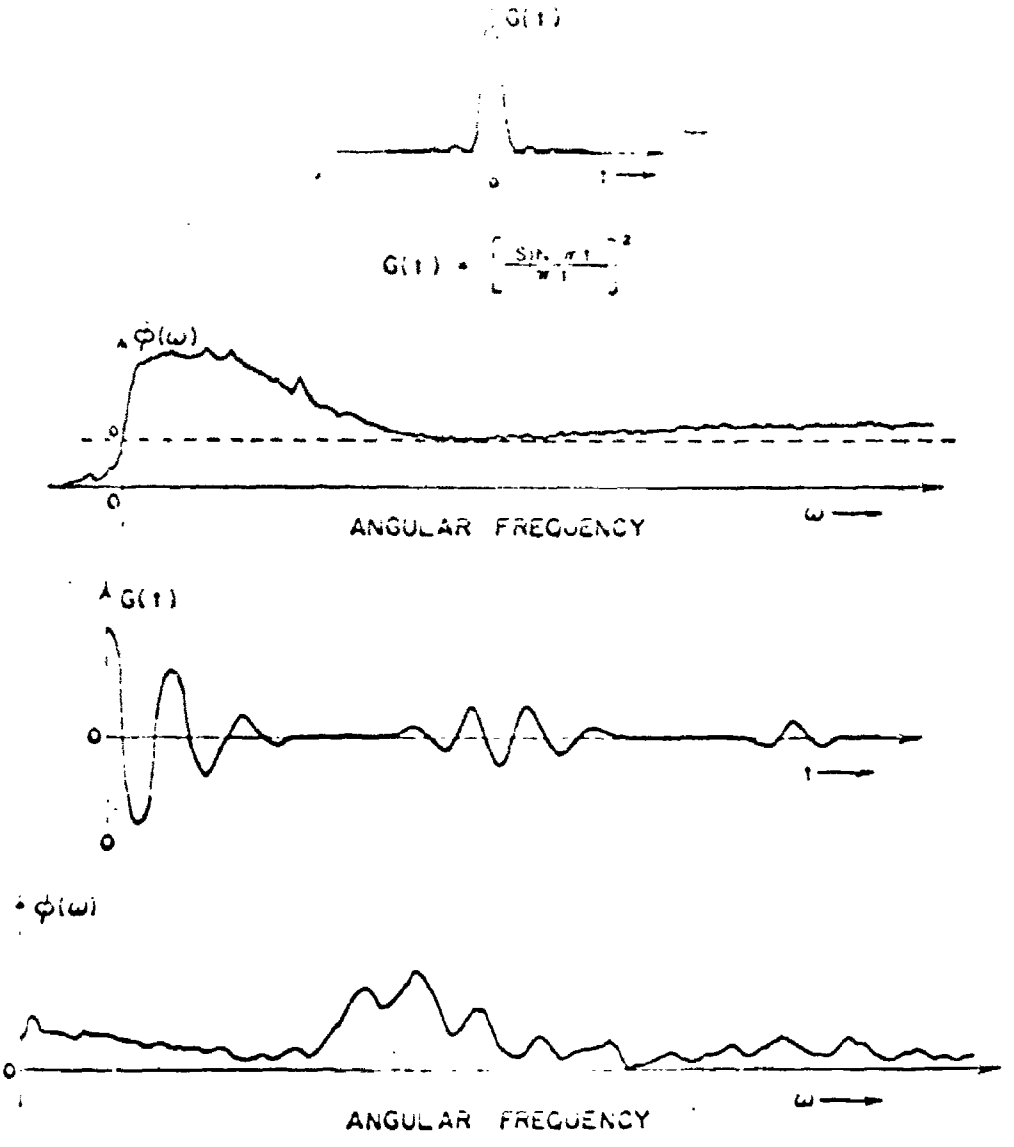

Figure 45

WAVEFORMS AND THEIR SYNTHESIZED SPECTRA

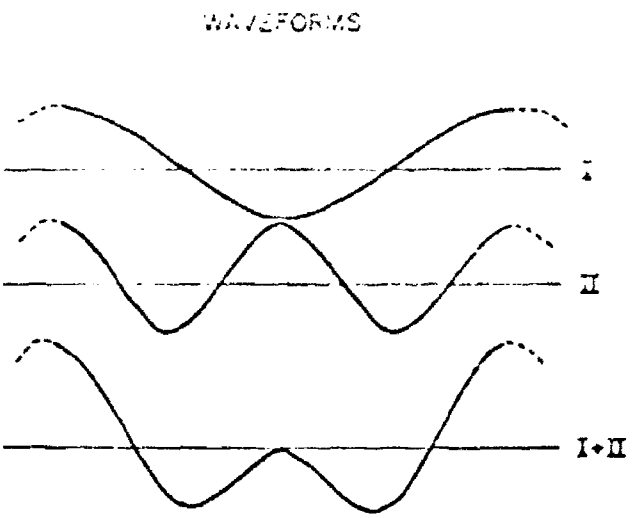

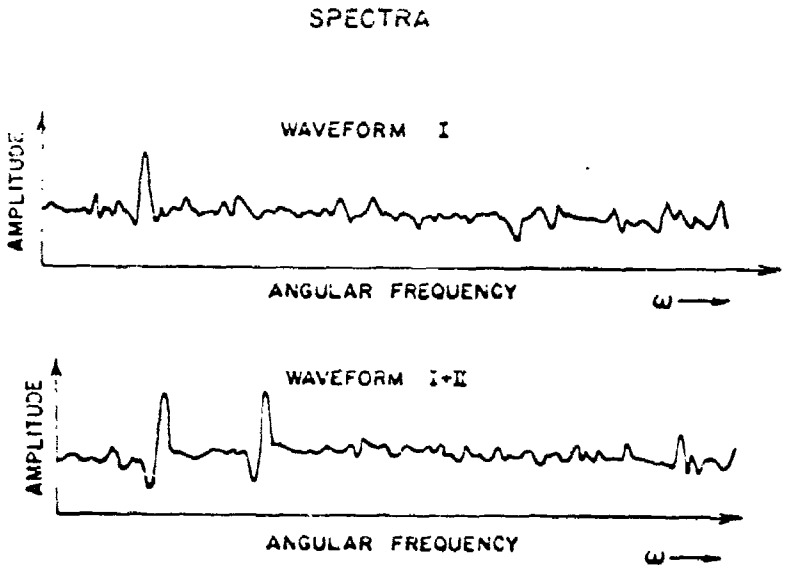

Figure 46

7. The film is non-linear and tends to saturate as a large number of samples are taken.

8. The time involved between the acquisition of the original data and the spectrum is excessive.

9. The accurate control of the polarizer setting is difficult.

Because of the large number of disadvantages, it was decided to abandon both schemes as a method of obtaining Fourier transforms in real time. An investigation was made to determine the feasibility of using storage tubes as a summation device, but they have all of the disadvantages of a CRT and are, therefore, not acceptable.

The system that is used is an all-electronic analog of the photographic system. It has the advantages of being automatic, of utilizing a linear summation scheme that will not saturate, and it is able to generate pure cosine functions of the desired frequency. The electronic scheme is also a real-time technique.

BIBLIOGRAPHY

1. Fellgett, P., Thesis, Cambridge University (1951).

2. Connes, J., Thesis, Laboratoire Aime Cotton, Bellevue (1961) Translation, NAVWEPS Report 80999, China Lake, California.

3. Stone, J.M., Radiation and Optics, McGraw-Hill Book Co., p. 307, (1963).

4. Vanasse, G.A., Thesis, Johns Hopkins University (1959).

5. Miller, D.C., Journal of the Franklin Institute, Vol. 182, pp. 285-322, September (1916).

6. Krantz, F.W., Journal of the Franklin Institute, Vol. 204, p. 245, August (1927).

7. Brown, S.L., Journal of the Franklin Institute, Vol. 228, p. 675, December (1939).

8. Robertson, J.H., Review of Scientific Instruments, Vol. 27, p. 276, October (1950).

9. Charp, S., Paper No. 49-163 presented at the AIEE Summer Meeting in Swampscott, Mass. (1949).

10. Montgomery, H.C., Bell System Technical Journal, p. 406 (1936).

11. Cutrona, L.J., Leith, E.N., Palerno, C.J., and Parcello, L.J., IRE Transactions on Information Theory, Vol. IT-6, No. 3, June (1960).

12. Firle, T.E., Review of Scientific Instruments, Vol. 27, No. 3, p. 140, March (1956).

13. Staake, D.B., Johns Hopkins University Report No. CM833, March (1958).

14. Pritchard, J., Paper presented at the Colloque de Spectroscopie Instrumentale, April (1966).

15. Beckel, H.J., IRE Wescon Convention Record, Part 3, p. 59 (1959).

16. Capon, J., Weiss, M.R., Proceedings of the IRE, Vol. 49, No. 11, p. 1717 (1961).

17. Schannon, C., Proceedings of the IRE, Vol. 37, p. 10, June (1949).

18. Goldman, S., Information Theory, Prentice Hall, Inc., Englewood Cliffs, N.J., p. 73 (1955).

19. Connes, J., op cit., p. 24.

20. Guillemin, E.A., Mathematics of Circuit Analysis, MIT Press, Chapter 7 (1949).

21. Vanasse, G.A., Journal of the Optical Society, Vol. 49, p. 844, No. 9 (1959).

22. Connes, J., op cit., p. 13.

23. Connes, J., op cit., p. 16.

24. Vanasse, G.A., Journal of the Optical Society, Vol. 52, No. 4, p. 472, April (1962).

25. Connes, J., op cit., p. 42.

26. Bracewell, R., The Fourier Transform and its Applications, McGraw-Hill Book Co., Chapters 4 and 5 (1965).

ACKNOWLEDGMENTS

The author wishes to express his appreciation to Professor Stuart for his guidance in this research. He is also indebted to Dr. Vanasse of Air Force Cambridge Research Laboratories for suggesting the research area and for many enlightening consultations. He wishes to thank Dr. Sakai of AFCRL for his consultations, and Messrs. Hirschy, Streeter and Ballio for their assistance in constructing the instrument and in preparing the diagrams. Appreciation is also due the Concord Radiance Laboratory staff, a division of Utah State University, for their assistance in carrying out this research.

This work was supported in part by the Laboratory Directors Fund, AFCRL, and by Contract AF19(628)-251.

DOCUMENT CONTROL DATA R&D

Electronics Laboratories, Dept. of Elec. Engr., Phys. and Chem.
Utah State University, Logan, Utah

Unclassified

A REAL TIME FOURIER TRANSFORM SYNTHESIZER

Scientific Report, Interim

Hoffman, Joseph E., Jr.

6. REPORT DATE: 1 November 1966	7a. TOTAL NO. OF PAGES: 118	7b. NO. OF REFS: 26
8a. CONTRACT OR GRANT NO.: AF19(628)-3825 ARPA Order No. 450 b. PROJECT AND TASK NO.: 8663 c. DOD ELEMENT: 62503015 d. DOD SUBELEMENT: N/A	9a. ORIGINATOR'S REPORT NUMBER(S): Scientific Report No. 7 9b. OTHER REPORT NO(S) (Any other numbers that may be assigned this report): AFCRL-67-0049	

10. AVAILABILITY LIMITATION NOTICES

Distribution of this document is unlimited.

11. SUPPLEMENTARY NOTES: Prepared for Hq. AFCRL, OAR (CRO) United States Air Force L. G. Hanscom Fld, Bedford, Mass	12. SPONSORING MILITARY ACTIVITY: Advanced Research Projects Agency

13. ABSTRACT

A study of the relationship between the interferogram F(x) obtained in Fourier spectroscopy and the corresponding spectral distribution E(ν) is made. It is found that the spectral distribution is the Fourier cosine transform of the interferogram. Various computational techniques for performing the required transformation are studied, and a Real-Time Fourier Transform Synthesizer is described. It has been designed to be compatible with a lamellar grating Michelson interferometer, but could be used just as well with a well-compensated Michelson interferometer. The system used to obtain the point of zero path difference is described in detail. A novel approach is used to obtain the cosine functions required in the synthesis of the cosine transform. All the computations except the summation are done in analog form, while the summation is done digitally. The result of the computation, the spectral distribution, is available as soon as the interferogram is obtained. Errors in the technique are discussed and methods of compensating for them are enumerated.

DD FORM 1 JAN 64 1473

Unclassified

Security Classification

Two-Beam Interferometer
Fourier Transform
Spectral Distribution
Interferogram
Synthesizer

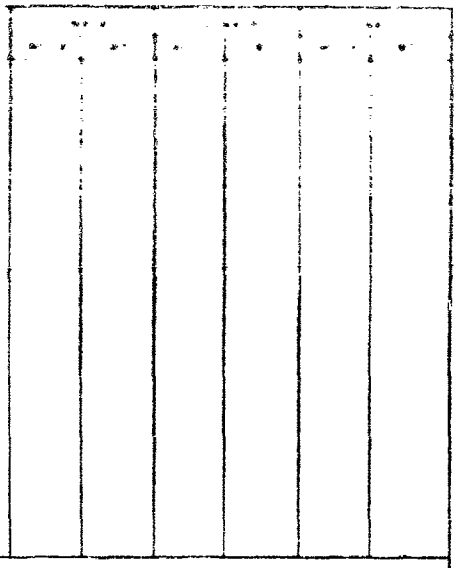

INSTRUCTIONS

1. ORIGINATING ACTIVITY: Enter the name and address of the contractor, subcontractor, grantee, Department of Defense activity or other organization *(corporate author)* issuing the report.

2a. REPORT SECURITY CLASSIFICATION: Enter the overall security classification of the report. Indicate whether "Restricted Data" is included. Marking is to be in accordance with appropriate security regulations.

2b. GROUP: Automatic downgrading is specified in DoD Directive 5200.10 and Armed Forces Industrial Manual. Enter the group number. Also, when applicable, show that optional markings have been used for Group 3 and Group 4 as authorized.

3. REPORT TITLE: Enter the complete report title in all capital letters. Titles in all cases should be unclassified. If a meaningful title cannot be selected without classification, show title classification in all capitals in parenthesis immediately following the title.

4. DESCRIPTIVE NOTES: If appropriate, enter the type of report, e.g., interim, progress, summary, annual, or final. Give the inclusive dates when a specific reporting period is covered.

5. AUTHOR(S): Enter the name(s) of author(s) as shown on or in the report. Enter last name, first name, middle initial. If military, show rank and branch of service. The name of the principal author is an absolute minimum requirement.

6. REPORT DATE: Enter the date of the report as day, month, year, or month, year. If more than one date appears on the report, use date of publication.

7a. TOTAL NUMBER OF PAGES: The total page count should follow normal pagination procedures, i.e., enter the number of pages containing information.

7b. NUMBER OF REFERENCES: Enter the total number of references cited in the report.

8a. CONTRACT OR GRANT NUMBER: If appropriate, enter the applicable number of the contract or grant under which the report was written.

8b, 8c, & 8d. PROJECT NUMBER: Enter the appropriate military department identification, such as project number, subproject number, system numbers, task number, etc.

9a. ORIGINATOR'S REPORT NUMBER(S): Enter the official report number by which the document will be identified and controlled by the originating activity. This number must be unique to this report.

9b. OTHER REPORT NUMBER(S): If the report has been assigned any other report numbers *(either by the originator or by the sponsor)*, also enter this number(s).

10. AVAILABILITY LIMITATION NOTICES: Enter any limitations on further dissemination of the report, other than those imposed by security classification, using standard statements such as:

(1) "Qualified requesters may obtain copies of this report from DDC."

(2) "Foreign announcement and dissemination of this report by DDC is not authorized."

(3) "U. S. Government agencies may obtain copies of this report directly from DDC. Other qualified DDC users shall request through _____."

(4) "U. S. military agencies may obtain copies of this report directly from DDC. Other qualified users shall request through _____."

(5) "All distribution of this report is controlled. Qualified DDC users shall request through _____."

If the report has been furnished to the Office of Technical Services, Department of Commerce, for sale to the public, indicate this fact and enter the price, if known.

11. SUPPLEMENTARY NOTES: Use for additional explanatory notes.

12. SPONSORING MILITARY ACTIVITY: Enter the name of the departmental project office or laboratory sponsoring *(paying for)* the research and development. Include address.

13. ABSTRACT: Enter an abstract giving a brief and factual summary of the document indicative of the report, even though it may also appear elsewhere in the body of the technical report. If additional space is required, a continuation sheet shall be attached.

It is highly desirable that the abstract of classified reports be unclassified. Each paragraph of the abstract shall end with an indication of the military security classification of the information in the paragraph, represented as *(TS), (S), (C), or (U)*.

There is no limitation on the length of the abstract. However, the suggested length is from 150 to 225 words.

14. KEY WORDS: Key words are technically meaningful terms or short phrases that characterize a report and may be used as index entries for cataloging the report. Key words must be selected so that no security classification is required. Identifiers, such as equipment model designation, trade name, military project code name, geographic location, may be used as key words but will be followed by an indication of technical context. The assignment of links, rules, and weights is optional.

Unclassified
Security Classification